UCL Université catholique de Louvain

École polytechnique de Louvain (EPL)

epl

Carbon dioxide capture using sodium hydroxide solution: comparison between an absorption column and a membrane contactor

Dissertation presented by
Nicolas CAMBIER

for obtaining the master's degree in
Chemical and Materials Engineering

Supervisor
Patricia LUIS ALCONERO

Tutor
Israel RUIZ SALMON

Readers
Juray DE WILDE, Joris PROOST

Academic year 2016-2017

Acknowledgements

Before beginning this report, I would like to address my acknowledgements to the people who helped me throughout the realisation of my master thesis.

First of all, nothing would have been possible without the support and advices of my promoter, the professor Patricia Luis. The working environment provided by her team and the meetings along the year were good opportunities to evolve for the best.

Secondly, I would like to thank Israel Ruiz Salmon who was a major actor of my work. He always helped me with my numerous questions and uncertainties. Without him, I certainly would not have managed to overcome the numerous challenges encountered during this work. His precious advices and corrections are certainly what helped me to finish this master thesis.

For their help with the preparation of solutions and in the lab, I thank Luc Wautier, Frédéric Van Wonterghem, Ronny Santoro and Nadine Deprez.

In addition, I would like to express my gratitude to Professors J. De Wilde and J. Proost who have accepted to be the readers of this thesis.

List of symbols

Symbols	Signification	Units
a	Specific area of packing per unit volume of column	m^2/m^3
A	Cross sectional area of the column	m^2
[A]	Concentration of species A	mol/L
a_{eff}	Effective interfacial area in membrane contactor	m^2
$CO_{2,I}$, $CO_{2,II}$	Composition of inlet and outlet flue gas in CO_2 (on the console screen)	%
E	Enhancement factor	−
F_a	Volumetric flow rate of absorption of CO_2	L/s
F_{air}, F_{CO_2}	Air and CO_2 flow rates (on the console screen)	L/min
G_{in}, G_{out}	Inlet and outlet gas flow rates	L/min
H	Column height	m
k_l, k_m, k_g	Individual mass transfer coefficient of the liquid phase, membrane and gas phase	$mol/(atm \cdot m^2 \cdot s)$
K_{Og}	Overall mass transfer coefficient	$mol/(atm \cdot m^2 \cdot s)$
L	Liquid flow rate	L/min
p_{atm}	Atmospheric pressure	atm
r	Pore radius	m
R	Ideal gas constant	J/(mol·K)
r_{CO_2}	Rate of absorption of CO_2	mol/s
V_i	Volume *i*	L
y_i, y_o	Inlet and outlet CO_2 partial pressures	%
Δp	Breakthrough pressure	atm
ΔP_{lm}	Logarithmic mean pressure	atm
γ	Interfacial tension	N/m
Θ	Geometric factor related to the pore structure	−

Abbreviations	Signification
AFOLU	Agricultural, forestry and other land use
AMP	Adenosine monophosphate
CCC	Carbon capture and conversion
CCS	Carbone capture and storage
DEA	Diethanolamine
GHGs	Greenhouse gases
GWP	Global warming potential
HFMC	Hollow fibre membrane contactor
IGCC	Integrated gasifier combined cycle
IPCC	Intergovernmental Panel on Climate Change
LLGHGs	Long-lived GHGs
MDEA	Methyl diethanolamine
MEA	Monoethanolamine
MO	Methyl orange
PCC	Post combustion capture
PP	Phenolphthalein
TETA	Triethylenetetramine

Contents

Introduction

Since the industrial revolution, human activities have contributed to increase drastically the atmospheric concentration of greenhouse gases. Carbon dioxide, even though it is not the more armful of them, is by far the most problematic of these gases. Indeed, its concentration is so high that its contribution is accountable to two third of the total contribution of warming gases [1].

In order to mitigate the CO_2 atmospheric concentration, the focus is made on the flue gas at the exit of the power plants. Indeed, the large increase of the last decades in atmospheric CO_2 is attributable by 75% to burning fossil fuels to produce power [2].

Industries have already reacted to help decrease their carbon dioxide release and the currently most developed method to capture CO_2 from flue gas is the use of absorption column using amine absorbents [3]. This method possesses drawbacks such as the toxicity of the liquid absorbents used or the Haber-Bosch process required to produce them which releases CO_2 hence reduces the overall mitigation of released carbon dioxide. In this context, researches are conducted to develop new way of CO_2 capture.

The present master thesis is part of a PhD project based on membrane technology for CO_2 absorption and recovery into Na_2CO_3 crystals using NaOH. The production of sodium carbonate is interesting in the prospect of creating a closed carbon loop in which CO_2 helps to create useful products instead of being stored underground [3]. Sodium carbonate is used as raw material in the cement and ceramic industry [4].

In this report, the chemical absorption of CO_2 with aqueous NaOH is studied using two technologies. The overall mass transfer coefficient of a packed column and a membrane contactor are measured with varying operating conditions and further analysed in order to compare their efficiency on the capture of CO_2 from a flue gas.

The content of this work is divided in five sections. First, a bibliographic review aims to detail the context of the carbon dioxide problematic and introduces the techniques used to mitigate its emission. This section focuses on the packed absorption columns and the membrane contactors. Then, the objectives of the master thesis will be fully explained in section two. Section three presents the materials and methods used to conduct the experiments that are explained and discussed in section four. Finally, section five provides further lines of inquiry for future researches on this topic.

1 Bibliographic review

1.1 Carbon dioxide problematic

Greenhouse effect has always been active on Earth. Without it, the average global surface temperature would be 33°C lower and life as we know could not be [5].Broadly speaking, this essential effect happens thanks to atmospheric gases know as greenhouse gases (GHGs). These gases (water vapour, N_2O, CH_4, CO_2, CFCs…) absorb and re-emit about 90% of the previously surface-radiated infrared energy from the atmosphere down to the surface (see Figure 1.1).

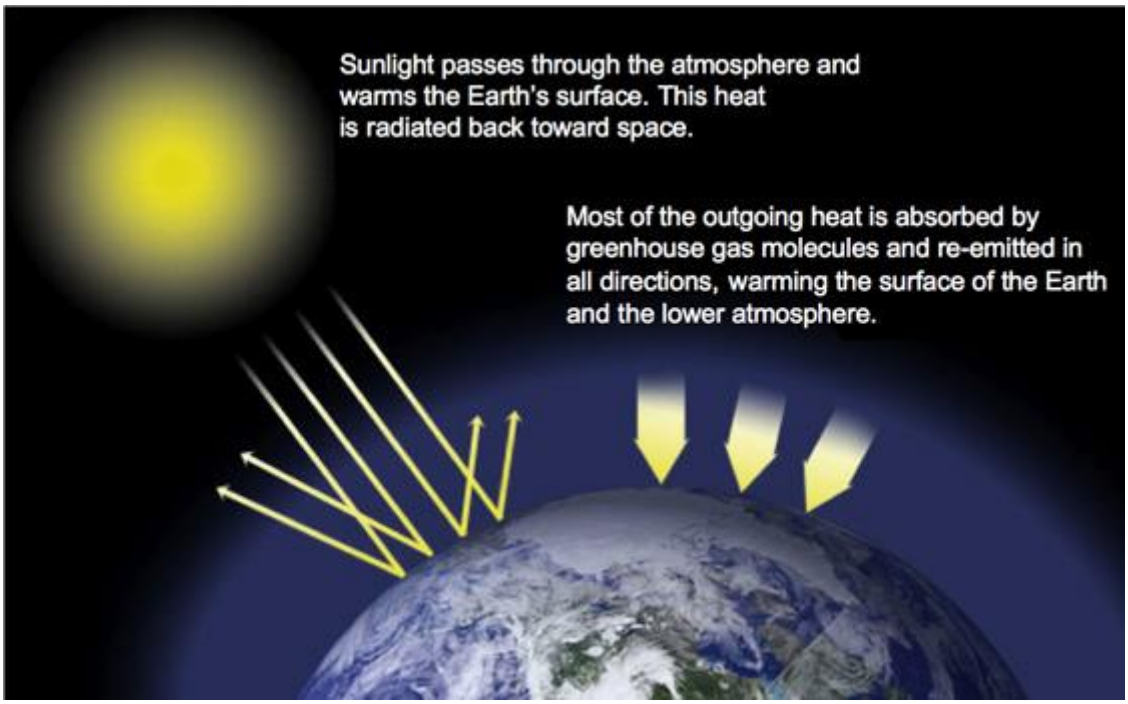

Figure 1.1: Greenhouse effect (from [6])

These GHGs can be classified in two categories. Gases that are physically or chemically impacted by changes in temperatures: the feedbacks; and the long-lived gases (LLGHGs) that are not affected by temperature changes and stay nearly permanently in the atmosphere [6]. The fifth assessment report of the Intergovernmental Panel on Climate Change (IPCC, [7]) concluded that the increase of atmospheric concentrations of LLGHGs is correlated with the global warming our planet is facing since the mid-twentieth century.

Climate on Earth has changed on all time scales. In the pre-industrial era (before 1750), ice ages and global warmings found their origins in natural causes mainly due to Earth's orbital changes involving variations of solar energy received by our planet [1]. Nonetheless, the industrial revolution has led to a huge increase in the concentrations of GHGs with amounts never achieved before. Human activity consisting in intensified agricultural practices, increase in land use and deforestation, industrialization and associated energy use from fossil sources is the cause of this increase [8]. Global temperature and sea level rise, warming oceans, shrinking ice sheets, glacial retreats, extreme events (hurricanes, intense

rainfalls…), ocean acidification and decrease of snow cover are all evidence of the rapid climate change that has been occurring since 1950 [6]. Figure 1.2 from [1] brings to light the relationship between temperature and sea level increase and concentrations of GHGs (CO_2 in ppm, other gases in ppb). Table 1.1 from [9] presents the main LLGHGs present in the atmosphere, their concentrations and their global warming potential (GWP). According to the data of this table, CO_2 is not the more active agent for climate change but its huge concentration in regard with the concentrations of other GHGs (409.01 ppm on the 5th May 2017, [10]) makes it the major actor for global warming. Figure 1.3 from [11] highlights that CO_2 concentration and temperature have always been linked – there was low CO_2 concentration during ice ages – but also that, for the last sixty years, there has been a tremendous increase of CO_2 concentration when compared with its evolution determined by analyse of ice cores.

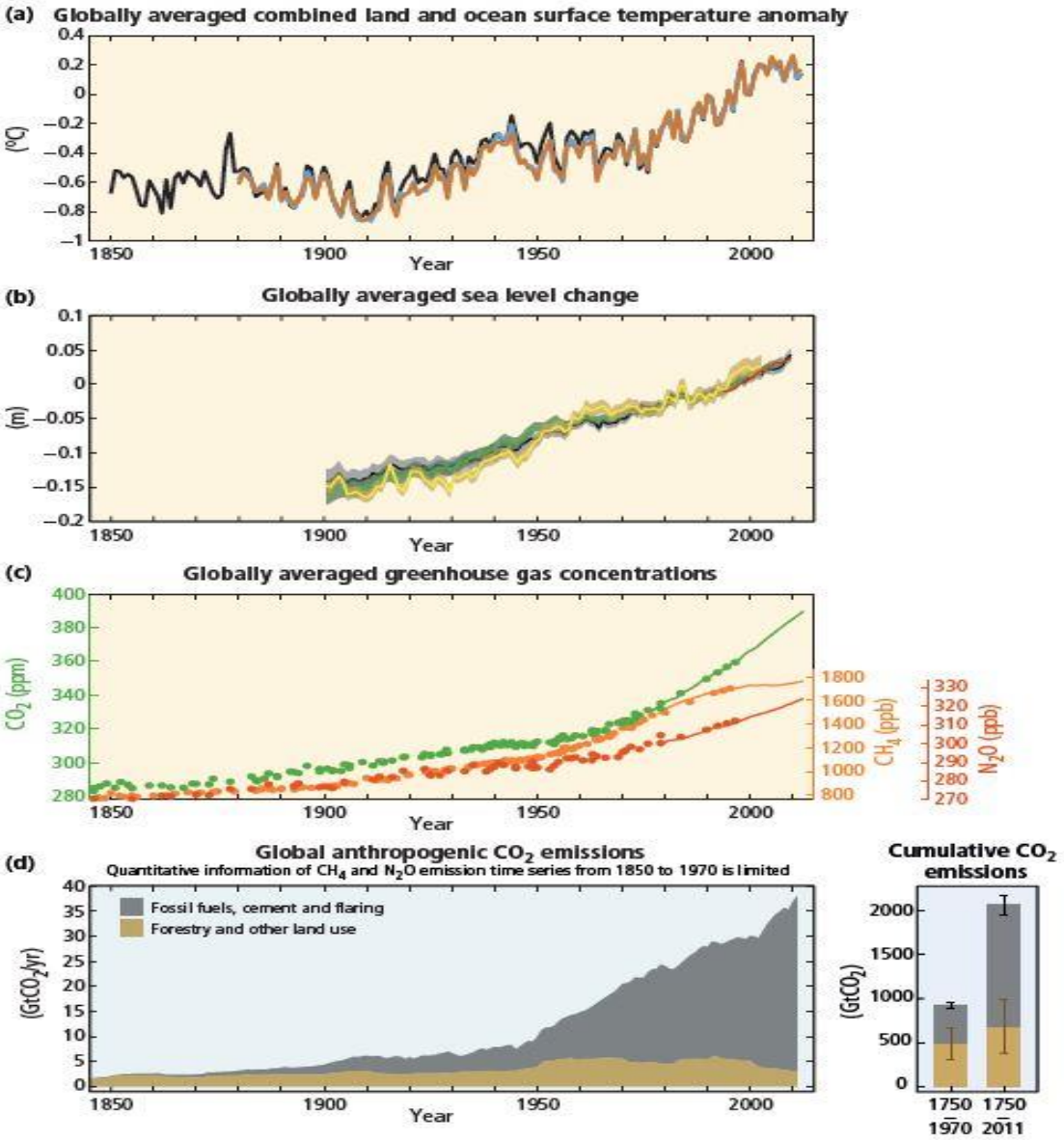

Figure 1.2: Evolution of temperature, sea level, GHGs concentrations and anthropogenic CO2 emissions (from [7])

The 2015 United Nations Climate Change Conference (COP21) led to the first global climate agreement and determined that, in order to preserve our planet, the increase in temperature from pre-industrial era cannot exceed 2°C [12]. In the next section will be presented the causes of the large increase in CO_2 concentration since 1950 and the techniques studied to mitigate its emissions in the atmosphere in order to handle the challenge COP21 has raised.

Compound	Pre-industrial concentration (ppmv*)	Concentration in 2005 (ppmv)	Atmospheric lifetime (years)	Main human activity source	GWP**
Carbon dioxide (CO_2)	280	379	variable	Fossil fuels, cement production, land use change	1
Methane (CH_4)	0.715	1.774	12	Fossil fuels, rice paddies, waste dumps, livestock	25
Nitrous oxide (N_2O)	0.27	0.319	114	Fertilizers, combustion industrial processes	298
HFC 23 (CHF_3)	0	0.000018	270	Electronics, refrigerants	14,800
HFC 134a (CF_3CH_2F)	0	0.000035	14	Refrigerants	1,430
HFC 152a (CH_3CHF_2)	0	0.0000039	1.4	Industrial processes	124
Perfluoromethane (CF_4)	0.00004	0.00008***	50,000	Aluminum production	7,390
Perfluoroethane (C_2F_6)	0	0.000003***	10,000	Aluminum production	12,200
Sulphur hexafluoride (SF_6)	0	0.0000042***	3,200	Dielectric fluid	22,800

*ppmv = parts per million by volume, **GWP = 100-year global warming potential, ***Concentration in 1998
Water vapor not included in table, see bullet.

Table 1.1: Main long-lived greenhouse gases (from [9])

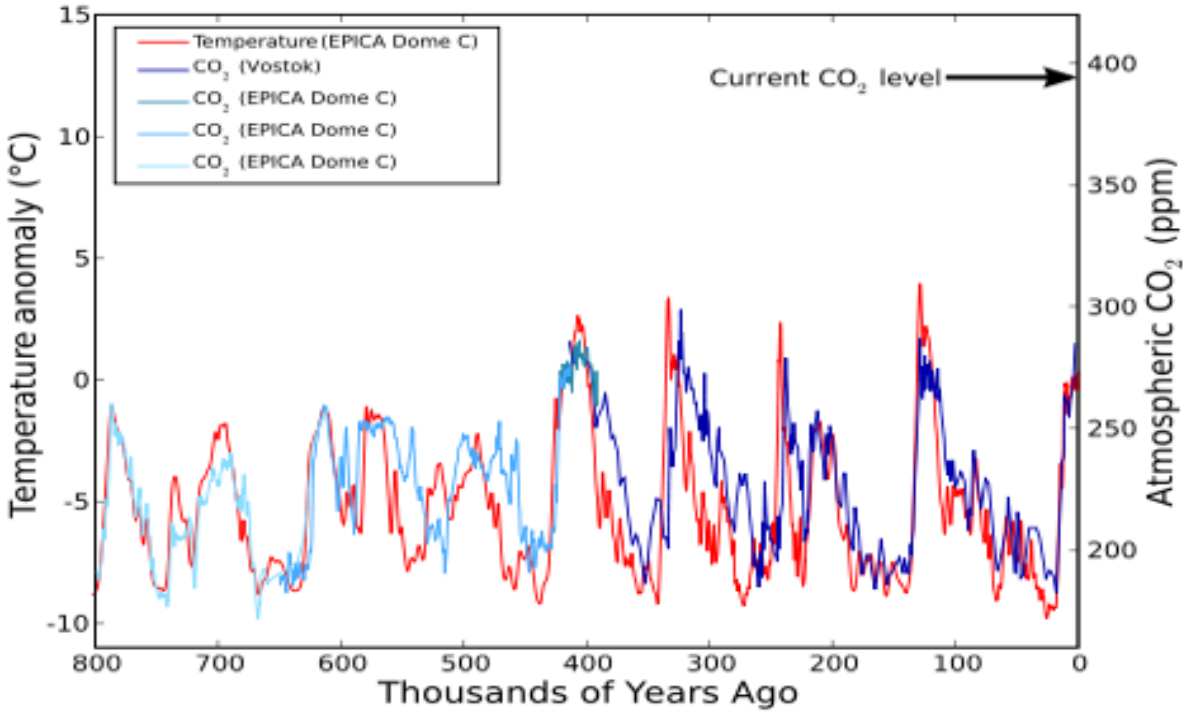

Figure 1.3: Temperature and CO_2 concentrations from ice cores (from [11])

1.2 Carbon dioxide sources and carbon capture and storage

As previously stated, anthropogenic CO_2 emission is the major issue regarding global warming. In order to meet the challenge of limiting the increase in the average global temperature to 2°C by 2100, the atmospheric concentration of CO_2 must be restricted to 450 ppm which will require a 50% cut-off of global CO_2 emissions compared to levels in 1990 [13]. In 2010, the energy sector released 35% of total GHGs emissions, 24% were released by AFOLU (agriculture, forestry and other land use) and 21% by industry (cement industry, iron and steel industry, etc.) (Figure 1.4 from [7]).

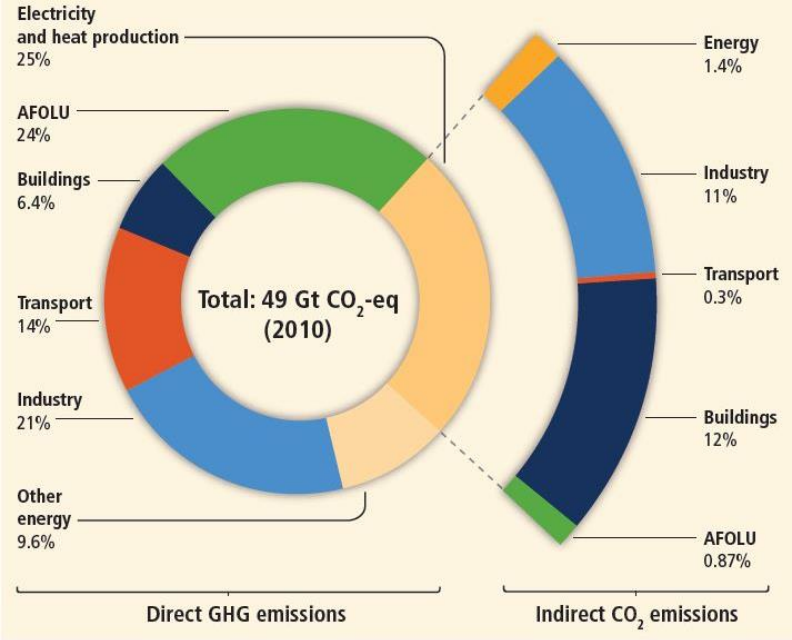

Figure 1.4: GHGs emissions by economic sectors in 2010 (from [7])

The large increase of the last decades in atmospheric CO_2 (see Figure 1.3) is attributable by 75% to burning fossil fuels in order to produce power for an amount of 23 Gton-CO_2/year [2]. Furthermore, the power plants represent large point sources of CO_2, therefore the major focus of searches on carbon capture and storage (CCS) is on actions to reduce the impact of power generation in the overall picture [14].

CCS is a "process consisting of the separation of CO_2 from industrial and energy-related sources, transport to a storage location and long-term isolation from the atmosphere" [15]. According to this definition, one can say that this is a three steps methodology (see Figure 1.5): CO_2 capture at the point of generation, compressing it to a supercritical fluid to transport it and finally storing it [16]. The capture is achieved by different methods such as absorption, adsorption, membrane separation or cryogenic separation [14; 16; 17; 18]. The transport of the compressed gas is done by pipeline or ship and the carbon dioxide is then stored by geological or ocean storage or via mineralisation [19].

One of the major goal of CCS is to modify as less as possible the processes and carbon-based infrastructures to minimise the cost linked to the mitigation of CO_2 emissions [16].The major contribution of the total cost of CCS is the capture of carbon dioxide which represents from 24 to 52 €/ton-CO_2. The transport costs that vary upon pipeline dimensions, pressure of CO_2 and landscape characteristics, are between 1 and 6 €/ton-CO_2 per 100 km of pipeline [16]. All these additional requirements lead to an increase in power production costs from 75% up to 100% for plants integrating CCS technologies. However, this may be reduced to 30% to 50% in the long term [20].

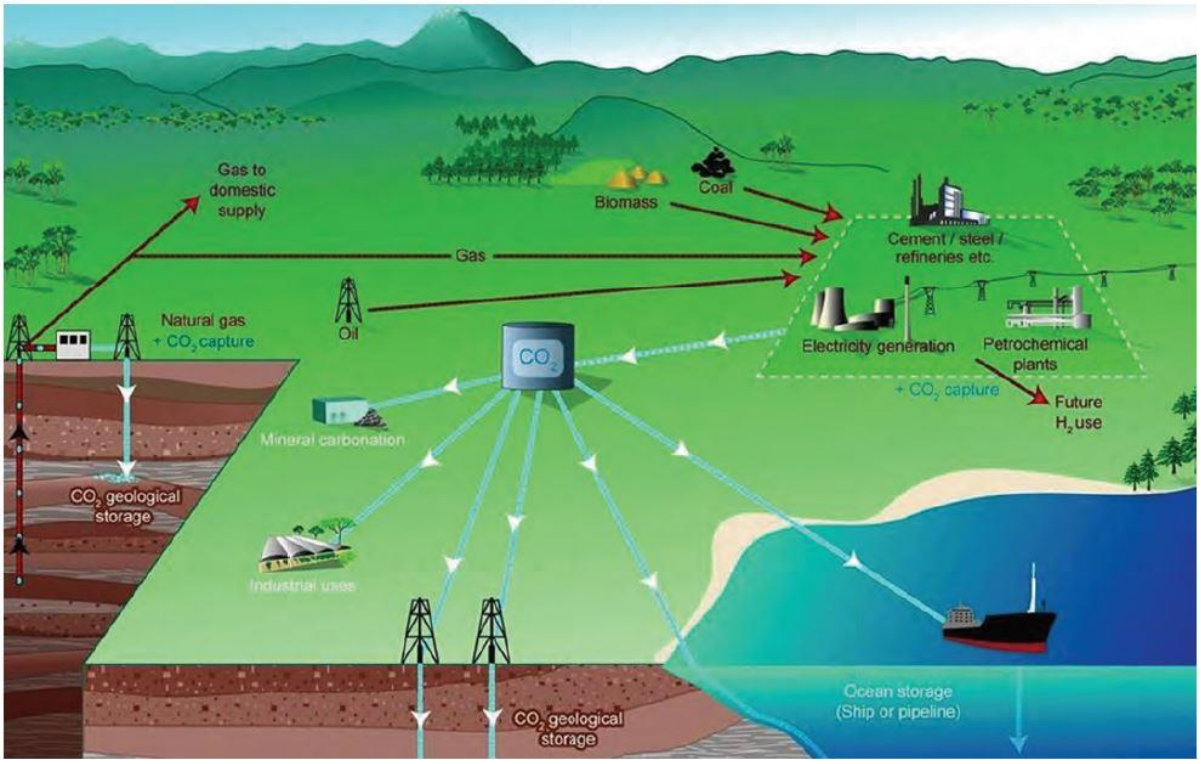

Figure 1.5: Carbon cycle in industry (from [14])

CCS is not the only possible way to mitigate carbon emissions. Professor Yoichi Kaya from the University of Tokyo has established a relationship to express the increase of atmospheric carbon dioxide [2]:

$$CO_2^{\uparrow} = POP * \frac{GDP}{POP} * \frac{BTU}{GDP} * \frac{CO_2^{\uparrow\uparrow}}{BTU} - CO_2^{\downarrow} \tag{1.1}$$

The CO_2 released to the atmosphere $\left(CO_2^{\uparrow}\right)$ is proportional to the population (POP), the standard of living measured by per capita gross domestic product (GDP/POP), the energy intensity given by the energy consumption per unit of GDP (BTU/GDP) and the carbon intensity represented by the amount of CO_2 released per unit of energy consumed $\left(CO_2^{\uparrow\uparrow}/BTU\right)$; $CO_2^{\downarrow}$ is the amount of CO_2 stored in ocean and lands sinks [2; 16].

In accordance with eq.(1.1), several actions may be taken to decrease the amount of CO_2 in atmosphere. That being said, the first two approaches are to reduce the population or the standard of living and are not policy-applicable. It then remains three approaches: reducing

energy intensity, reducing carbon intensity by use of carbon-free fuel (renewable and nuclear energy) and increase of CCS efficiency. Investment costs, lack of intergovernmental policies (already reduced with COP21), lack of technology maturity are all associated to dampen the establishment of CCS technologies. The three previously mentioned approaches to meet CO_2 mitigation must be investigated. However, the use of non-fossil fuels such as nuclear or renewable also presents defaults as they cannot meet our energy needs and can lead to dangerous waste and reducing energy intensity seems hardly considerable in the near future. Considering the present energy needs highly reliable on power production from fossil fuels, CCS is the best way to maintain CO_2 level under control [2].

1.3 Carbon capture technologies

Because power generation is the major actor in CO_2 emissions, the focus will be on the technologies dedicated to mitigate the emissions of this particular industrial sector. Figure 1.6 presents the three possible ways of CO_2 capture: post-combustion, pre-combustion and oxyfuel combustion. As previously stated, the capture of carbon dioxide represents the major cost of CCS and needs to become a more mature technology before the industrial sector heavily applies it. The choice of the capture technology depends on the concentration of the flue gas, the pressure of the gas stream and the fuel type [2].

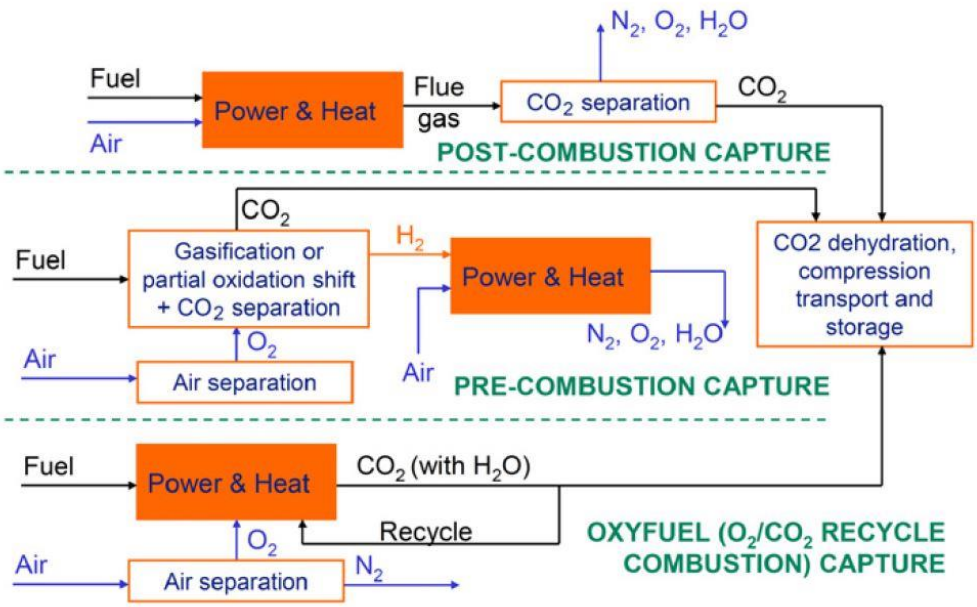

Figure 1.6: Carbon capture technologies (from [19])

1.3.1 Post-combustion CO_2 capture

Post-combustion capture (PCC) means that the carbon dioxide is separated from other exhaust gases produced by combustion of fossil fuel just before its release in the atmosphere. Exiting gas of power plant has a low CO_2 concentration (between 4 and 14%) and is at atmospheric pressure resulting in low thermodynamic driving force for CO_2 capture and large volume of gas to be handled. The low concentration of CO_2 implies that powerful chemical

solvents need to be used to separate carbon dioxide from flue gas meaning that their regeneration will require a large amount of energy. Despite these technical difficulties, post-combustion capture is the most advanced technique because it can be retrofitted to existing units. The techniques used for post-combustion separation are absorption, membrane separation and cryogenic separation that will be explained later on this report [2; 17].

1.3.2 Pre-combustion CO_2 capture

CO_2 is of course not available for capture before combustion. Nonetheless, by modifying the conventional power unit, one can achieve the separation of CO_2 from other gases before the production of power [21]. This can be achieved if fuel is reacted with oxygen, air or steam to give mainly carbon monoxide and hydrogen by a process called gasification, partial oxidation or reforming (eq.(1.2)) [2]. This mixture rich in H and CO is passed through multiple catalyst beds to achieve the "water-gas shift" reaction (eq.(1.3)) producing more CO_2. The latter will be separated while H_2 is used as a fuel in a gas turbine combined-cycle plant.

$$2C + O_2 + H_2O \Leftrightarrow H_2 + CO + CO_2 \quad (1.2)$$

$$CO + H_2O \Leftrightarrow CO_2 + H_2 \quad (1.3)$$

The separation is typically achieved using a physical solvent. Because CO_2 is more concentrated and has a higher partial pressure than in post-combustion, it is more easily separated from flue gas and the regeneration operation requires less energy. Furthermore, the installations are smaller than in the post-combustion case [2; 21]. Pre-combustion technique does induce an energy penalty with the gasification but the overall energy balance is much more favourable than in the post-combustion case [21].

The main advantage of pre-combustion capture relies on the use of carbonless fuel. Indeed, the reforming transforms the chemical energy of carbon to chemical energy of hydrogen [16]. The combustion of hydrogen offers advantages such as the absence of SO_2 emissions [2] but the efficiency of hydrogen-burning gas turbines is smaller than conventional units [21]. It seems that pre-combustion technology is applicable for integrated gasifier combined cycle (IGCC) that relies on coal gasification but is less attractive to treat liquid or solid fuels for which more energy losses would be involved in the gasification step [21].

1.3.3 Oxyfuel combustion

Oxyfuel combustion switches the major separation step to separation of O_2 and N_2 prior to combustion which can be achieved by cryogenic separation or membranes [17]. This operation offers a modified post-combustion technique where fuel is burnt with this oxygen-enriched gas (more than 95% volume) resulting in high concentration of CO_2 in flue gases (over 80%) mixed with H_2O. The final separation step is easily performed by water condensation. Fuel combustion with pure oxygen rather than air produces a much higher flame temperature which requires the recycling of flue gas to act as heat sink instead of N_2 in conventional post-combustion process. Another advantage of this technology is that it does not produce NO_x and the final volume of treated gas is greatly reduced thanks to the high CO_2 concentration in the exhaust gas. Even though this technique still demands flue gas desulphurization, there will be no solvents involved in the separation steps (O_2/N_2 and CO_2/H_2O separations) [2; 16; 17; 21].

The major issue of oxyfuel combustion is in the oxygen production costs of the air separation unit. Cryogenic distillation is a very expensive and energy intensive process. This is why the major investigations are in the reduction of the oxygen purification costs. The solution may be found in hybrid systems combining a permeable O_2/N_2 membrane and cryogenic distillation in which the membrane leads to a stream of oxygen enriched air further oxygen-concentrated by cryogenic distillation [16]. Yet, this technology appears to be uncompetitive at the time being.

The advantages and disadvantages of these capture technologies are presented in Table 1.2.

Capture technology	Advantages	Disadvantages
Post-combustion	Existing technology Retrofit to existing power-plant designs Extra removal of NO_x and SO_x	Energy penalty due to solvent regeneration Loss of solvent
Pre-combustion	Existing technology Very low emissions	Cooling of gas to capture CO_2 is necessary Efficiency loss in water-gas shift section
Oxyfuel combustion	Existing technology Absence of nitrogen → no NO_x emissions Absence of nitrogen → low volume of gases and reduction of the entire process size	High energy input for air separation Combustion in pure oxygen is complicated

Table 1.2: Advantages and disadvantages of CO_2 capture technologies (from [2])

1.4 CO_2 separation techniques in post-combustion separation

The detailed analysis of separation techniques will focus on PCC because this technology is the most advanced one and is the simplest to effectively implement as a retrofit option to working plants. There are several common techniques used in post-combustion separation: physical or chemical absorption, adsorption, cryogenic distillation and membrane separation. Whatever way used, the best solution would ultimately be to involve a closed carbon loop in which CO_2-based products with economical value would emerge. This involves a global overview not limited to the strict capture of CO_2 from a flue gas [3].

1.4.1 Absorption

Absorption is a process by which a species in a gas mixture in contact with a liquid phase is dissolved to the liquid bulk by selective mass transfer. Chemical absorption by use of monoethanolamine (MEA) is by far the most advanced and used technique for CCS. This

process implies that CO_2 reacts with the solvent that will further be regenerated with heat giving the original solvent and a stream of pure CO_2 [15]. MEA is currently the preferred solvent because it is cheap, it reacts rapidly with CO_2 in low partial pressure (i.e. at the outlet of combustion plant, the concentration of CO_2 is about 15% [15]). Nonetheless, this solvent shows some weaknesses: it is corrosion-sensitive, its regeneration cost is quite high [15], it shows a low carbon dioxide loading capacity (g CO_2 absorbed/g solvent) [2], it implies amine degradation by SO_2, NO_2 and O_2 inducing a high solvent makeup rate, large equipment size [22] and, above all, it is not environmentally friendly. Firstly, its production involves the use of ammonia (NH_3) that is synthesised by the Haber-Bosch in which CO_2 is a by-product. On a global overview, this could lead to a negative balance in the overall capture process. Furthermore, these amines show a strong toxicity that could lead to soil pollution in case of leakage [3; 23].

Many studies have been conducted for the use of novel solvents such has mixed amines (MEA mixed with diethanolamine (DEA) for example), sterically hindered amines (piperazine derivatives) [2], ionic liquids or even hot potassium carbonate (K_2CO_3) [3; 23]. These show that the regeneration duty can be lowered but still these derivatives present undesirable environmental effect. Yet, the emerging solutions of interest in the overall carbon balance are in other fields such as adsorption on a sorbent, calcium looping, carbon capture and conversion (CCC) and membranes.

1.4.2 Adsorption

Adsorption differs from absorption in that the gas is in contact with a solid called the sorbent. The species selectively diffuses through the surface of the solid and in its pores. For CO_2 adsorption, some sorbents are of interest such as activated carbon, soda-lime and some organic and inorganic solids. As for the solvent in absorption, sorbents must fulfil some requirements to be efficient: high adsorption capacity and selectivity for CO_2, fast adsorption/desorption kinetics, mechanical strength, low heat of adsorption to decrease the energy duty of the regeneration step and, of course, they should be cheap [23].

1.4.3 Calcium looping

Calcium looping is based on carbonation/calcination cycles in two fluidized bed reactors. CO_2 is removed from flue gas in an absorber according to the chemical reaction below (eq.(1.4)) that can be reverted when the system is heated in the regenerator producing a concentrated stream of CO_2 at higher temperature.

$$CaO_{(s)} + CO_{2(g)} \leftrightarrow CaCO_{3(s)} \quad \Delta H_{r,298K} = -178\ \text{kJ/mol} \tag{1.4}$$

The major drawback of this process is the rapid decay of CO_2 adsorption capacity of the sorbent with the number of cycles. It could be used to capture as much as 94% of CO_2 emissions in the cement industry which represents 20% of all industrial carbon emissions [16; 23].

1.4.4 Carbon capture and conversion

As previously stated, the optimal process of CO_2 capture should involve its re-introduction in a closed carbon loop on the form of a CO_2-based products. This is the aim of CCC. Carbon dioxide itself is not of great value (carbon is in its highest oxidation level) and – despite its use as feedstock in urea plants, in the fertilizer or methanol production, in the

beverage industry or as coolant gas in nuclear reactor – in its pure form, the only way to mitigate its emission, is for it to be stored by CCS [3]. CCC, on the other hand, aims to chemically transform the recovered CO_2 in useful and valuable products such as fuels or chemicals [23].

The main drawback of this approach is that CO_2 requires high heat duty for its reduction. Nevertheless, some processes are under study.

Sodium hydroxide (NaOH) for sodium carbonate (Na_2CO_3) production

The use of NaOH as an alternative solvent is of interest. Sodium hydroxide can be obtained as waste from different industrial processes (such as treatment of waste streams from Merox towers) and its reaction with CO_2 forms sodium carbonate which can be used as raw material in the cement and ceramic industry [4].

Ammonia (NH_3) for ammonium bicarbonate (NH_4HCO_3) production

Liquid ammonia can be used as an alternative solvent for the absorption of CO_2 to produce NH_4HCO_3. This chemical is a synthetic N-fertilizer and is then valuable. Furthermore, the process of CO_2 absorption using NH_3 is less energy consuming than the use of MEA and does not show the same corrosion issues. The drawbacks related to this technology are to be found in the big ammonia makeup needed involving a large solvent production by the Haber-Bosch process which releases CO_2 as previously stated [17; 3].

Photocatalytic conversion into fuels

Another technique is based on the use of solar thermal and/or photonic energy instead of fossil fuels in order to convert CO_2. Its major advantage is to use a renewable energy instead of using the conventional way releasing carbon dioxide hence being less favourable for the global carbon emissions balance. This process can be used to produce Na_2CO_3 and HCl [24].

1.5 Closer look on the reactive absorption of CO_2 using NaOH

In section 1.4.1, it was mentioned that MEA presented several drawbacks and, in section 1.4.4, that sodium hydroxide can be used as an alternative solvent in order to eliminate CO_2 from a flue gas. It appears that the absorption efficiency of NaOH is higher than that of MEA. Indeed, the capture of a ton of CO_2 would theoretically require 0.9 and 1.39 tons of NaOH and MEA respectively [25]. Another advantage of NaOH is its abundance relative to MEA [25] and it is and industrial waste in some chemical technologies (e.g. chlorine production) [26].

When the absorption process occurs for a sufficient time, all NaOH is depleted and the final product obtained is bicarbonate ($NaHCO_3$). However, the aim of this technology is to obtain sodium carbonate (Na_2CO_3) instead. This species will further be processed to be re-injected for industrial use in cement or ceramic industries [27].

To better address the reaction between NaOH and CO_2, one should consider the different steps involved in the absorption mechanism. Firstly, due to its high alkalinity, sodium hydroxide in aqueous solution provides nearly immediately completely ionized Na^+ and OH^-. Also, CO_2 is physically absorbed to form aqueous CO_2 (see eq.(1.5)) [25].

$$CO_{2(g)} \rightarrow CO_{2(aq)} \tag{1.5}$$

Then, the two major steps of the reaction mechanisms can occur [28]:

$$CO_{2(aq)} + OH^-_{(aq)} \leftrightarrow HCO^-_{3(aq)} \tag{1.6}$$

$$HCO^-_{3(aq)} + OH^-_{(aq)} \leftrightarrow H_2O_{(l)} + CO^{2-}_{3(aq)} \tag{1.7}$$

These two reactions are reversible and exothermic in the forward direction. They are both characterized by high reaction rates at high pH-values [28] but the rate controlling step is the absorption of CO_2 reaction (eq.(1.6)) because the second step (eq.(1.7)) is considered to be instantaneous. Aqueous carbon dioxide is then not present in solution. According to Figure 1.7, one can say that the equilibrium of the absorption is pH-dependent which involves that reaction (1.7) is dominant early in the process. Hence, when the concentration of hydroxide ions is high so is the pH and carbonic acid exists only in the form of carbonate ions [25; 28]. This leads to the following global reaction for the first step of the reactive absorption (eq.(1.8)):

$$2OH^-_{(aq)} + CO_{2(g)} \rightarrow CO^{2-}_{3(aq)} + H_2O_{(l)} \tag{1.8}$$

When almost all hydroxide has reacted leading to the formation of carbonate ions CO_3^{2-}, pH has lowered and bicarbonate (HCO_3^-) starts to form via the inverse reaction (1.7). The hydroxide ions provided are instantly consumed by reaction (1.6). The pH will again be lowered in this second step that can be described by this global reaction (eq.(1.9)):

$$CO^{2-}_{3(aq)} + CO_{2(g)} + H_2O_{(l)} \leftrightarrow 2HCO^-_{3(aq)} \tag{1.9}$$

After reaction (1.9) is at equilibrium, assuming the pH is low enough, CO_2 is present in solution via physical absorption which will be described as the third reaction step.

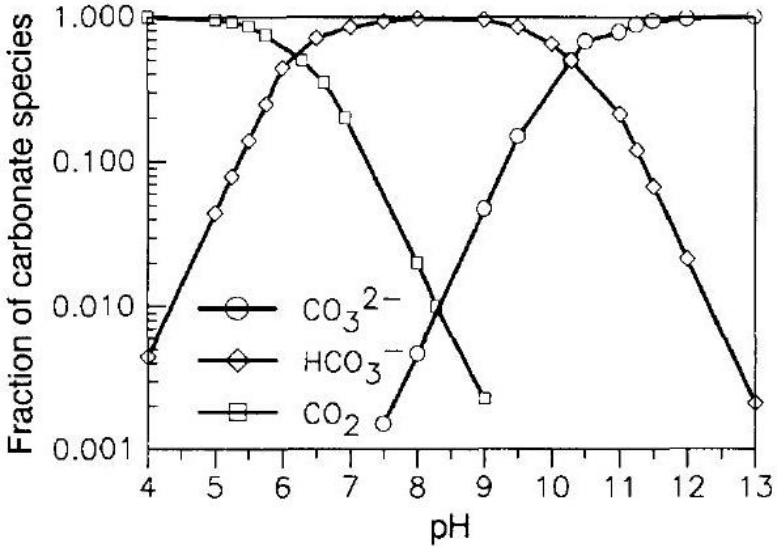

Figure 1.7: Fractions of different carbonate species at chemical equilibrium (from [28])

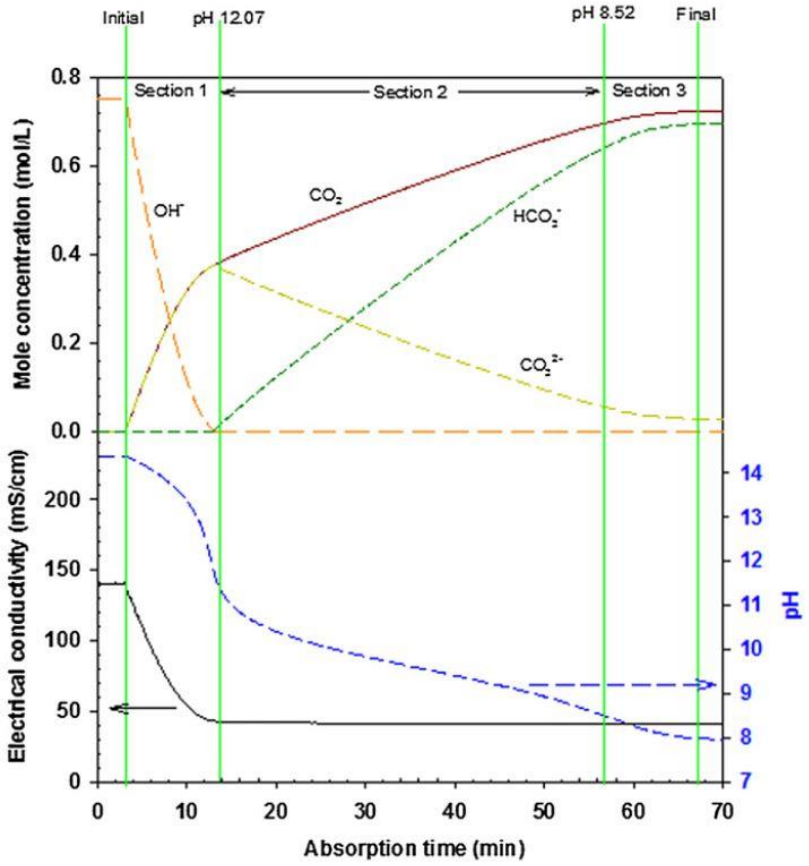

Figure 1.8: Concentration variation of absorbed CO_2 and of carbonate species and pH (from [25])

Yoo et al. [25] highlighted the correlation between the carbonate species in solution and the different steps of the overall CO_2 absorption, these results are shown in Figure 1.8. The three reactions steps can be associated with the three sections represented in the figure. As previously detailed in this section, the concentration of species is correlated with the pH of the solution. The latter drops heavily in the first section when hydroxide ions react with CO_2, in the second section, the decrease is less intense while carbonate reacts with carbon dioxide to produce bicarbonate. Finally, the absorption section is characterized by a nearly constant pH. These graphs were obtained by a lab-scale experiment conducted in a batch reactor containing 3wt.% NaOH in which a flue gas composed of approximately 31.5% CO_2 was absorbed for 70 minutes [25]. The previous example gives an overview of the trend of reaction; of course some variations may appear in function of particular experimental conditions.

This absorption technique has been studied for different configurations such as packed columns, spray towers, venturi towers, rotating packed beds and membrane contactors. The next sections will further analyse the behaviour of this reactive absorption in packed columns and membrane contactors.

1.6 Randomly packed columns for CO_2 absorption

This section aims to explain the working principles of the absorption of CO_2 using absorption column and gives an overview of the state of the art of this technology (see Table 1.3). Absorption columns are devices that have been used for decades in the chemical field. In this report, the focus is on randomly packed columns. Their working principle relies on the contact between the two phases flowing in the column through the random packing (i.e. the gas containing the species to be absorbed and the absorbent flowing counter-currently). The internals can be of many shapes (see Figure 1.9) and are commonly made of metal, ceramic or polymers [29].

Figure 1.9: Column internals (from [30])

Absorption columns are commonly used in the process of CO_2 absorption from flue gas according to the schema represented in Figure 1.10. This unit illustrates the absorption of CO_2 with MEA (or another amino-based solvent) and its further regeneration in the stripping unit. As previously stated, the major energy requirement is imputable to the regeneration of the solvent and is about 3.5 GJ per ton of CO_2 to recover an aqueous solvent of 30 wt% MEA [31]. Even though this technology is more voluminous than membranes, it is being used in industry

due to its reliability. Nevertheless, it is also well-known for the operational problems related to its use: high gas phase pressure drop, liquid channelling and flooding of the packing materials all resulting in poor gas-liquid contact [32].

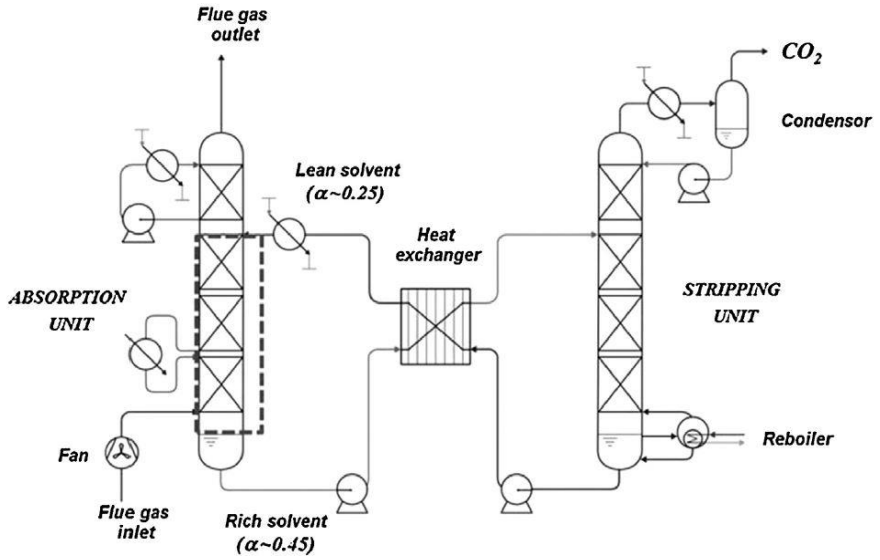

Figure 1.10: Schema of a typical post combustion CO_2 capture unit (from [31])

The absorption of the solute gas in the absorbent involves three steps that can be modelled via the resistance-in-series model. Figure 1.11 represents the mass transfer that occurs in an absorption column. The contact between the gas and the liquid takes place at the surface of the packing elements and is characterized by the molecular diffusion of CO_2 through the gas film followed by its absorption in the liquid phase and its diffusion through the liquid film. The major difference with membrane contactors in the diffusion mechanism is the absence of the membrane resistance in the overall process. The chemical reaction of CO_2 with NaOH being instantaneous (see section 1.5), it will take place only in the liquid film [32].

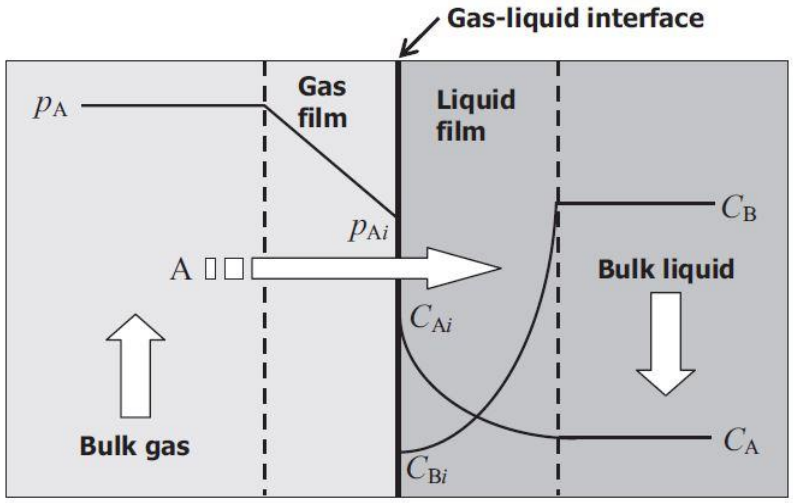

Figure 1.11: Reactive absorption model based on the two-film theory (from [32])

Experimentally speaking, the overall mass transfer coefficient will be calculated according to eq.(1.10) (from [33]):

$$K_{Og} = \frac{r_{CO_2}}{a \cdot AH \cdot \Delta P_{lm}} \ [\text{mol}/(\text{atm} \cdot \text{m}^2 \cdot \text{min})] \tag{1.10}$$

where r_{CO_2} is the rate of absorption of CO_2 [mol/min]; a is the specific area of packing per unit volume of tower [m^2/m^3]; A is the cross-sectional area of the tower [m^2]; H is the packing height [m] and $\Delta P_{lm} = \frac{y_i - y_o}{\ln(y_i/y_o)} \cdot \frac{p_{atm}}{100}$ is the logarithmic mean driving force [atm] (y_i and y_o are the column inlet and outlet CO_2 partial pressures [%] and p_{atm} is the atmospheric pressure [atm]).

1.6.1 Liquid holdup and flooding

One of the main operational limitation for the use of columns in absorption processes is flooding. This phenomenon occurs at high liquid and gas flow rates and drastically reduces the efficiency of the column. Figure 1.12 from [29] shows the evolution of pressure drop and liquid holdup in function of the gas velocity. Those data were collected from an experiment conducted at 1 bar and 20 °C with a 0.15 m diameter column randomly packed with 1 in. Bialecki rings to a height of 1.5 m.

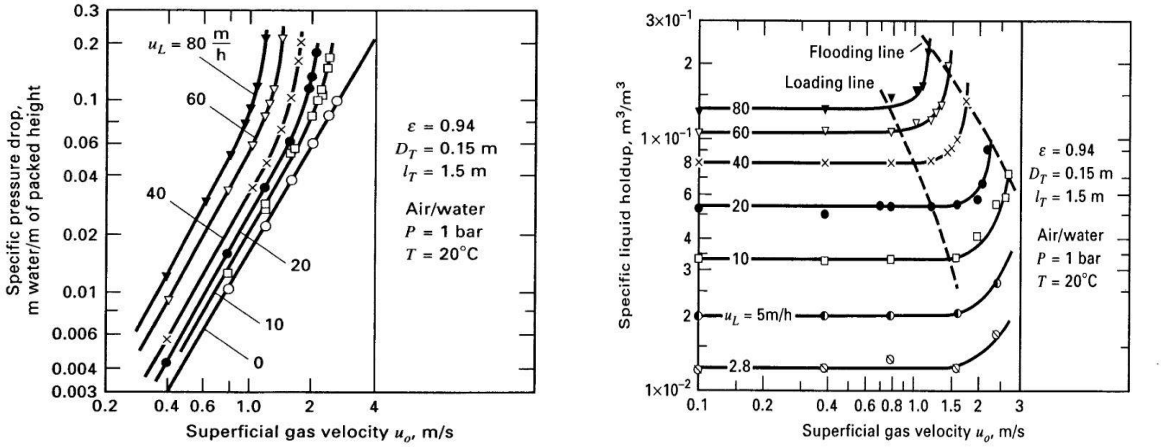

(a) Pressure drop (b) Liquid holdup

Figure 1.12: (a) Evolution of pressure drop in function of gas velocity for different water flow rates (b) Evolution of liquid holdup in function of gas velocity for different water flow rates (from [29])

In Figure 1.12.a, the lowest curve corresponds to the dry pressure drop (i.e. when no liquid is flowing down the column) and shows a linear profile. When the liquid flow rate increases, the pressure drop for a given gas velocity increases as well. This is due to the resistance added by the liquid flowing counter-currently to the gas at increasing flow rate. Nonetheless, below a specific gas velocity, the pressure drop profiles are parallel to the dry pressure drop. Figure 1.12.b shows that under that specific gas velocity, the liquid holdup is constant. Once the critical gas velocity is attained (i.e. the loading point), liquid holdup increases and reduces the void fraction available for gas to flow through leading to an increase in pressure drop. Between the loading and the flooding point, liquid accumulates at the top of the column until pressure drop increases infinitely due to a continuous liquid phase. At this point, the system is unstable and mass transfer efficiency decreases drastically. Operating

conditions are chosen so that the system operates below the loading point to ensure a proper wetting of the packing. A minimum liquid flow rate also exists to ensure that the liquid holdup is sufficient to properly wet the packing.

1.7 State of the art on reactive absorption of CO_2 with NaOH using packed columns

Reference	Title	Experimental conditions	Results
Kordylewski et al. [26]	Laboratory test on the efficiency of carbon dioxide capture from gases in NaOH solutions	Absorption in a Dreschel washer. Flue gas composed of 15% CO_2; 140 L/min. NaOH solution between 0 and 50 %wt. concentration, 25 or 61.5 °C.	1. Na_2CO_3 is generated until the exhaustion of NaOH. 2. After the exhaustion of NaOH, sodium bicarbonate is created. 3. The efficiency of CO_2 capture depends mainly on NaOH concentration in the solution (85% efficiency for 50%wt NaOH) 4. The efficiency of CO_2 capture with NaOH is ten times higher than with Na_2CO_3. 5. The increase of solution temperature increases the efficiency of CO_2 capture.
Onda et al. [34]	Gas absorption with chemical reaction in packed columns	Absorption column filled with 15mm Raschig rings and ½-in and 1-in Spheres. Absorbent solution: aqueous NaOH 0.05, 0.1, 0.25, 0.5 and 1 N; 30 ± 1°C; [8-80]*10^3 kg/m^2hr. Flue gas: mixture of CO_2 and gas (unknown composition and flow rate).	1. An increase in liquid flow rate increases the overall mass transfer coefficient ($K_G a \propto L^n$; $n = 1/3 \sim 1/2$). 2. The effective interfacial area increases when the liquid flow rate increases. 3. There is a maximum NaOH concentration after which $K_G a$ decreases when the concentration increases due to the increased viscosity of the solution.
Zeng et al. [35]	Mass transfer coefficients for CO_2 absorption into aqueous ammonia solution using a packed column	Absorption column filled with ceramic Raschig rings 8mm inner diameter. Absorbent solution: aqueous ammonia 2%~16%, 0.76-3.06 $m^3/(m^2h)$. Flue gas: up to 15 kPa partial pressure of CO_2, 61-214 $m^3/(m^2h)$.	1. The increase of CO_2 partial pressure leads to a slight decrease on the overall mass transfer coefficient. 2. The increase of the liquid flow rate increases the value of the overall mass transfer coefficient due to the increase in interfacial area per unit volume. 3. The increase in gas flow rate leads to a higher mass transfer coefficient, especially when the ammonia concentration is high. 4. The increase of the solvent concentration leads to an increase in the mass transfer coefficient. 5. The value of the overall mass transfer coefficient increases with the temperature when the temperature of the solution is lower than 40°C due to the dependence of the reaction steps of CO_2 absorption into NH_3 on temperature.

Table 1.3: Key references on reactive absorption using packed columns

1.8 Membrane technology for post combustion capture

Membranes were already cited as viable alternatives to conventional technologies for CCS. There are two types of membrane technologies that can be used in order to properly handle the mitigation of industrial CO_2 emissions: membranes acting as selective barriers and membrane contactors.

Membranes acting as selective barriers offer the possibility to selectively permeate one compound faster than the others in gas/liquid or liquid/liquid separation processes [23]. Permeability and selectivity will then be the main parameters to be optimised for this technology. Nevertheless, it is known that a trade-off needs to be achieved between those two parameters meaning that a membrane with a higher selectivity generally means a lower permeability hence a smaller flux [36]. The techniques achieved with this technology are gas permeation and supported liquid membranes, the driving force of the separation process is carried out by a pressure gradient as can be seen on Figure 1.13.

On the other hand, membrane contactors are devices acting like physical barriers showing no selectivity at all (involving a high permeability and a higher flux). In the process of reactive absorption, the selectivity is achieved by the absorbent liquid. The purpose of those membranes is to increase the surface for mass transfer between the gas and the absorbent using a much smaller operational volume (i.e. applying process intensification) [37]. The technique is referred to as non-dispersive contact and is achieved via a microporous membrane, the driving force of the separation process is a difference of chemical potential characterized by a concentration gradient (see Figure 1.13). Membrane contactors will be further detailed in section 1.9 and their advantages against conventional columns in section 1.12.

1.9 Membrane contactors

After having briefly explained how membranes could be used in PCC, let us focus on membrane contactors, their characteristics and their working principle. Membrane contactors are membrane devices that show no selectivity and act only as physical barriers to efficiently "keep in contact" two phases [38]. Those membranes are generally composed of symmetric micro-pores in which the desired interphase contact takes place. In order to avoid the interpenetration of phases, contactors are made of hydrophobic or hydrophilic materials depending on the polarity of the phase that should not pass through the pores. Thanks to the membrane, no dispersion nor mixing of one phase in the other occur and the species are transferred only by diffusion. The conventional membrane contactors in CCS are hollow fibres membranes contactors (HFMC). Nonetheless, membrane contactors can be of any shape, the fluids on both side of the membranes can be in co/counter-current, in radial or longitudinal flows, etc.

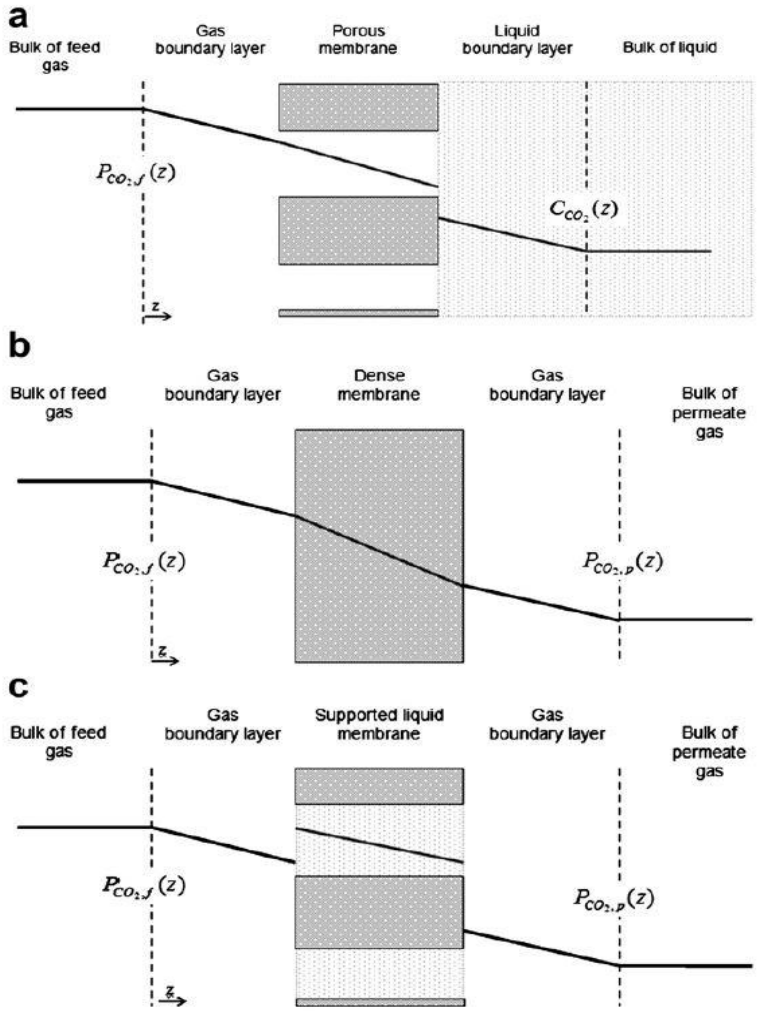

Figure 1.13: Schema of mass transfer in the systems: a) non-dispersive contact; b) gas permeation; c) membrane contactor (from [37])

The best way to maximise exchange area between both phases is to use tubular modules. One phase circulates in the outlet of the fibres (shell side) while the other circulates in the fibres (lumen side). In order to avoid maldistribution of the liquid phase flowing in shell side (distribution tube), manufacturers introduced baffles to deviate the fluid and create a transverse flow as well as a local turbulence (see Figure 1.14).

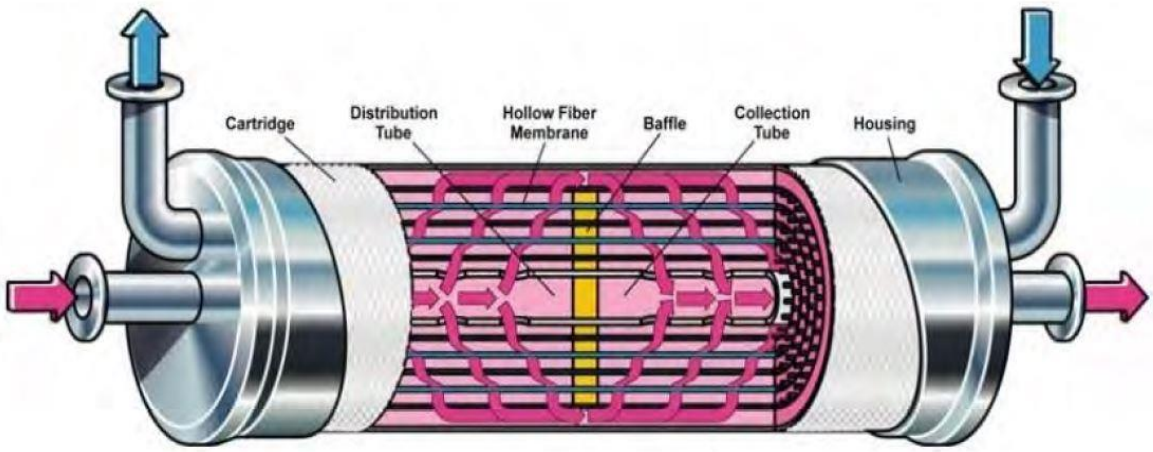

Figure 1.14: Hollow fibre membrane contactor with central baffle manufactured by Liqui-Cel® (from [48])

Membrane contactors have many applications but this report focuses on their use in reactive absorption of a gas species into a liquid solvent. The liquid solvent will flow in shell side counter currently to the gas mixture flowing in lumen side. A hydrophobic membrane is used to prevent the liquid penetrating in the pores because the volatile species has higher effective diffusivity in gas than in liquid [38]. In the following section, this configuration will be presented.

1.10 Reactive absorption in membrane contactors

1.10.1 Membrane contactors as scrubbers

In membrane scrubbers, a species contained in the gas phase will be absorbed in the liquid phase. In order to achieve this operation, the species will first need to diffuse from the bulk gas phase to the outer surface of the membrane then through the membrane pores to finally diffuse in the liquid and be dissolved in the absorbent [36]. Due to the large size of pores, a mechanism of viscous flow or Knudsen flow is considered for the diffusion in the membrane media.

These three steps involve resistances to the mass transfer. Figure 1.15 (from [31]) illustrates the resistance-in-series model that represents the concentration gradient of the species which is the driving force of the diffusion. According to the two-film theory, the resistance of gas and liquid phases are to be found in boundary layers close to the membranes [39]. When considering a membrane composed of hollow fibres with the fluid flowing in the shell side and the gas in the lumen side, the overall mass transfer coefficient is expressed based on the liquid phase (K_{Ol}) or on the gas phase (K_{Og}). According to the resistance-in-series

model, one can express the overall mass transfer coefficients as follow (adapted from [38; 39; 40]):

$$\frac{1}{K_{Ol}} = \frac{1}{E \cdot k_l} + \frac{1}{H \cdot k_m} \cdot \frac{d_o}{d_{lm}} + \frac{1}{H \cdot k_g} \cdot \frac{d_o}{d_i} \tag{1.11}$$

$$\frac{1}{K_{Og}} = \frac{H}{E \cdot k_l} + \frac{1}{k_m} \cdot \frac{d_o}{d_{lm}} + \frac{1}{k_g} \cdot \frac{d_o}{d_i} \tag{1.12}$$

where k_l, k_m and k_g are the individual mass transfer coefficients of the liquid phase, the membrane and the gas phase respectively; d_o, d_{lm} and d_i are the outer, log-mean and inside diameters of the hollow fibres; $E = \frac{J_{chem}}{J_{phy}}$ is the enhancement factor induced by the reactive absorption (J_{chem} and J_{phy} are the rate of chemical and physical absorption of CO_2 respectively) and H is the Henry's law constant relating the partial pressure of the gas species being absorbed in the gas phase and its concentration in the liquid phase at equilibrium (i.e. $p_i = H_i \cdot c_i$).

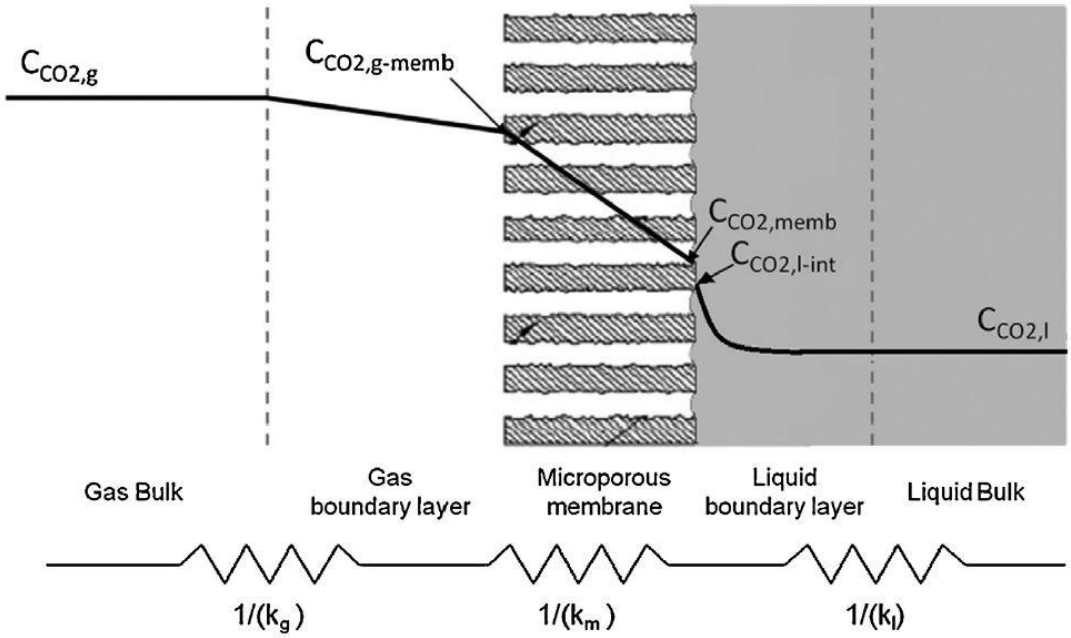

Figure 1.15: Resistance-in-series model (from [31])

Eqs.(1.11) and (1.12) are based on several assumptions (from [40]). First of all, assumption is made that the system is at steady state and that equilibrium exists at the fluid/fluid interface which curvature does not affect the rate of mass transfer, the equilibrium solute distribution or the interfacial area. The pore size and wetting characteristics must be uniform throughout the membrane. It is required that the two fluids are virtually insoluble in each other so that no bulk flow correction is necessary and mass transfer is described adequately by simple mass transfer coefficients. Finally, the equilibrium solute distribution is constant over the concentration range of interest.

Experimentally speaking, the overall mass transfer coefficient will be evaluated according to eq.(1.13) (adapted from [36]):

$$K_{Og} = \frac{r_{CO_2}}{a_{eff} \cdot \Delta P_{lm}} \text{ [mol/(atm} \cdot \text{m}^2 \cdot \text{min)]} \quad (1.13)$$

where r_{CO_2} is the rate of absorption of CO_2 [mol/min]; a_{eff} is the effective gas-liquid contact area [m^2] and $\Delta P_{lm} = \frac{y_i - y_o}{\ln(y_i/y_o)} \cdot p_{mean}$ is the logarithmic mean driving force [atm] (y_i and y_o are the contactor inlet and outlet CO_2 partial pressures [%] and p_{mean} is the average pressure in the lumen side [atm]).

According to eq.(1.11) and eq.(1.12), one needs to determine the individual mass transfer coefficients as well as the enhancement factor to be able to compute the overall mass transfer coefficients. This is beyond the scope of this report but further information can be found on Appendices A and B.

After the presentation of the theory of chemical absorption using membranes, the working parameters of interest will be presented.

1.10.2 Breakthrough pressure

When using a hydrophobic membrane, the liquid phase needs to be maintained at a higher pressure than the wetting fluid (i.e. the fluid present in the pores), the gas in our situation, in order to avoid the latter to permeate in the liquid phase [38]. Even though the liquid pressure needs to be slightly higher than the gas pressure, it cannot exceed a critical pressure called the breakthrough pressure, Δp, which is determined by [38]:

$$\Delta p = -\frac{2\Theta\gamma \cos\theta}{r} \quad (1.14)$$

where Θ is a geometric factor related to the pore structure; γ is the interfacial tension given by the Young's equation; θ is the liquid-solid contact angle (which is increased with increasing polarity difference between the membrane and the wetting liquid) and r is the pore radius. The usual values of the breakthrough pressure are between 100 and 400 kPa [38].

The breakthrough pressure is of outmost importance since it allows to avoid wetting of the pores by the liquid. In the case of chemical absorption where the major resistance lies in the liquid phase, wetting of the pores has a strongly bad influence on the performance.

1.10.3 Membrane fouling and plugging

The ability of using membrane technology on industrial scale is restricted to the fouling and plugging issues that can be encountered in the membranes. Due to the small diameters of the fibres, pre-treatment of flue gas may be needed to ensure that it does not contain suspended particles. Nonetheless, gas absorption contactors are less sensitive to fouling since there is no convective flow through the pores [36].

1.11 State of the art on reactive absorption of CO_2 with NaOH using membrane contactors

This section aims to provide an overview of the state of the art of membrane contactor used for the absorption of CO_2 with NaOH solutions.

Reference	Title	Experimental conditions	Results
Kim et al. [41]	Absorption of carbon dioxide through hollow fiber membranes using various aqueous absorbents	Absorbent solution (lumen side): water – AMP – MDEA – MEA (12%wt.). Gas phase (shell side): CO_2-N_2 mixture (40:60 volume ratio), 170 cc/min. System at 20-40 or 60°C.	1. The increase of the absorbent flow rate induces the increase of the mass transfer coefficient of CO_2. 2. The efficiencies of the absorbents are: MEA > AMP > MDEA > water. 3. The increase in temperature induces an increase in absorbed CO_2 concentration for amine solutions but a decrease for water because absorption occurred physically. 4. The absorption efficiency increases with the concentration of amine in the absorbent solution until the saturation point reached at the equilibrium.
Wang et al. [42]	Influence of membrane wetting on CO_2 capture in microporous hollow fiber membrane contactors	Absorbent solution (lumen side): 2M DEA or water. Gas phase (shell side): pure CO_2 or CO_2-N_2 mixture (volume ratio 20/80). Room temperature (25°C).	1. The CO_2 absorption rate in the non-wetted mode is six times higher than in the wetted mode due to the appearance of the mass transfer resistance imposed by the liquid in the membrane pores. 2. The reduction of overall mass transfer coefficient may reach 20% even if the wetting is as low as 5%. 3. The increase of gas flow rates leads to a large increase in CO_2 absorption rate when the DEA solution is the absorbent.
Chabanon et al. [43]	Study of an innovative gas-liquid contactor for CO_2 absorption	Two composite membranes are studied (Oxypluus® and a PP porous fiber). Absorbent solution (shell side): MEA (20 and 30 %wt.) or MDEA (25 and 50 %wt.) or MDEA (18 and 25 %wt.) + TETA (6 %wt.) Gas mixture (lumen side): mixture of CO_2 and N_2, unknown composition.	1. The higher CO_2 removal efficiency is obtained for high liquid velocity, high alkanolamine mass fraction in the liquid phase and a low CO_2 fraction in the gas phase. 2. Dense layer of the membrane governed the CO_2 mass transfer, the polymer used as the dense layer and the coating ensuring the physical-chemical properties are maintained must be chose carefully.

Table 1.4: Key references on reactive absorption using membrane contactors

Table 1.4 continued

Reference	Title	Experimental conditions	Results
Rangwala [39]	Absorption of carbon dioxide into aqueous solutions using hollow fiber membrane contactors	One HFMC of 0.0254m diameter and 0.2m and one of 0.051m diameter and 0.61M length. Absorbent solution (lumen side): water or NaOH (2N) or DEA (0.5M). Gas phase (shell side): air + CO_2 (1-10 %mol CO_2).	1. The nominal surface area of lumen side is bigger than the effective interfacial area which is then related to the actual gas-liquid contact area and not the geometric area. 2. The overall mass transfer coefficients experimentally obtained were lower than the theoretical values assuming non-wetted pores. This indicates that the HFMC suffer from wetting. 3. Using correlations, it was found that the mass transfer coefficient of HMFC is 3 to 9 times higher than in packed columns.
Mansourizadeh et al. [44]	Effect of operating conditions on the physical and chemical CO_2 absorption through the PVDF hollow fiber membrane contactor	Absorbent solution (lumen side): water or NaOH (0.2 or 1M). Gas phase (shell side): pure CO_2.	1. The increase in liquid flow leads to an increase in CO_2 flux. When increasing the liquid flow rate, the membrane mass transfer resistance increases as well (from 25% of the total resistance at a velocity of 0.18 m/s to 75% of the total resistance at a flow rate of 1 m/s). This is due to the increase in liquid mass transfer coefficient when increasing the liquid flow rate. 2. The increase of temperature is favourable for the chemical absorption (due to the increase in reaction rate) while it has a negative effect on the physical absorption with water (due to the decrease in CO_2 solubility). 3. The CO_2 pressure has a strong effect on the physical absorption (it increases its efficiency due to the increase in driving force) while it has a small impact on chemical absorption (due to the faster saturation of liquid in lumen side).

1.12 Comparison between membrane contactors and packed columns

Membrane contactors show advantages in regard to conventional devices such as packed tower, spray tower, venturi scrubber and bubble column [36; 40]:

- The main advantage is undoubtedly the intensification factor offered by the increased interfacial area of the membranes. The specific exchange area of membrane contactors can be as much as 10 times higher than the area of a classical column packing [31]. Kreulen et al. reported specific exchange areas as high as 8000 m^2/m^3 for membrane contactors and about 800 m^2/m^3 in conventional columns [45].
- Membranes are much more compact than columns leading to a reduction over 70% in size and 66% in weight [36] involving an easier retrofit to existing plants. Furthermore, membranes are less energy-consuming, combined with their less voluminous aspect, they are more economic.
- Another advantage of the exchange area of contactors is that it is known and constant, even at high flow rates. Indeed, the two fluids are independent contrarily to columns that are subjected to flooding at high flow rates and unloading at low ones. With the two fluids not being in contact, no foaming nor channelling can occur. This allows an easier performance prediction than with dispersive contactors and operational flexibility.
- Membranes allow a linear scale-up hence a predictable increase in capacity simply by adding modules in regards with the limitations of support equipment.
- Finally, membranes show a low solvent holdup which is interesting when dealing with expensive solvents.

Nonetheless, even though membranes show some advantages against columns, some challenges remain [36; 40; 46]:

- First of all, the membrane itself introduces a large mass-transfer resistance. Nonetheless, due to its bigger interfacial area, this disadvantage to columns can be minimised.
- Membrane fouling can occur, especially in pressure-driven devices. Membrane contactors are then less likely to suffer from this issue.
- Gas and liquid flows are laminar due to the membrane configuration involving a less efficient mass-transfer coefficient than in columns where turbulent flows occur. Thanks to the use of baffles and other equipment modifications, turbulent flows could be achieved ensuring a better mass transfer coefficient.
- The long-term stability of membranes is questionable. Indeed, membrane contactors made of polymers should be tested for their thermal resistance as well as their chemical stability with the solvents used.
- Membranes are subjected to pore wetting after some operating time. When liquid enters the pore, the resistance to mass-transfer increases considerably. Wang et al. showed that if the pores are 5% wetted, the overall mass-transfer coefficient could be reduced as much as 20% [42].

In conclusion, membranes should be the devices of tomorrow but still need to overcome some challenges. The biggest being to achieve good performance while being cheap. Indeed, fouling and wetting of the membranes tend to decrease their efficiency in CO_2 recovery and the ability to replace them when they lose performance instead of trying to keep them operational is of interest [37].

2 Objectives of the master thesis

So far in this report were addressed the issues arising from the increase in concentration of atmospheric CO_2 as well as the techniques currently used for its mitigation, especially focussing on the reactive absorption using NaOH with HFMC and absorption columns. This review was carried out to give the overview needed to properly handle the definition of the objectives of this thesis and how they will be achieved.

2.1 Framework of the master thesis

This thesis takes part in the doctoral thesis of Israel Ruiz Salmón: "CO_2 capture with NaCl: An approach based on membrane technology" and promoted by Pr. Patricia Luis Alconero. Figure 2.1 presents the flowsheet of the entire process studied in the PhD, this section will briefly present each step.

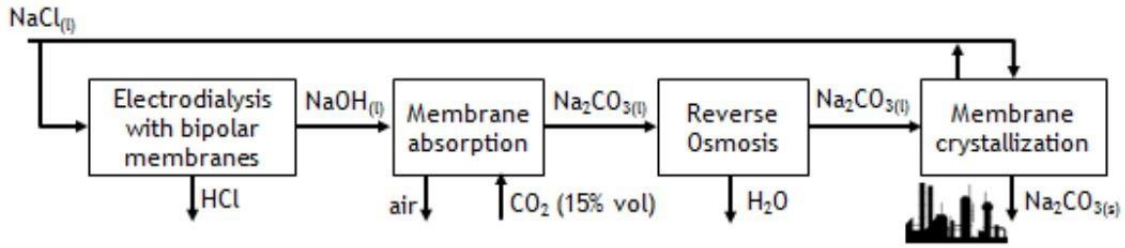

Figure 2.1: Overview of the whole CO_2 capture process studied in Israel Ruiz Salmón's PhD (from [42])

The first step aims to produce NaOH by a membrane technology – electrodialysis with bipolar membranes – using liquid NaCl as inlet.

Membrane absorption is then used to perform the chemical absorption of an inlet gas containing 15% vol CO_2 (which is the conventional outlet content of flue gas in combustion plants [15]) in aqueous NaOH. This step is the focus of the present thesis and was already documented in sections 1.5 and 1.10. It involves the global reaction of NaOH and CO_2 leading to the formation of aqueous Na_2CO_3 (soda ash):

$$2\ NaOH_{(aq)} + CO_{2(g)} \rightarrow Na_2CO_{3(aq)} + H_2O \qquad (2.1)$$

The previously produced aqueous soda ash is concentrated in a reverse osmosis process in which it will be brought close to saturation [47].

In the final membrane crystallisation step, soda ash will be obtained as solid products to be reused as raw material in the cement or ceramic industry. This step is achieved by use of aqueous NaCl as osmotic solution [4].

2.2 Objective of the master thesis

The general objective of this thesis is to compare the efficiency of two distinct technologies – column absorption and hollow fibre membrane contactor – for the reactive absorption of CO_2 gas with the help of aqueous NaOH. This comparison is done on the technical and economic approaches to determine which technology will be the most suitable for different working conditions.

The specific objectives for the two technologies are:

Absorption column

- to determine the absorption rate and the mass transfer coefficient at different absorbent sodium hydroxide concentrations (0.2, 0.5, 1M) and flow rates (1, 3, 5, 7 L/min) and flue gas flow rates carbon dioxide concentrations (10, 15% vol)

Membrane contactor

- to adapt the initial setup in order to use the membrane contactor instead of the absorption column
- to determine the absorption rate and the mass transfer coefficient at different absorbent sodium hydroxide concentrations (0.2, 0.5, 1M) and flow rates (1, 1.5, 3 L/min) and flue gas carbon dioxide concentrations (10, 15% vol)

3 Materials and methods

This section will present the chemicals used both for the experiments lead with the membrane contactor and the absorption column and will specifically review the working principle of both setups as well as the experimental procedures applied with them. The characterization method will finally be introduced.

3.1 Chemicals

The absorption solution is made by diluting NaOH pellets (sodium hydroxide, NaOH solid – AnalaR Normapur) in Deionized water (electrical resistivity of 18.2 MΩ/cm). The flue gas was composed of CO_2 (industrial carbon dioxide at 20 bars, Praxair) mixed with air (piston compressor entrained by an electric motor and delivering a maximum pressure of 8 bars).

In order to analyse the liquid samples, the double indicators method will be used (see section 3.5.2 for detailed procedure). This method involves the use of HCl (hydrochloric acid, HCl 37% - AnalaR Normapur) and two indicators: phenolphthalein (PP) and methyl orange (MO).

3.1.1 Preparation of the solution

The solution of NaOH used to chemically absorb CO_2 is the outcome of the precipitation of NaOH solid in deionised water. In order to fill the sump tank of the installation, a solution of five times the required concentration was prepared and further distilled with water in the sump tank to reach the desired concentration. The detailed procedure to produce 25L of aqueous NaOH is explained in Table 3.1. Each experiment was conducted with 25L of solution so that the sampling did not influence the total volume hence the absorption.

Step n°	Action
1.	Weight the required amount of solid NaOH (M_{NaOH} = 40 g/mol) in a beaker
2.	Pour the solid NaOH in a stirred beaker containing deionised water
3.	Wash the first beaker and pour the washing water in the second
4.	Pour deionised water (e.g. 200mL) in a 2000mL flask
5.	Pour the aqueous NaOH in the flask
6.	Let the flask rest for 12 hours in a hood so that it cools down
7.	Adjust the volume of the flask
8.	Fill a 10L plastic tank (T1) with 2L of deionised water
9.	Pour the 2000mL of aqueous NaOH in T1
10.	Wash the flask with 1000mL deionised water and pour it in T1
11.	Pour 10L of deionised water in the sump tank (T2)
12.	Pour the 5L of aqueous NaOH in T2
13.	Wash T1 with 10L of deionised water and pour it in T2

Table 3.1: Procedure for the preparation of the NaOH solution

3.2 Equipment

3.2.1 Absorption column

Experiments were conducted with a packed absorption column (UOP7-MKII Gas Absorption Column, Armfield Ltd, England) represented in Figure 3.1. Its characteristics are summarised in Table 3.2. The pipes wherein the gas and liquid flow are made of rigid PVC. The column is made of two parts separated by a liquid redistributor.

Parameters	Data from manufacturer
Column configuration	Packed column
Column walls material	Acrylic
Column diameter [mm]	80
Column length [m]	1.4
Column packing	Raschig rings
Raschig rings material	Glass
Raschig rings dimensions [mm x mm]	10 x 10
Raschig rings specific area [m^2/m^3]	440
Packing volume [L]	7

Table 3.2: Characteristics of the absorption column

A centrifugal air blower provides the air flow (up to 200 L/min) that will be mixed with CO_2 flowing from an external cylinder. The liquid is pumped from its storage tank by a submersible centrifugal pump (up to 10 L/min).

The installation is equipped with an electrical console that displays the information from the many sensors of the surrounding of the column. On this screen can be found information about pressure, gas and liquid flows, temperature and CO_2 concentrations at the inlet and outlet of the column. The tubing used for the conveying of gases from the sampling points to the console are 6 mm diameter rigid nylon tubing. A detailed list of the sensors is presented in Table 3.3, refer to Figure 3.1 and Figure 3.2 to get an overview of the installation and of the sensors locations.

Sensor name	Type of sensor	Range of readings
F1: Liquid flow rate	Turbine flow	0 – 10 [L/min]
F2: Air flow rate	Microbridge mass flow	0 – 200 [L/min]
F3: CO_2 flow rate	Microbridge mass air flow featuring a Venturi type flow housing	0 – 20 [L/min]
ΔP1: Pressure drop in upper section of column	Tappings 743 mm apart connected to 50 mbar differential pressure sensor inside electrical console	0 – 50 [mbar]

ΔP2: Pressure drop in lower section of column	Tappings 700 mm apart connected to 50 mbar differential pressure sensor inside electrical console	0 – 50 [mbar]
CO_2 concentration	Compact flow aspirated CO_2 measurement module (operating flow rate < 1 L/min, selector switch to measure CO_{2In} or CO_{2Out})	0 – 20 [%]
T1: Temperature of liquid tank	Thermistor	Not mentioned
T2: Temperature of inlet gas	Thermistor	Not mentioned

Table 3.3: Characteristics of the sensors of the absorption column

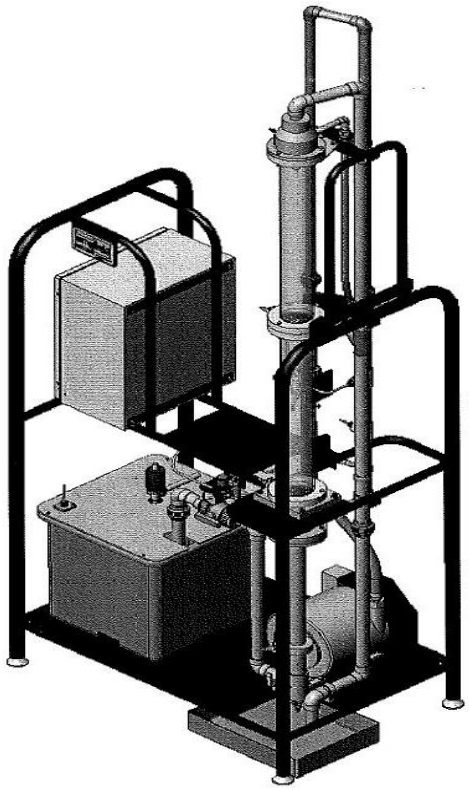

Figure 3.1: UOP7 MKII Gas Absorption Column (from [33])

3.2.2 Membrane contactor

Membrane technology was analysed by using a hollow fibre membrane contactor (2.5 x 8 Extra-Flow Module™ Liqui-Cel®, Membrana GmbH, Germany). The characteristics of the membrane are detailed in Table 3.4.

This HFMC is provided with an internal central baffle in order to get transverse flow and create turbulence (see section 1.9).

Parameters	Data from manufacturer
Module configuration	Hollow fibres
Membrane/potting material	Polypropylene/Polyethylene
Fibre i.d./o.d. [µm]	240/300
Wall thickness [µm]	40
Effective pore size [µm]	0.04
Porosity [%]	40
Effective fibre length [m]	0.16
Effective membrane surface area [m^2]	1.4
Number of fibres	10 200
Burst strength [bar]	27
Contact angle [°]	112

Table 3.4: Characteristics of the hollow fibre membrane contactor (from [48])

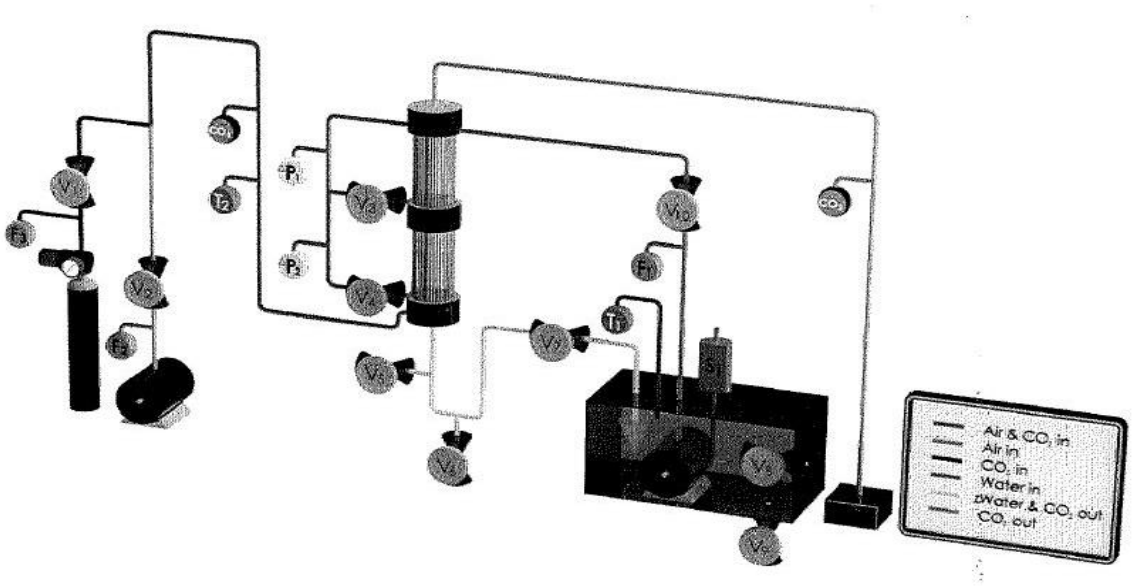

Figure 3.2: Column process flow diagram (from [33])

3.3 Experimental setups

In order to get a clear overview of the setups used to conduct the experiment, some pictures are available in Appendix C.

3.3.1 Absorption column

The UOP7-MKII Gas Absorption Column provides a fully integrated setup allowing to perform absorption experiment (see Figure 3.1 and Figure 3.2). The flowsheet of the experimental setup is provided in Figure 3.3.

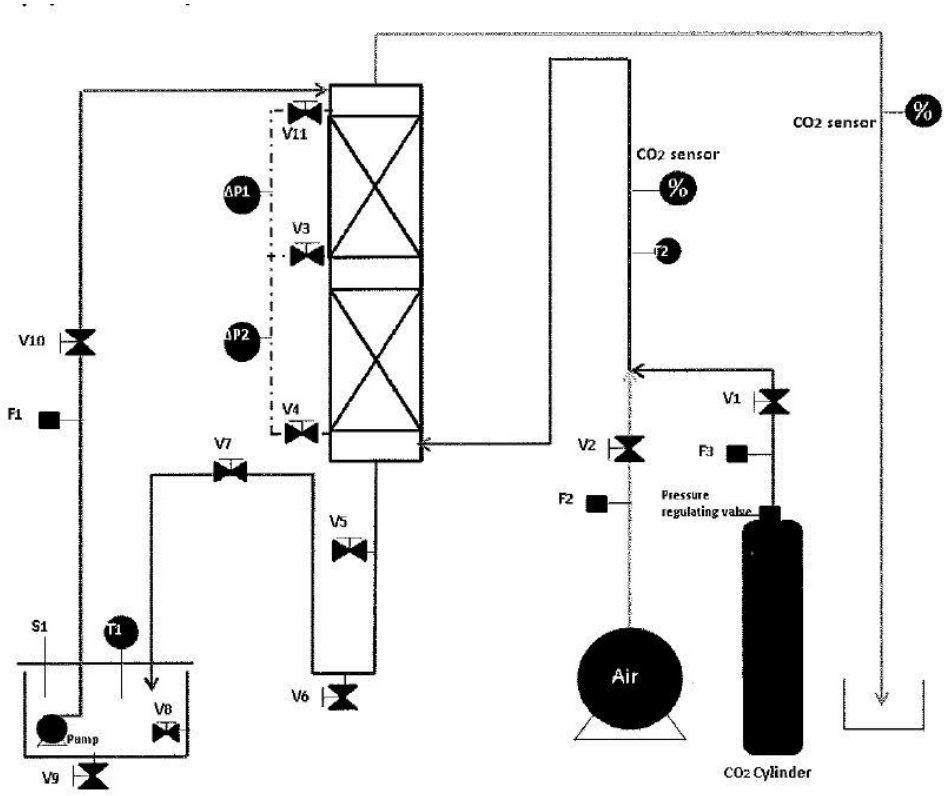

Figure 3.3: Absorption column flowsheet (from [33])

From the sump tank, the aqueous NaOH is pumped up to the top of the column where it falls by gravity through the packing and counter-currently comes into contact with the rising gas mixture (air + CO_2) that enters at the bottom of the column. At this point, CO_2 diffuses through the gas film and is chemically absorbed by NaOH in the liquid film surrounding the packing material. The liquid flows in closed loop and returns to the sump tank via a "U-bend" that forms a liquid seal and prevents the gas from escaping. Samples are taken both from the sump tank and the bottom of the column through pipes closed by valves (V6 and V9 on Figure 3.3) for further CO_2 concentration analyses by the double indicators method. The water flow meter F1 (see Figure 3.3) displaying the flow rate of liquid entering the top of the column is placed just before the valve allowing the control of the liquid flow (V10). Liquid temperature is given by a thermistor placed on the sump tank (T1).

The gas mixture is composed of air from the centrifugal air blower and CO_2 from the cylinder of compressed CO_2 gas and goes up the packed column from its bottom. Air is provided by the centrifugal air blower and its flow rate can be adjusted via a control diaphragm valve (V2), its value is displayed on the electric console via a flow meter (F2). Carbon dioxide is taken from a cylinder of compressed CO_2 gas, its flow rate is controlled by a pressure regulator (V1) and its value is displayed on the electrical console (via F3). Two small tapping points in the inlet and outlet lines containing the gas mixture connect to a solenoid inside the electrical console which computes the concentration of CO_2 in the gas and displays it on the screen. A switch allows to display one concentration at a time ($CO_{2,I}$ or $CO_{2,II}$; I is the inlet and II the outlet). Gas temperature is given by a thermistor placed in the inlet line (T2). Finally, three tappings with isolating valves are present at the top (V11), centre (V3) and bottom (V4) of the column to measure the pressure drop in the two sections of the column via electronic pressure sensors placed inside the console. These pressure drop values are displayed on the screen. The gas then exits the column from the top and is conveyed to floor level in a liquid PVC and released.

3.3.2 Membrane contactor

Experiments conducted with the membrane contactor used the UOP7-MKII Gas Absorption Column setup that was modified in order to use the HFMC instead of the packed absorption column. This section will present all the modifications that were performed on the initial setup to conduct membrane experiments.

About the liquid closed loop

The liquid is still pumped via the submersible centrifugal pump from the sump tank. The pipe previously ensuring the connection with the top of the column is deviated so that the liquid is injected in the shell side of the membrane contactor. A second pipe connects the exit of shell side to the sump tank and is equipped with a valve allowing to take samples for further CO_2 concentration analyses.

The maximum flow provided with this setup is of 3 L/min due to the pressure drop induced by the membrane that the liquid must overcome.

About the gas circuit

To connect the air flow with the membrane contactor, it was needed to modify the piping. Air no longer flows through the rigid PVC pipe to the bottom of the column but is blocked just after the former CO_2 connection and exits through the tapping that was previously used to inject carbon dioxide in the system. A rigid nylon tubing conveys air to inlet of lumen side of the membrane contactor. Before entering the membrane, air is mixed with CO_2 which enters the line via a “T-connection”.

The first observation was that the centrifugal air blower did not provide enough pressure so that air could flow through the membrane contactor against the pressure drop created by the membrane itself. After some thinking, it was decided to connect the compressor of the lab (see section 3.1) which will provide the required air flow. However, this

compressor does not allow to properly select the desired pressure and flow rates so a system of reducer was installed.

CO_2 is still provided by the external cylinder of compressed CO_2 gas and is mixed with air as previously explained, no major changes for CO_2 delivery was made.

In order to use the CO_2 inlet sensor (i.e. $CO_{2,I}$), a deviation was made between the mixing point of air and carbon dioxide and the inlet of lumen side. In order not to flood the sensor, an exit allows the gas to exit the pipe before reaching the sensor ensuring that only a fraction of the gas will reach the sensor. Just before the membrane, a pressure gauge was disposed in order to know what the inlet pressure of the gas phase in the contactor is.

At the exit of lumen side, a rigid pipe conveys the gas mixture to $CO_{2,II}$ sensor. In order not to flood the sensor, an outlet allows the gas to exit the pipe before reaching the sensor ensuring that only a fraction of the gas will reach the sensor. At this exit, a gas flow meter allows to determine the outlet flow rate of the gas phase.

3.4 Experimental procedure

Both for the absorption column and the membrane contactor, experiments were conducted in order to determine the influence of operating conditions on the overall mass transfer coefficient and to compare the efficiency of the two technologies. Experiments were also conducted to evaluate the flooding of the column and the evolution of pressure drop in the membrane contactor.

3.4.1 Absorption column

Flooding experiments

In order to determine the flooding of the column and to ensure that the conducted experiments are done in good operating conditions, a flooding experiment was performed.

The sump tank is filled with tap water that is pumped to the top of the column, its flow rate adjusted with V10. When the system is stabilised, air is injected in the column and its flow rate is adjusted with V2. The pressure drop across the column is obtained via the addition of ΔP_1 and ΔP_2 that can be read on the console screen. Results are then reported in a table.

A second experiment was then conducted to get the pressure drop when a mixture of air and CO_2 is used that will be needed for the calculation of the overall mass transfer coefficient (see section 3.5.1). This experiment is conducted following the same procedure as when only air is used.

Mass transfer coefficient experiments

The operating conditions of the experiments conducted with the absorption column are reviewed in Table 3.5.

	Liquid		Gas	
N°	**[NaOH] [mol/L]**	**Flow rate [L/min]**	**[CO_2] [%]**	**Flow rate [L/min]**
1.	0.2	1-3-5-7	10	33
2.	0.2-0.5-1	5	10-15	33

Table 3.5: Experimental conditions for the absorption column

The first set of experiments aims to determine the influence of the liquid flow rate on the mass transfer coefficient while the second one aims to determine the influence of both the liquid concentration in NaOH and of the gas mixture in CO_2.

All the experiments achieved with the column followed the same procedure. After the preparation of the solution (see section 3.1.1), the liquid flow is started and the desired flow rate maintained via the control valve V10. A first liquid sample is taken from the sump tank to be further analysed to check the initial concentration of the aqueous NaOH. Then, the air blower is turned on and the flow rate adjusted via V2 before CO_2 is allowed to enter the setup at the desired flow rate (adjusted with V1). After five minutes of steady operation, samples are taken every twenty minutes from the outlet of the absorption column (V6) and the sump tank (V9). The information displayed on the console screen are carefully noted every time samples are taken as well.

The total duration of an experiment from the first sampling procedure is 80 minutes. When the experiment is over, CO_2 arrival is first closed followed by the air blower. Then, the liquid pump is turned off and all the liquid contained in sump tank and column is washed out via V9 and V6. Before proceeding to a new experiment, tap water is passed on the setup in order to clean it.

3.4.2 Membrane contactor

Pressure drop experiments

A first experiment was realised in order to determine the pressure drop across the membrane. Water is introduced in the membrane from the sump tank and, once the system is stabilised, air from the compressor is introduced as well. Data for varying gas flow rates are carefully reported in a table. The same experiment was conducted for gas mixtures of air and CO_2.

Mass transfer coefficient experiments

The operating conditions of the experiments conducted with the membrane contactor are reviewed in Table 3.6:

	Liquid		Gas	
N°	**[NaOH] [mol/L]**	**Flow rate [L/min]**	**[CO_2] [%]**	**Flow rate [L/min]**
1.	0.2	1.5	10-15	6.5
2.	0.2-0.5-1	1	10-15	6.5
3.	0.2-0.5-1	3	15	6.5

Table 3.6: Experimental conditions for the membrane contactor

The first set of experiment aims to determine the influence of CO_2 concentration in the gas mixture on the overall mass transfer coefficient. The second set of experiment aims to evaluate both gas and liquid concentration interactions with the mass transfer coefficient. Finally, the third set of experiment aims to compare the influence of the liquid concentration on the mass transfer coefficient.

The experiments realised with the membrane contactor followed a procedure similar to the ones of the absorption column. The major difference lies in the air injection because in the case of the membrane, it is provided by a compressor as explained in section 3.3.2.

When the experiment is over, the closing procedure is the same as for the column. Before conducting a new experiment, the membrane is washed with tap water and dried by injecting air at high pressure in it for five minutes so that all remaining liquid is evacuated.

3.5 Characterisation and analyse procedures

3.5.1 Mass transfer coefficient

Absorption column

The mass transfer coefficient based on the gas side is given by the following equation (from [33]):

$$K_{Og} = \frac{r_{CO_2}}{a \cdot AH \cdot \Delta P_{lm}} \text{ [mol/(atm} \cdot \text{m}^2 \cdot \text{min)]} \quad (3.1)$$

where r_{CO_2} is the rate of absorption of CO_2 [mol/min] (see sections 3.5.2 and 3.5.3 for calculation details); a is the specific area of packing per unit volume of tower [m^2/m^3]; A is the cross-sectional area of the tower [m^2]; H is the packing height [m] and $\Delta P_{lm} = \frac{y_i - y_o}{\ln(y_i/y_o)} \cdot \frac{p_{atm}}{100}$ is the logarithmic mean driving force [atm] (y_i and y_o are the column inlet and outlet CO_2 partial pressures [%] and p_{atm} is the atmospheric pressure [atm]). This formula assumes that the pressure drop in the column is small enough so that it can be neglected (see section 4.1.1).

Membrane contactor

The mass transfer coefficient of the membrane contactor is given by the following equation (adapted from [36]) which is very similar to the one used for the absorption column:

$$K_{Og} = \frac{r_{CO_2}}{a_{eff} \cdot \Delta P_{lm}} \text{ [mol/(atm} \cdot \text{m}^2 \cdot \text{min)]} \quad (3.2)$$

where r_{CO_2} is the rate of absorption of CO_2 [mol/min]; a_{eff} is the effective gas-liquid contact area [m^2] and $\Delta P_{lm} = \frac{y_i - y_o}{\ln(y_i/y_o)} \cdot p_{mean}$ is the logarithmic mean driving force [atm] (y_i and y_o are the contactor inlet and outlet CO_2 partial pressures [%] and p_{mean} is the average pressure in the lumen side [atm]).

3.5.2 Titration method (double indicators method)

The reactive absorption of CO_2 with NaOH was previously detailed in section 1.5. The process takes place in two distinct steps. While NaOH is still present in solution, the reaction is:

$$CO_2 + 2OH^- \rightarrow CO_3^{2-} + H_2O \quad (3.3)$$

When all NaOH has reacted, a second reaction occurs:

$$CO_2 + CO_3^{2-} + H_2O \leftrightarrow 2HCO_3^- \quad (3.4)$$

The liquid samples taken in inlet and outlet of the column or membrane may then contain three chemical species of interest: OH^-, CO_3^{2-} and HCO_3^-; the determination of their concentration allows to compute the rate of absorption of carbon dioxide.

In order to determine the concentrations of interest, the double indicators method was used. The sample which is alkaline is titrated with HCl and two indicators (phenolphthalein

and methyl orange) that change colour and indicate what species is in solution during titration. This method is used differently whether or not NaOH is still present in solution.

NaOH in solution

Sodium hydroxide being a strong base, it reacts first with HCl according to this reaction:

$$OH^- + H^+ \rightarrow H_2O \tag{3.5}$$

Once all hydroxide has reacted, the carbonate reacts in turn with HCl following a two-step reaction:

$$CO_3^{2-} + H^+ \rightarrow HCO_3^- \tag{3.6}$$

$$HCO_3^- + H^+ \rightarrow H_2CO_3 \tag{3.7}$$

Hence, two moles of HCl are required to neutralise one mole of Na_2CO_3.

Phenolphthalein is first added to the sample which turns purple. HCl is then added drop by drop until solution becomes colourless after addition of a volume V_1 of HCl which indicates that only bicarbonate is present in solution.

Methyl orange is then poured in the sample that turns yellow and HCl is again added drop by drop until solution becomes pink after addition of a volume V_2 of HCl which indicates that all bicarbonates have reacted to form H_2CO_3.

The determination of the species concentration is summarised in Table 3.7 (V_s is the volume of the sample):

$V_{tot} = V_1 + V_2$	$V_{CO_3^{2-}} = 2 \cdot V_2$	$V_{OH^-} = V_{tot} - V_{CO_3^{2-}}$
$[OH^-] = \frac{[HCl] \cdot V_{OH^-}}{V_s}$		$[CO_3^{2-}] = \frac{[HCl] \cdot V_{CO_3^{2-}}}{V_s}$

Table 3.7: Computation of species concentration when NaOH is present in solution

NaOH has already reacted

When all NaOH has already reacted, the absorption occurs according to reaction (3.4) and the species in presence are carbonate and bicarbonate. The titration method will again use phenolphthalein and methyl orange.

Titration follows reactions (3.6) and (3.7). After addition of V_1 mL of HCl, all carbonate has reacted to form bicarbonate and after further addition of V_2 mL of HCl, only H_2CO_3 remains. The determination of the species concentration is summarised in Table 3.8:

$V_{CO_3^{2-}} = 2 \cdot V_1$	$V_{HCO_3^-} = V_2 - V_1$
$[CO_3^{2-}] = \frac{[HCl] \cdot V_{CO_3^{2-}}}{V_s}$	$[HCO_3^-] = \frac{[HCl] \cdot V_{HCO_3^-}}{V_s}$

Table 3.8: Computation of species concentration when NaOH is not present in solution

The rate of absorption of CO_2 is then calculated following the operations summarised in Table 3.9 where L stands for the liquid flow rate in L/min:

NaOH in both inlet and outlet	$r_{\mathrm{CO_2}} = ([\mathrm{OH^-}]_{in} - [\mathrm{OH^-}]_{out}) \cdot L \cdot 0.5$
NaOH not present in inlet nor outlet	$r_{\mathrm{CO_2}} = ([\mathrm{HCO_3^-}]_{out} - [\mathrm{HCO_3^-}]_{in}) \cdot L \cdot 0.5$
NaOH in inlet but not in outlet	$r_{\mathrm{CO_2}} = ([\mathrm{OH^-}]_{in} + [\mathrm{HCO_3^-}]_{out}) \cdot L \cdot 0.5$

Table 3.9: Computation of the rate of absorption of CO_2

3.5.3 Sensors method

This alternative method to get the rate of absorption of CO_2 uses the information displayed on the console screen. The analysis of the inlet and outlet partial pressures of CO_2 should allow to determine the variation of the absorption rate.

Absorption column

The absorption rate of CO_2 will be determined according to this equation (adapted from [33]):

$$r_{\mathrm{CO_2}} = F_a \cdot \frac{p_{atm}}{R \cdot T_{column}} \tag{3.8}$$

where; $F_a = \frac{(\mathrm{CO_{2,I}} - \mathrm{CO_{2,II}})}{100} \cdot \frac{F_{air} + F_{\mathrm{CO_2}}}{60}$ [L/s] is the volumetric rate of absorption of CO_2; $\mathrm{CO_{2,I/II}}$, F_{air}, $F_{\mathrm{CO_2}}$, and T_{column} are the readings on the console screens respectively giving the inlet/outlet CO_2 concentration in gas stream, air flow rate, CO_2 flow rate and temperature of the column; p_{atm} is the atmospheric pressure and R is the gas constant.

Membrane contactor

The absorption rate of CO_2 for the membrane contactor device will use a quite similar equation than what is used for the column device (adapted from [33] and [49]):

$$r_{\mathrm{CO_2}} = F_a \cdot \frac{p_{atm}}{R \cdot T_{column}} \tag{3.9}$$

Where $F_a = \left(\mathrm{CO_{2,I}} \cdot G_{in} - \mathrm{CO_{2,II}} \cdot G_{out}\right) \cdot \frac{1}{100 \cdot 60}$ [L/s] is the volumetric rate of absorption of CO_2; G_{in} and G_{out} are the total gas flow rates at the inlet and the outlet of the membrane respectively.

4 Results and discussion

4.1 Absorption column

4.1.1 Analysis of the setup

Before presenting the results obtained for the analysis of the operating parameters, it seems relevant to introduce this section with the different experiments realised to evaluate the behaviour of the column.

Pressure drop and flooding

The analysis of flooding allows to determine the maximum liquid and gas flow rates that will be achievable for the conducted experiments. The data were collected by increasing the gas flow rate for constant liquid flow rate and taking the readings of P1 and P2 on the console screen. All the data were then plotted in a log-log graph presented in Figure 4.1.

The evolution of the pressure drop shows a linear profile with a slope slowly changing. For low air flow rate, the pressure drop is characterized by the resistance to air flow induced by the liquid falling counter-currently. At higher air flow rate, the change of slope is due to the liquid holdup which is an additional resistance to the air flow hence an additional pressure drop. For liquid flow rates of 1 and 2 L/min, this change in slope is less obvious yet exists. As explained in section 1.6.1, flooding occurs for high liquid and gas flow rates and is observable on Figure 4.1 by the absence of relevant data. When considering a constant liquid flow rate, an increase in the gas flow rate has a lower influence than the increase of liquid flow rate for a given gas flow rate.

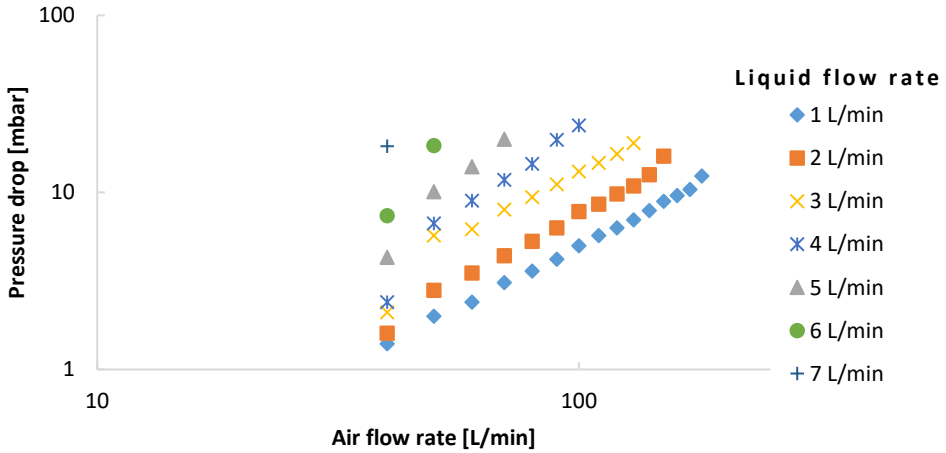

Figure 4.1: Evolution of the pressure drop across the column in function of the air flow rate for different liquid flow rates (1 to 7 L/min)

Given the small values of the pressure drop across the column for the operating conditions used, it will be assumed that it is null in further calculations.

CO_2 sensors

An experiment was conducted to determine the precision of the two sensors provided in the column setup. For every operational conditions, theoretical and observed values were compared, all the results are presented in Table 4.1.

The observed values are given by the sensors of the column installation while the theoretical values are given by the following relation (F_{CO_2} and F_{air} are the displayed flow rates of CO_2 and air respectively):

$$y_{CO_2} = \frac{F_{CO_2}}{F_{CO_2} + F_{air}} \cdot 100\ [\%] \tag{4.1}$$

Air	CO_2	Theoretical value	Observed value	Error
30	3	9.1%	9.9%	8.1%
28	5	15.2%	16.7%	9%
60	6	9.1%	10%	9%

Table 4.1: Evaluation of the error of sensors measurements

4.1.2 Comparison between sensors and titration methods

To introduce this section about the obtained results, an experiment will be fully developed for the two methods available to determine the rate of CO_2 absorption hence the overall mass transfer coefficient in order to compare them as well as to analyse how the system evolves. The experiment was conducted with a 0.2M solution of NaOH flowing at 1 L/min and a flue gas containing 10% CO_2 and flowing at 33 L/min.

Figure 4.2 shows the evolution of ions concentrations at inlet and outlet of the column (i.e. samples from the sump tank and the bottom of the column). According to section 1.5, species concentrations evolve following reactions (1.8) and (1.9) respectively. The inlet hydroxide concentration determined from samples taken in the large liquid volume of the sump tank declines smoothly until all ions are used for the creation of carbonate ions (Figure 4.2.a).

On the other hand, for each time step, the outlet concentration of OH^- is way smaller than the inlet one (Figure 4.3.a) suggesting that the formation of carbonate ions across the column occurs rapidly. In the first 20 minutes of experiment, the carbonate concentration increases accordingly to the depletion of OH^- and then it seems that carbonates level off (Figure 4.2). This behaviour can be explained by reaction (1.9) that begins as soon as no more hydroxide is present in the column. The formation of bicarbonate ions consumes carbonate. This species is then produced in the top of the column while NaOH reacts with CO_2 and then consumed in the lower part of the absorber. Eventually, the outlet concentration of carbonate exceeds its inlet concentration when only reaction (1.9) occurs in the column (after 80 minutes of experiment, Figure 4.3.b). Of course, once its production begins, the concentration of HCO_3^- is always higher at the bottom of the column than in the sump tank (Figure 4.3.c).

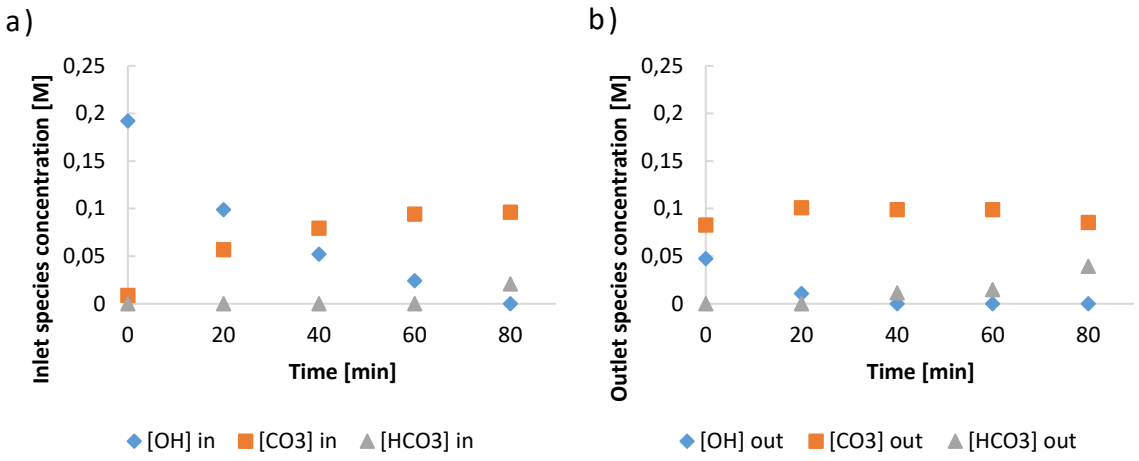

Figure 4.2: Evolution of species concentration as a function of time. NaOH initial concentration is 0.2M and liquid flow rate is 1 L/min; CO_2 inlet gas concentration is 10% and gas flow rate is 33 L/min

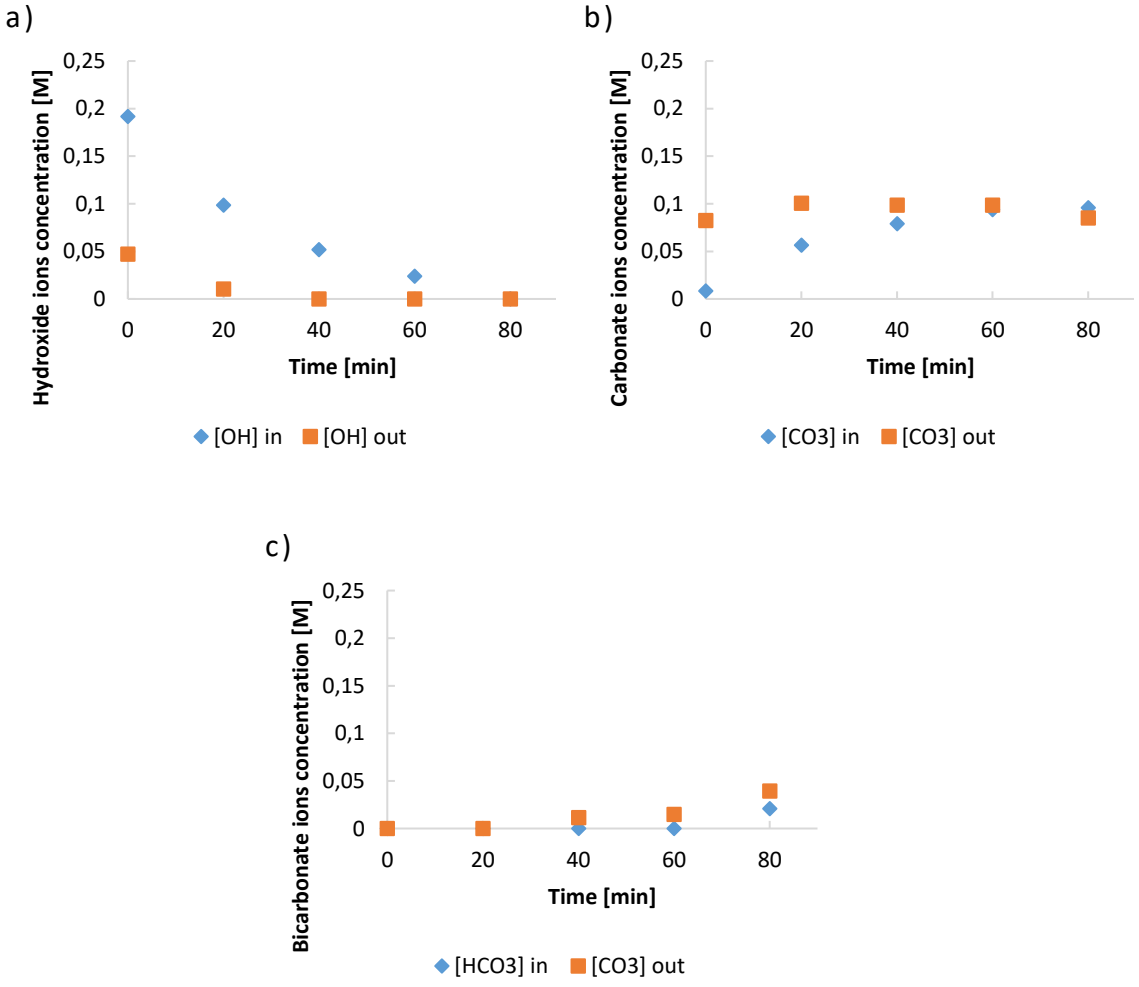

Figure 4.3: Evolution of inlet and outlet species concentration as a function of time. NaOH initial concentration is 0.2M and liquid flow rate is 1 L/min; CO_2 inlet gas concentration is 10% and gas flow rate is 33 L/min

The results obtained in Figure 4.2 using the titration method allow to determine the rate of CO_2 absorption and the overall mass transfer coefficient which is compared with the value obtained via the sensors method in Figure 4.4. For both methods, the overall mass transfer coefficient reduces with time which means that absorption efficiency gradually decreases. This trend is related with the rapid saturation of the sodium hydroxide solution given the instantaneous rate of carbonate production. Once all NaOH has reacted, the production of bicarbonates starts at a lower rate. Eventually, solution becomes entirely saturated and no more chemical absorption is possible (physical absorption by water still happens).

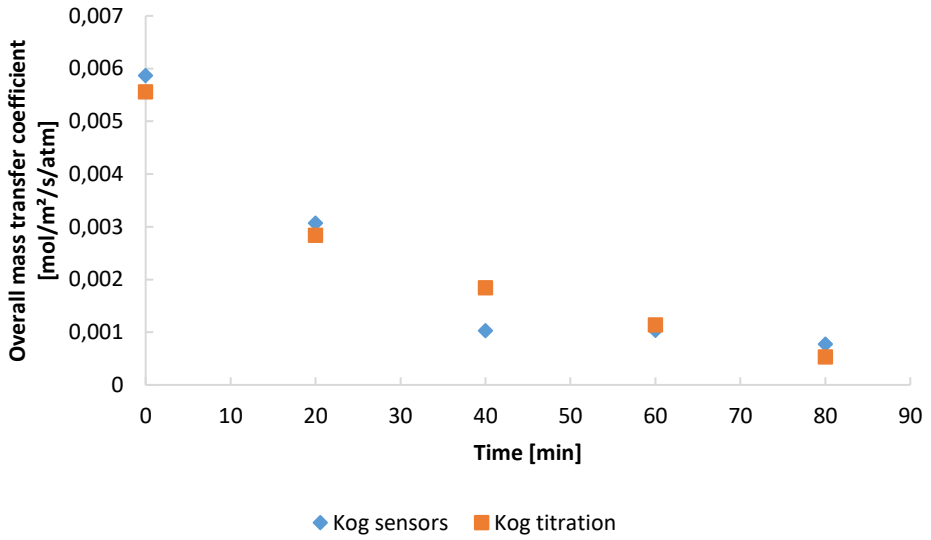

Figure 4.4: Overall mass transfer in function of time using the sensors and the titration methods. NaOH initial concentration is 0.2M and liquid flow rate is 1 L/min; CO_2 inlet gas concentration is 10% and gas flow rate is 33 L/min

As expected, some deviations happen between the two methods. Given the graphs computed for all experiments, the sensors method was proved more reliable (see Appendix D for the graphs of the variation of overall mass transfer coefficient in function of time for all conducted experiments). Indeed, the titration method is subject to manipulation errors (the methyl orange turn is hard to reproduce) while the sensors gives results easily reproducible. According to this choice, all further presented graphs will rely on the results given by the sensors method.

4.1.3 Influence of the liquid and gas flow rates

The influence of liquid flow rate on the overall mass transfer coefficient has been studied for a sodium hydroxide solution of 0.2M flowing at 1-3-5-7 L/min counter-currently to a gas composed of 10% CO_2 and flowing at 33 L/min. Figure 4.5 shows the evolution of K_{Og} in function of the experiment time. Regardless of the liquid flow rate, after 20 minutes of experiment, all configurations present a greatly reduced mass transfer coefficient which then stabilises to a value near zero.

Figure 4.6 presents the obtained mass transfer coefficient after 20-40-60-80 minutes of experiment. For every time step, two distinct groups are visible. The values of K_{Og} for 1 and 3 L/min and the values for 5 and 7 L/min are respectively quite similar. After 20 minutes, for a liquid flow rate of 1 or 3 L/min, K_{Og} is around 0.0031 and for a flow rate of 5 or 7 L/min, it is

around 0.0045 mol/m^2/s/atm. This highlights a dependence between the liquid flow rate and the performance of the chemical absorption. Considering what was explained in section 4.1.1 and the conclusions of the work of Onda et al. [34], this is related with the increased liquid holdup that allows a better wetting of the packing material hence a more efficient absorption between the gas and the liquid in the liquid film surrounding the packing. After 40, 60 and 80 minutes of experiment, the dependence between the liquid flow rate and the overall mass transfer coefficient is less important because after some time, independently of the liquid flow rate, all hydroxide ions has reacted and the absorption occurs only with the formation of bicarbonate ions following a less performant reaction (see [26]).

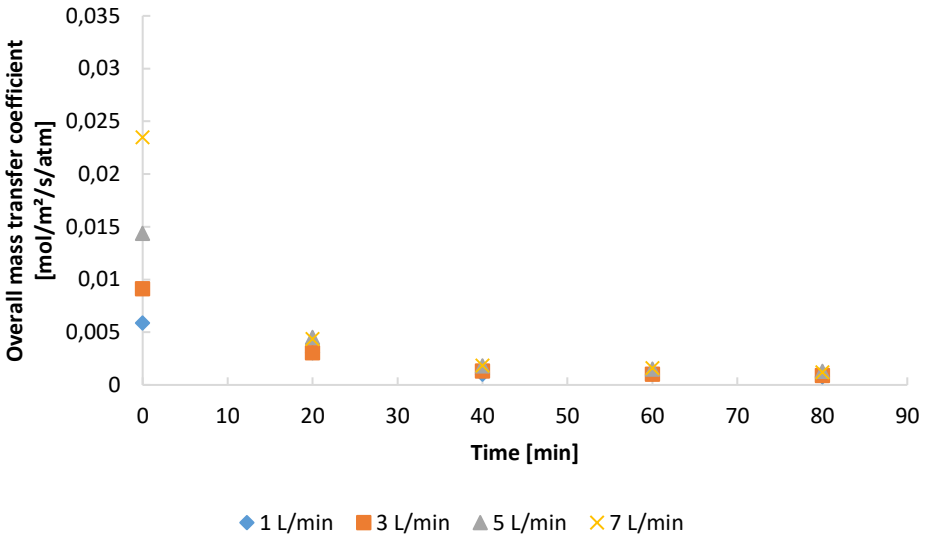

Figure 4.5: Overall mass transfer coefficient in function of the time for varying liquid flow rates. NaOH initial concentration is 0.2M; CO_2 inlet gas concentration is 10% and gas flow rate is 33 L/min

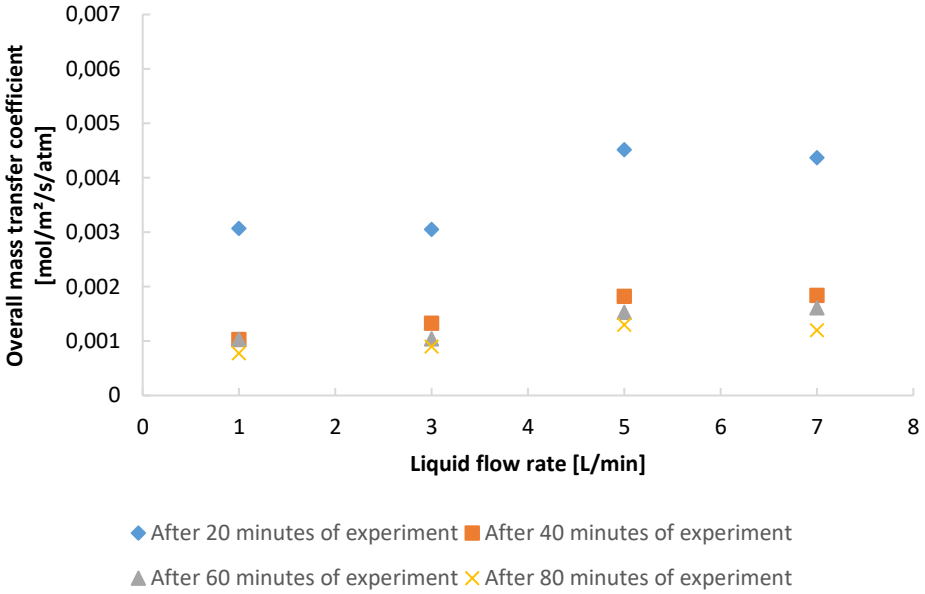

Figure 4.6: Overall mass transfer coefficient taken after 20-40-60-80 minutes of experiment in function of liquid flow rate. NaOH initial concentration is 0.2M; CO_2 inlet gas concentration is 10% and gas flow rate is 33 L/min

The influence of the gas flow rate was then evaluated. A solution of 0.2M NaOH at a flow rate of 5 L/min and a flue gas composed of 10% CO_2 flowing at 33 and 66 L/min were used. Figure 4.7 presents the evolution of the overall mass transfer coefficient in function of the time for these two gas flow rates. Both series decrease in a similar trend with close K_{Og} values. For the 60 first minutes of experiment, the mass transfer coefficient is higher at a higher gas flow rate which indicates that more CO_2 is absorbed at each time step when more gas pass through the column. After 80 minutes of experiment, the tendency is reversed because, at 66 L/min gas flow rate, the liquid flowing through the absorption column is saturated in CO_2 and only physical absorption still occurs. This behaviour is quite logical since at a higher flow rate, a bigger quantity of CO_2 is continuously delivered to the solution.

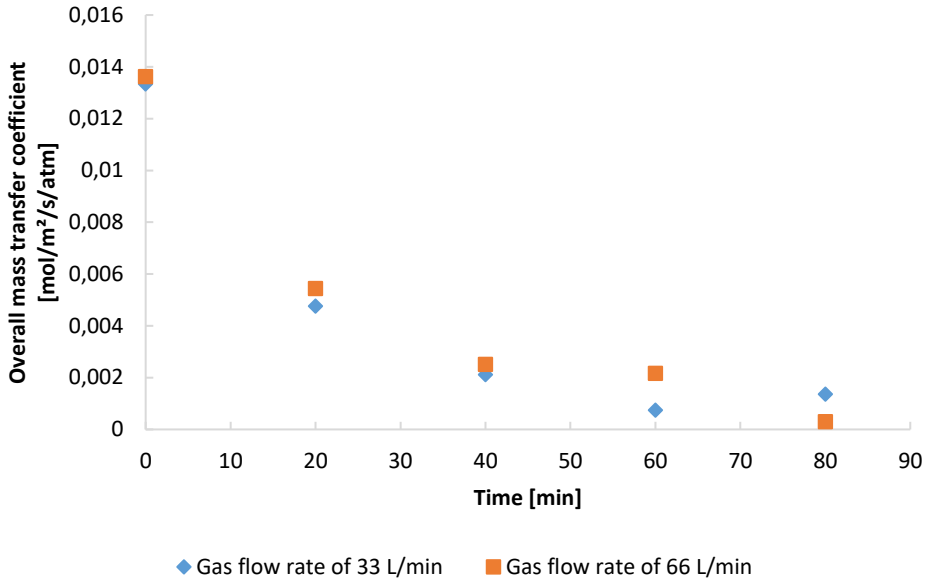

Figure 4.7: Overall mass transfer coefficient in function of the time for a flue gas flowing at 33 or 66 L/min. NaOH flow rate is 5 L/min and initial concentration is 0.2M; CO_2 inlet gas concentration is 10%

Given the small difference in performance for a higher gas flow rate, it seems that the only true influence is that liquid becomes saturated in carbon dioxide faster when more gas passes through the absorption column.

In conclusion, the overall mass transfer coefficient is dependent on the liquid flow rate given the increased liquid hold up but this dependence is not of much importance and loses its influence with time and saturation of the liquid NaOH. On the other hand, the gas flow rate has not much influence on K_{Og} while it stays under the critical pressure ensuring that the system is not working between the loading and flooding points (see section 1.6.1).

4.1.4 Influence of the liquid and gas concentrations

The influence of liquid and gas concentrations on the overall mass transfer coefficient for 0.2, 0.5 and 1M NaOH and 10 and 15% CO_2 was examined. The liquid and gas flow rates were 5 and 33 L/min respectively. Figure 4.8 presents the evolution of K_{Og} in function of time for different couple of liquid and gas concentrations. Once again, the mass transfer coefficient follows a decreasing trend due to the depletion of sodium hydroxide in solution. It is easily noticeable that the higher the initial liquid concentration in NaOH, the bigger the coefficient. This is accountable to the availability of hydroxide groups to react with carbon dioxide.

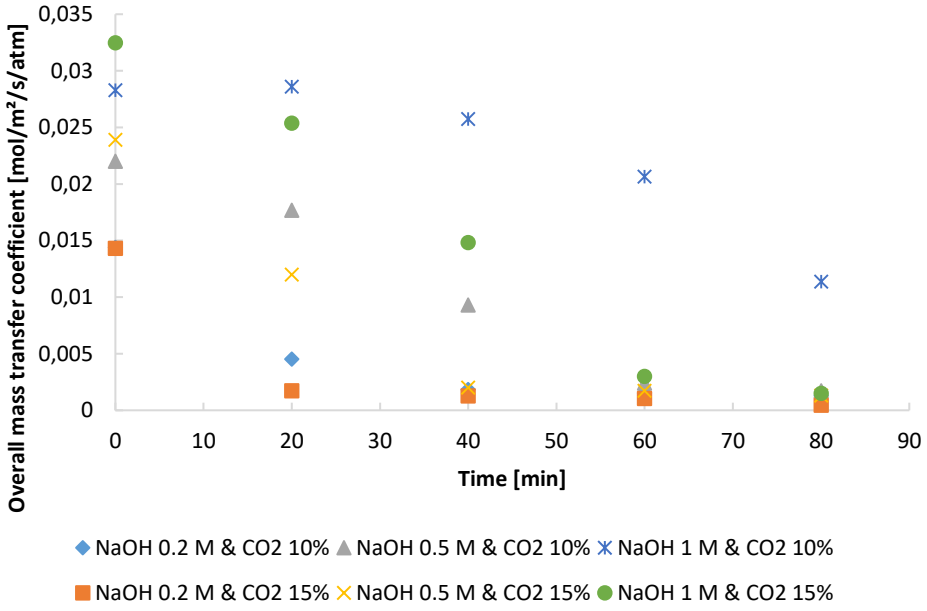

Figure 4.8: Variation of overall mass transfer coefficient in function of time for varying liquid and gas concentrations. Liquid flow rate is 5 L/min and gas flow rate is 33 L/min

Figure 4.9 strengthens the existence of the dependence between the overall mass transfer coefficient and the reaction between NaOH and CO_2. Indeed, the values displayed in this graph are taken after 20 minutes of experiment and it is clear that for a flue gas less concentrated in CO_2, K_{Og} remains bigger at any liquid concentration. This is due to the fact that less hydroxide groups have reacted with the carbon dioxide since less CO_2 was delivered in the same time interval. All NaOH remaining in the sump tank and entering the column is able to chemically absorb CO_2 while passing through the packing ensuring a high value of K_{Og}.

In conclusion, the overall mass transfer coefficient strongly depends on both the concentration of the liquid and the gas because the more unreacted NaOH remains in solution, the more CO_2 can be absorbed via reaction (1.8) which is more efficient than equation (1.9) (see section 1.5).

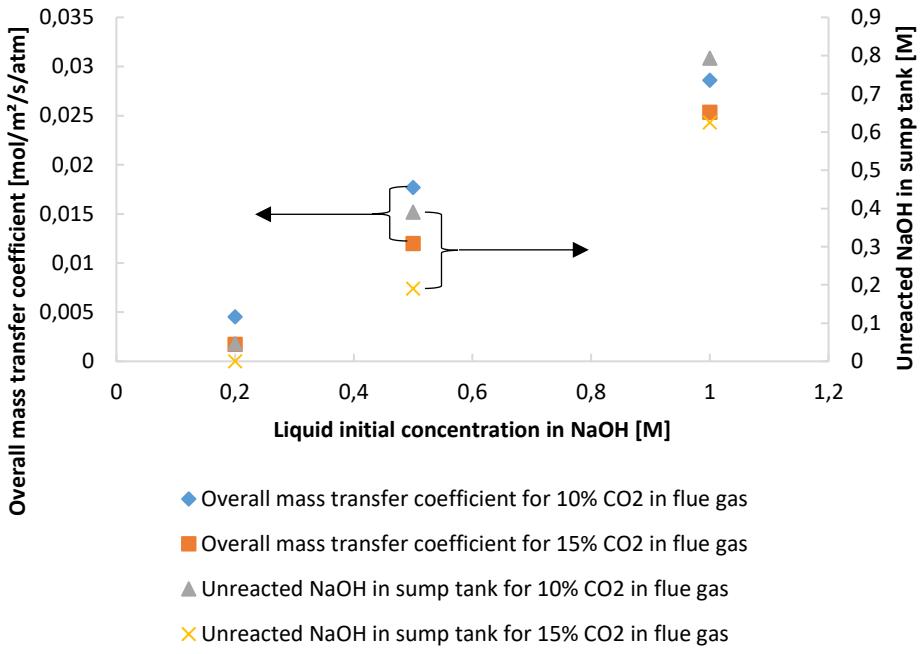

Figure 4.9: Overall mass transfer coefficient and unreacted NaOH in sump tank after 20 minutes of experiment in function of the liquid concentration in NaOH for 10 and 15% CO_2 in flue gas. Liquid and gas flow rates are 5 and 33 L/min respectively

4.2 Membrane contactor

4.2.1 Observations about the results of the membrane

Figure 4.10 presents the evolution of species in function of time for a liquid flow rate of 1 L/min of a solution of initial concentration in NaOH of 0.2M and a gas containing 10% CO_2 flowing at 6.5 L/min. The first observation is that after 80 minutes of experiment, the liquid concentration in NaOH remains quite high compared to what was obtained when using the column (see Figure 4.2). Also, at each time step, the small decrease in hydroxide ions concentration between the inlet and the outlet of the membrane expresses that the reactive absorption is slow. This is due primarily to the lower gas flow rate used in the membrane contactor. To understand why the gas flow rate used was small, it is necessary to explain in details how the membrane contactor setup was used.

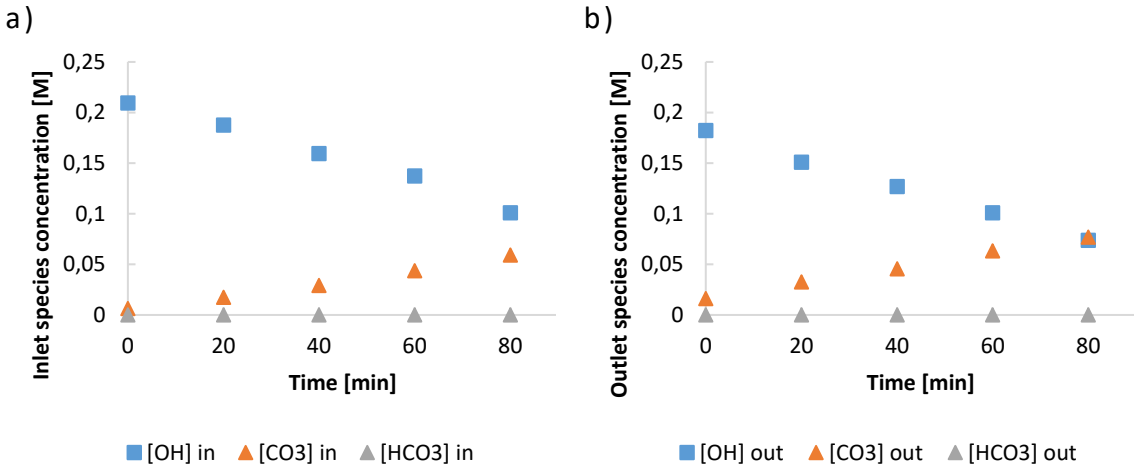

Figure 4.10: Evolution of species concentration as a function of time. NaOH initial concentration is 0.2M and liquid flow rate is 1 L/min; CO_2 inlet gas concentration is 10% and gas flow rate is 6.5 L/min

As explained in section 3.3.2, a deviation was made before the inlet of the lumen side of the membrane contactor in order to deviate a portion of the flue gas to the sensor allowing to determine its CO_2 composition. An exit ensures that this sensor is not flooded by an excessive gas flow. This solution was the only way to properly use the CO_2 sensors provided with the initial column setup. Nonetheless, by allowing the gas to exit the circuit, a very little amount of gas was actually flowing through the contactor and allowed to react with the liquid sodium hydroxide. This may explain why the absorption of CO_2 is so slow while using the contactor.

Furthermore, the pump used to inject the liquid in the contactor is the one of the column device and it was noticed than the pressure delivered by this pump is too small to ensure that the liquid pressure in the contactor is bigger than the gas pressure as required in order to avoid the interpenetration of both phases. In fact, bubbles were formed in the liquid outlet stream meaning that some gas was directly mixed with the liquid in the membrane. Table 4.2 presents the pressures measured at the inlet of the membrane for both the gas and liquid streams. The pressure of the liquid stream was determined using a mercury manometer connected to the liquid circuit just before the inlet of the membrane contactor while the gas pressure was determined using a pressure gauge placed on the gas circuit before the gas enters the membrane.

Liquid flow rate [L/min]	1	1.5	3
Liquid inlet pressure [mbar]	6.9	9.3	26
Gas inlet pressure for a 23.5 L/min flow rate [mbar]	34.7		

Table 4.2: Liquid and gas pressures at the inlet of the membrane contactor

These observations about the membrane setup led to the conclusion that the results obtained with this device were to take with caution due to the uncertainty of the absorption mechanism that was happening.

In order to evaluate the behaviour of the membrane contactor when all the gas dispensed by the lab compressor is flowing through it, one experiment was conducted with a new setup. The deviation of gas to the CO_2 sensor allowing to determine its inlet composition was removed ensuring that no loss of gas had to be made in order not to flood the sensor. Figure 4.11 presents the evolution of species concentration with time for this new setup. The liquid flow rate is 1 L/min and the NaOH initial concentration is 0.2M while the gas composition is 10% CO_2 and the gas flow rate is 6.7 L/min. Once again, the liquid pressure in the membrane is not sufficient to avoid the formation of air bubbles in the liquid outlet stream.

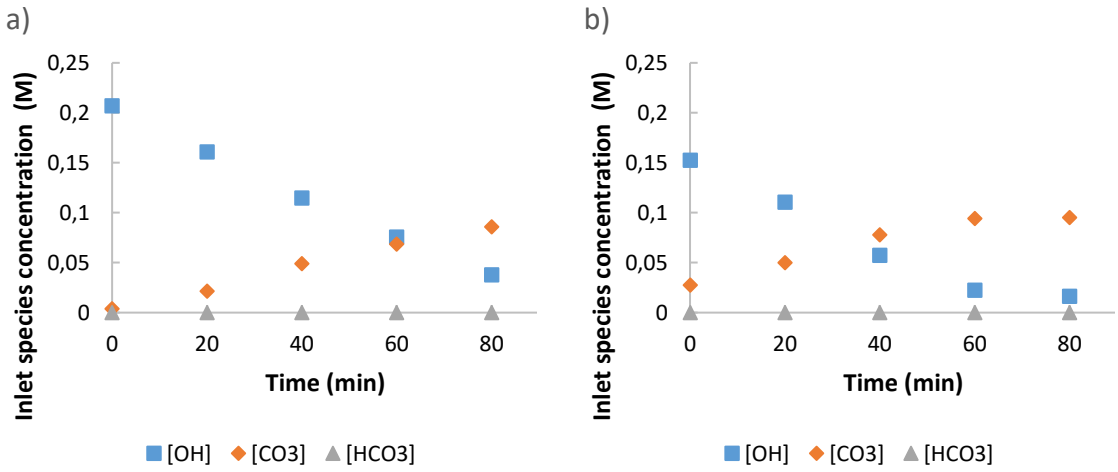

Figure 4.11: Evolution of species concentration as a function of time. NaOH initial concentration is 0.2M and liquid flow rate is 1 L/min; CO_2 inlet gas concentration is 10% and gas flow rate is 6.7 L/min

When comparing Figure 4.11.a and Figure 4.11.b, one can observe how the reactive absorption happens in the membrane contactor. The decrease of hydroxide ions concentration combined with the increase in carbonate ions between the inlet and the outlet of the membrane ensures that the reaction is happening. However, the slow evolution of species concentrations with time highlights that the setup used with these initial operating conditions is not very efficient to conduct the absorption. Nonetheless, Figure 4.12 presents the evolution of K_{0g} for the two different setups used (i.e. with the gas exit opened or closed) and shows that, when the gas exit is opened, K_{0g} is constant and that it decreases when the gas exit is closed.

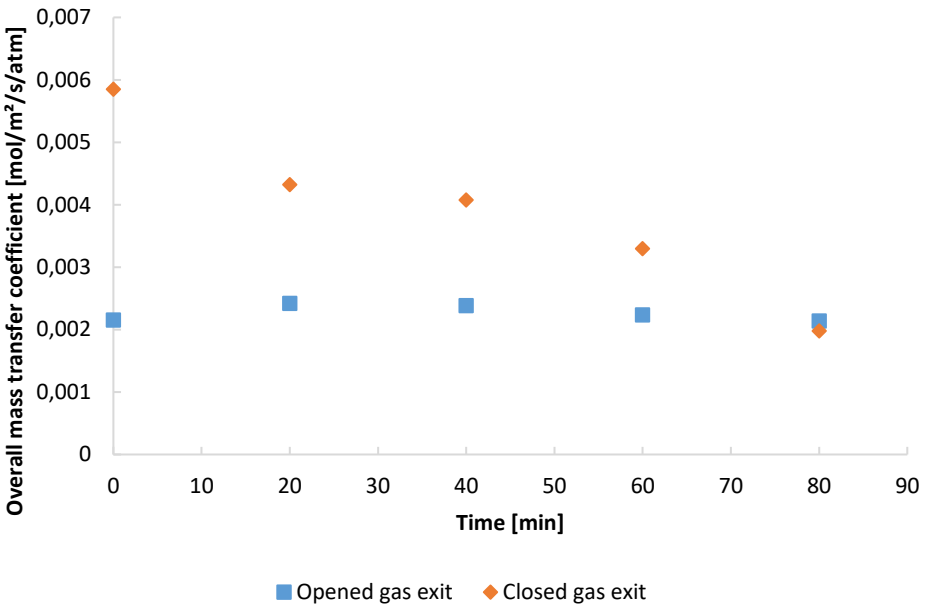

Figure 4.12: Evolution of the overall mass transfer coefficient in function of the time for the two membrane setups. NaOH initial concentration is 0.2M and liquid flow rate is 1 L/min; CO_2 inlet gas concentration is 10% and gas flow rate is 6.5 L/min

Obviously, the setup using the closed gas exit presents more interesting results in terms of the overall mass transfer coefficient evolution because the expected decrease is visible.

Pressure drop

Figure 4.13 presents the evolution of the pressure drop across the membrane contactor in function of the inlet gas flow rate. The results allow to conclude that the variation of the pressure drop is higher in the configuration using the closed gas exit. This can be explained because all the gas is eventually flowing in the contactor when the flow rate is increased while, when using the opened gas exit setup, more and more gas is flowing out the membrane contactor via the exit.

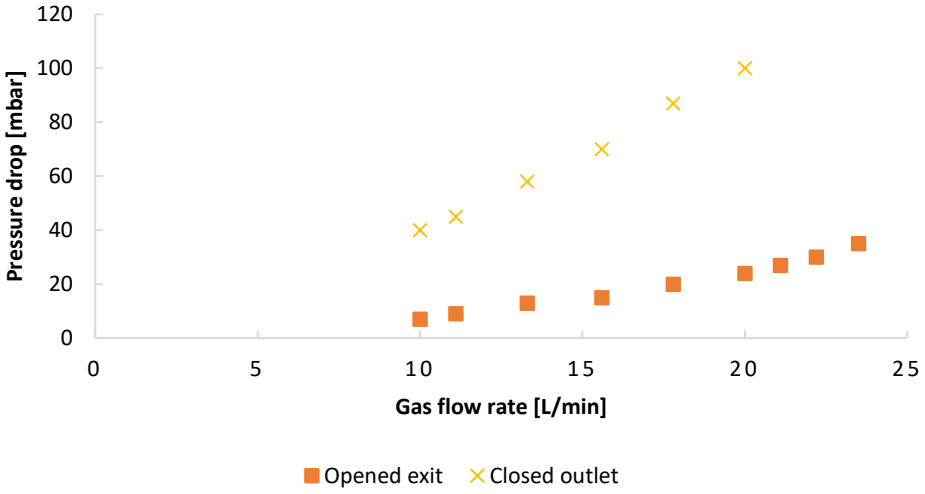

Figure 4.13: Evolution of the pressure drop across the membrane contactor in function of the air flow rate for the two setups

4.2.2 Influence of the liquid flow rate

The influence of the liquid flow rate on the overall mass transfer coefficient has been studied with the setup using the opened gas exit. The solution was of concentration 0.2M NaOH flowing at 1-1.5-3 L/min counter-currently to a gas composed of 15% CO_2 and flowing at 6.5 L/min. Figure 4.14 presents the evolution of K_{Og} in function of the time for varying liquid flow rates. The first observation is that regardless of the liquid flow rate, K_{Og} decreases with time. The evolution of the coefficient for 1 and 1.5 L/min shows that the solution becomes saturated faster at a higher flow rate due to the faster injection of fresh liquid in the contactor. Nonetheless, the coefficient remains higher for a liquid flow rate of 3 L/min. This might arise from the higher liquid pressure decreasing the penetration of the gas phase in the liquid phase and ensuring a better mass transfer coefficient.

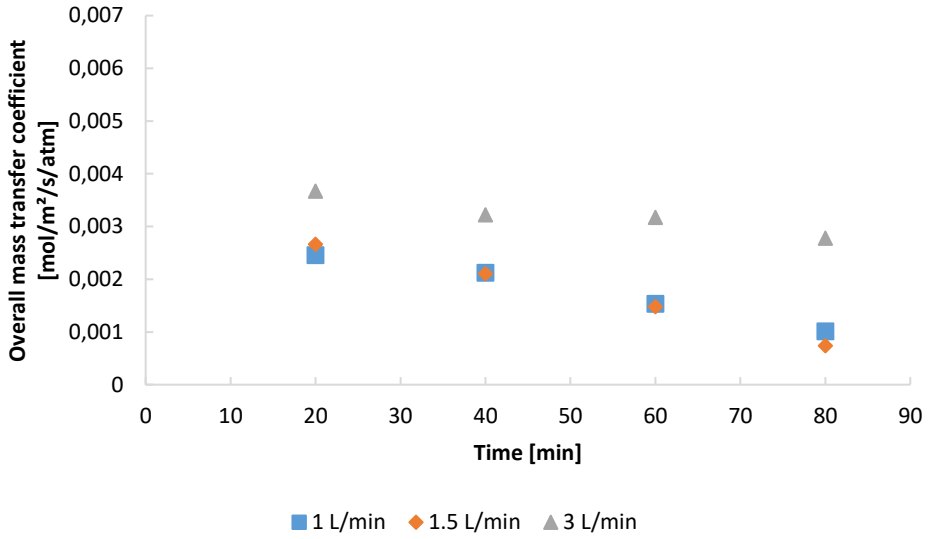

Figure 4.14: Overall mass transfer coefficient in function of the time for varying liquid flow rates. NaOH initial concentration is 0.2M; CO_2 inlet gas concentration is 15% and gas flow rate is 6.5 L/min

Figure 4.15 presents the overall mass transfer coefficient computed after 20 minutes of experiment for different liquid flow rates and initial NaOH concentrations of 0.2, 0.5 or 1M. The series presenting the data collected for 0.2M can be compared with Figure 4.14. It can be observed that, after 20 minutes, the smaller the flow rate or the liquid concentration, the smaller K_{Og}.

In conclusion, the overall mass transfer coefficient is related to the liquid flow rate and evolves proportionally to it. The higher the liquid flow rate, the more rapidly fresh NaOH enters the contactor ensuring that CO_2 is efficiently absorbed.

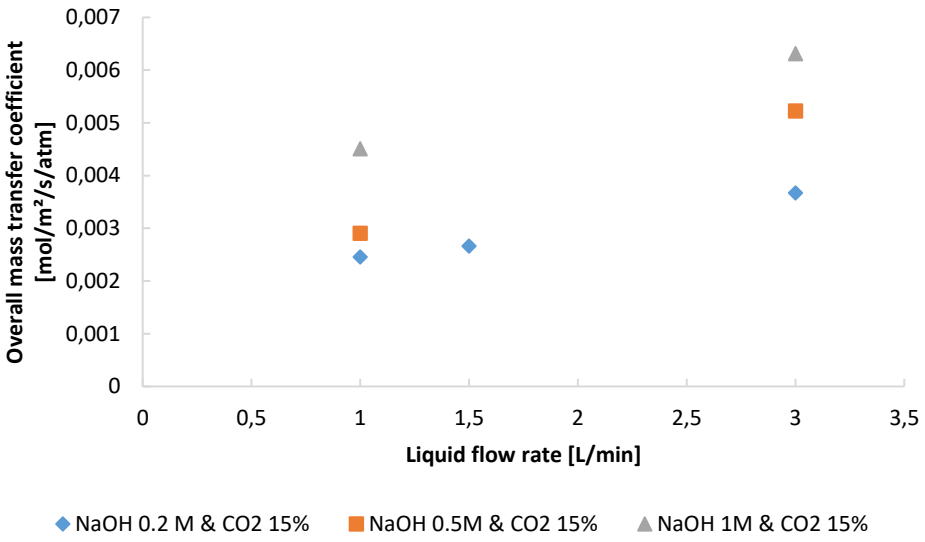

Figure 4.15: Overall mass transfer coefficient taken after 20 minutes of experiment in function of liquid flow rate and NaOH concentration. NaOH initial concentration is 0.2M-0.5M or 1M; CO_2 inlet gas concentration is 15% and gas flow rate is 6.5 L/min

4.2.3 Influence of the gas flow rate

The influence of the gas flow rate on the overall mass transfer coefficient has been studied with the setup using the closed gas exit. The solution was of concentration 0.2M NaOH flowing at 1 L/min counter-currently to a gas composed of 10% CO_2 and flowing at 6.7 or 10 L/min. Figure 4.16 presents the evolution of the overall mass transfer coefficient in function of the time for these two gas flow rates. K_{Og} is higher for a higher flow rate due to the faster continuous intake in CO_2 from the flue gas. Indeed, more CO_2 flowing through the membrane implies a better absorption rate of the device.

In conclusion, the overall mass transfer coefficient is less dependent on the gas flow rate than on the liquid flow rate.

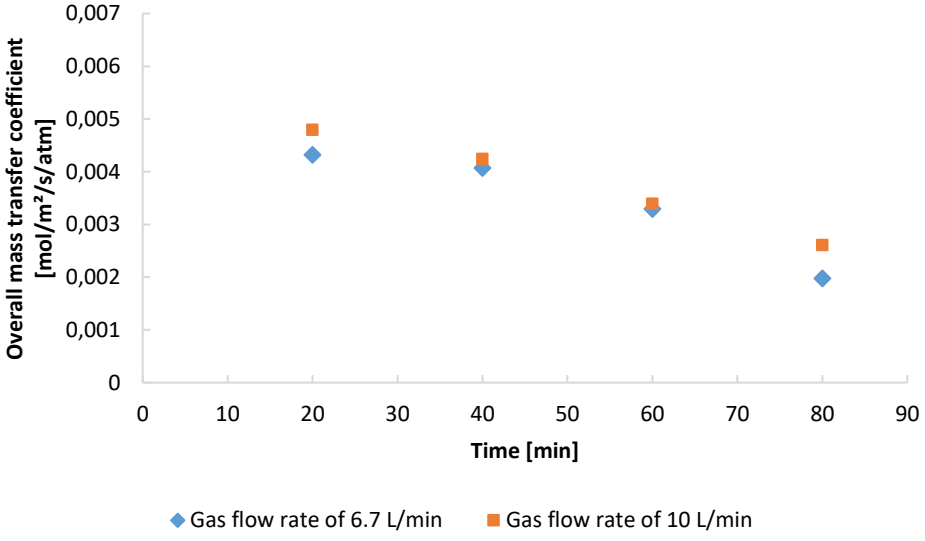

Figure 4.16: Overall mass transfer coefficient in function of the time for a flue gas flowing at 6.7 or 10 L/min. NaOH initial concentration is 0.2M; CO_2 inlet gas concentration is 10%

4.2.4 Influence of the liquid and gas concentrations

The influence of liquid and gas concentrations on overall mass transfer coefficient for 0.2, 0.5 and 1M NaOH and 10 and 15% CO_2 was examined for the device using the opened gas exit. The liquid and gas flow rates were 1 and 6.5 L/min respectively. Figure 4.17 presents the evolution of K_{0g} in function of time for different couple of liquid and gas concentrations. At first, one can observe that when the flue gas is composed of 10% CO_2, K_{0g} remains nearly constant during the experiment while when it is composed of 15% CO_2, the coefficient presents a slight decrease. The higher values of the overall mass transfer coefficient are observed for higher initial liquid concentrations in sodium hydroxide due to the larger presence of initial hydroxide ions that remains available longer during the experiment to react with carbon dioxide.

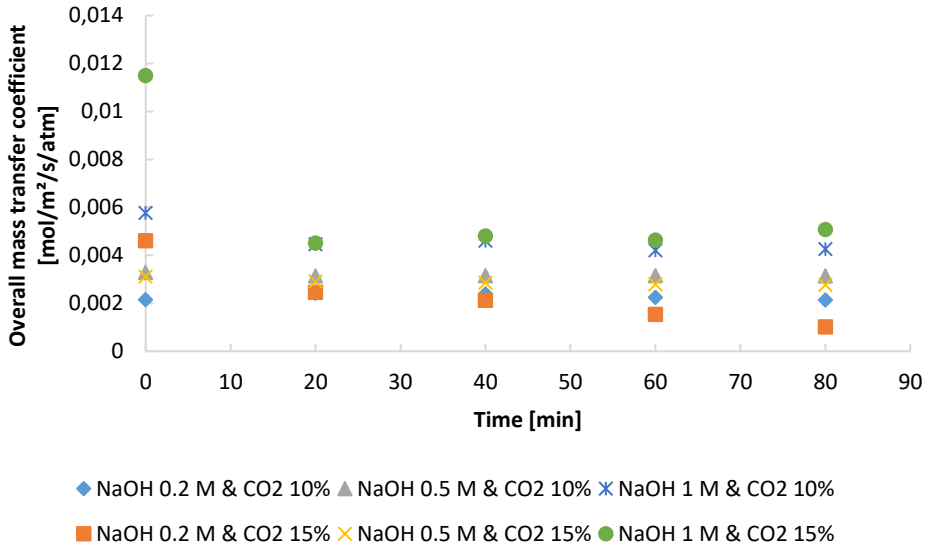

Figure 4.17: Variation of overall mass transfer coefficient in function of time for varying liquid and gas concentrations. Liquid flow rate is 1 L/min and gas flow rate is 6.5 L/min

Figure 4.18 presents the overall mass transfer coefficient and the amount of unreacted NaOH in solution after 20 minutes of experiment for varying liquid initial concentration in NaOH and composition of flue gas at the inlet of the membrane. Unexpectedly, the concentration of sodium hydroxide remains nearly the same as the initial one after 20 minutes of experiment whatever the composition of the flue gas in CO_2. This leads to a small amount of absorbed CO_2 and explains why the overall mass transfer coefficient does not vary much with the gas composition.

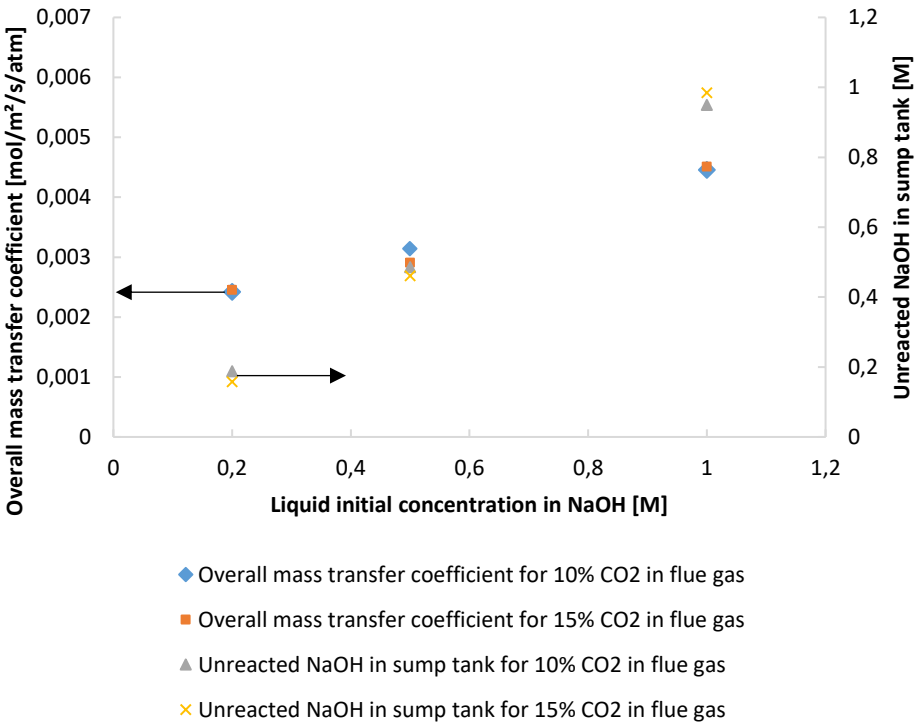

Figure 4.18: Overall mass transfer coefficient and unreacted NaOH in sump tank after 20 minutes of experiment in function of the liquid concentration in NaOH for 10 and 15% CO_2 in flue gas. Liquid and gas flow rates are 1 and 6.5 L/min respectively

Figure 4.19 presents the same results taken after 80 minutes of experiment. The depletion of sodium hydroxide ions is more noticeable than in Figure 4.18 and, accordingly to what was stated for the column, more NaOH remains unreacted when the composition of the flue gas in CO_2 is smaller. The results obtained for the solution of 1M NaOH are contradictory with this statement because more OH^- remains in sump tank for a gas containing 15% CO_2 than for a gas containing 10% CO_2. This might be due to the large initial concentration in NaOH that becomes saturated way more slowly than when the liquid is of 0.2 or 0.5M. According to this observation, a flue gas composed of more CO_2 allows more hydroxide ions to react hence leads to a higher overall mass transfer coefficient. If the experiment was conducted longer, the trend would have been reversed and K_{Og} would have become greater for a flue gas composed of 10% CO_2.

The results obtained in this section indicate that the overall mass transfer coefficient depends both on the liquid and gas concentrations. The best operating conditions involve a highly concentrated liquid allowing to handle a flue gas composed of 15% CO_2 with better results than a flue gas of 10% CO_2.

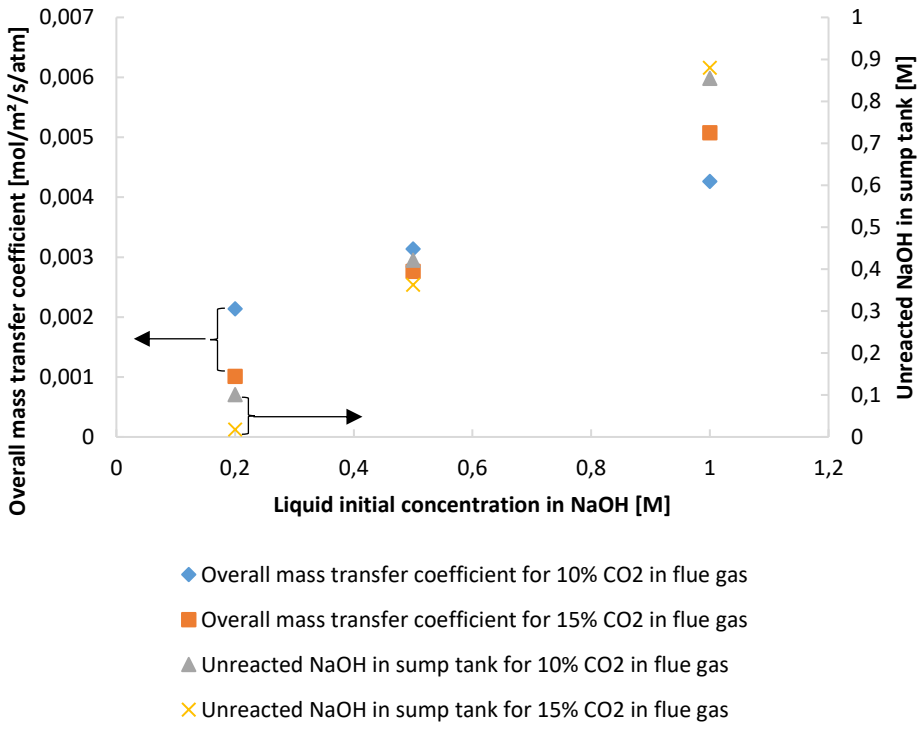

Figure 4.19: Overall mass transfer coefficient and unreacted NaOH in sump tank after 80 minutes of experiment in function of the liquid concentration in NaOH for 10 and 15% CO2 in flue gas. Liquid and gas flow rates are 1 and 6.5 L/min respectively

4.3 Comparison between the two devices

The effective interfacial area of the column is $a_{specific} \cdot \pi \cdot r_{column}^2 \cdot L_{column} = 3.1\text{m}^2$ and is of 1.4m^2 for the membrane contactor (see sections 3.2.1 and 3.3.2). There is then twice as much exchange area for the absorption to occur when using the column. This section aims to compare the efficiency of both devices and how they evolve with the variation of the operating conditions.

4.3.1 Evolution of the mass transfer coefficient

Figure 4.20 presents the evolution of the overall mass transfer coefficient and the unreacted NaOH in sump tank with time for the absorption column and the membrane contactor when the initial liquid concentration is 0.2M NaOH and its flow rate 1 L/min and the flue gas is composed of 10% CO_2. The gas flow rate is 33 L/min for the column and 10 L/min for the membrane. This graph allows to determine that, for both devices, K_{0g} decreases accordingly to the depletion of remaining hydroxide ions concentration in the sump tank. After 80 minutes of experiment, there is no more sodium hydroxide in the sump tank when using the absorption column hence the overall mass transfer coefficient is greatly reduced; this is not the case when using the membrane contactor.

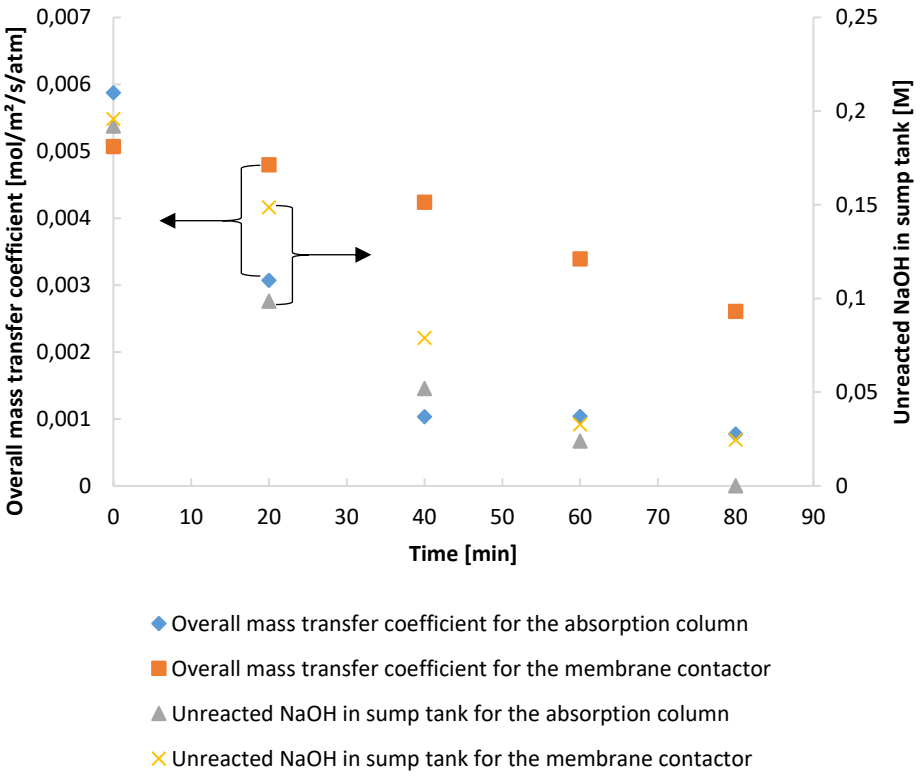

Figure 4.20: Evolution of the overall mass transfer coefficient and the unreacted NaOH in sump tank in function of the time for the absorption column and the membrane contactor. NaOH initial concentration is 0.2M and liquid flow rate is 1 L/min; CO_2 inlet gas concentration is 10% and gas flow rate is 33 L/min for the column and 10 L/min for the membrane

The first observation of interest than can be made is that, at lower gas flow rate and a two-time smaller exchange area, the membrane contactor gives a mass transfer coefficient in the same range than the absorption column. This is the strength of intensification. Then, the faster depletion of K_{0g} for the column device comes from the more abundant flow of CO_2 in the inlet flue gas given the higher gas flow rate. The solution of sodium hydroxide becomes saturated faster and is less efficient to remove carbon dioxide from the flue gas.

4.3.2 Influence of the liquid and gas flow rates

Liquid flow rate

Figure 4.21 allows to compare the influence of the variation of liquid flow rate on the overall mass transfer coefficient. The column was operated using a 0.2M solution and a gas composed of 10% CO_2flowing at 33 L/min while the membrane used a 0.2M solution and a gas composed of 15% CO_2 flowing at 6.5 L/min. According to the data obtained, K_{0g} increased by 47% for the column and for liquid rates increasing from 1 to 7 L/min and it increased by 50% for the membrane and liquid flow rates increasing from 1 to 3 L/min.

In conclusion, the absorption efficiency of both devices varies with the liquid flow rate but the membrane contactor is more dependent on this operating condition than the column.

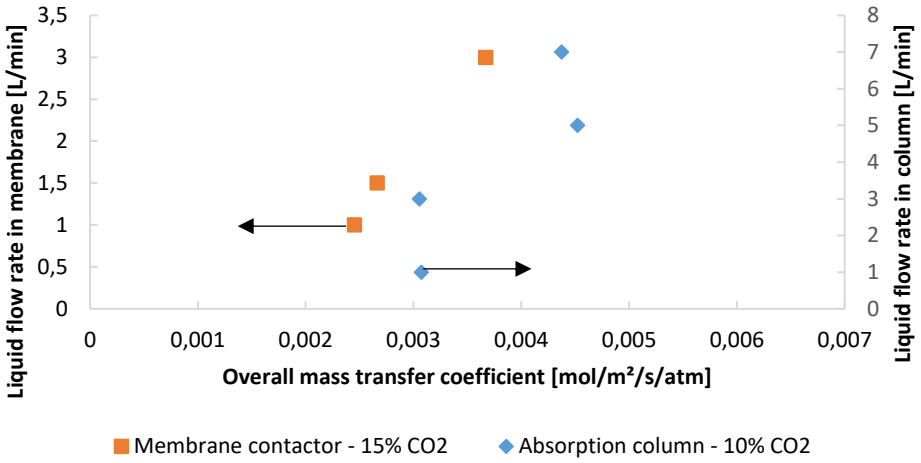

Figure 4.21: Comparison of the evolution of the overall mass transfer coefficient in function of the liquid flow rate for the membrane contactor (flue gas composed of 15% CO_2 flowing at 6.5 L/min) and the absorption column (flue gas composed of 10% CO_2 and flowing at 33 L/min). The initial concnetration of the liquid is 0.2M for both devices

Gas flow rate

Figure 4.22 presents the evolution of K_{Og} in function of the gas flow rate for the two devices. Both the column and the membrane use a liquid of initial concentration 0.2M NaOH and a flue gas composed of 10% CO_2. The liquid flow rate is 5 L/min for the column and 1 L/min for the membrane.

As explained in sections 4.1.4 and 4.2.4, the gas flow rate is not of much importance for the chemical absorption of CO_2 when using the absorption column or the membrane contactor. The efficiency of the column is improved by 14% when using a flow rate of 66 L/min rather than 33 L/min and the efficiency of the membrane is increased by 11% when using a flow rate of 10 L/min rather than 6.7 L/min.

Once again, the membrane is more dependent on the variation of the parameter than the column.

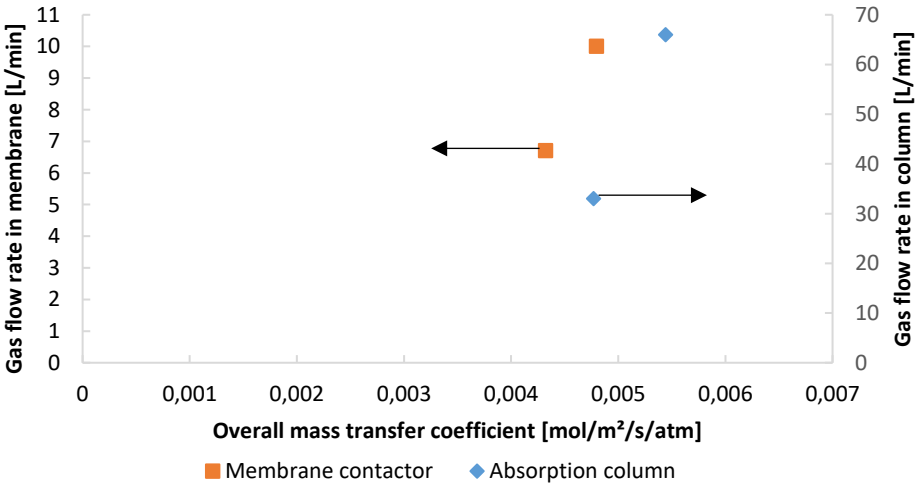

Figure 4.22: Comparison of the evolution of the overall mass transfer coefficient in function of the gas flow rate for the membrane contactor and the absorption column. The initial concentration of the liquid is 0.2M for both devices flowing at 1 L/min for the membrane and 5 L/min for the column. The gas is composed of 10% CO_2 for both devices

4.3.3 Influence of the liquid and gas concentrations

Liquid concentration

Figure 4.23 presents the evolution of K_{Og} in function of the liquid initial concentration for the two devices. Both the column and the membrane use a flue gas composed of 15% CO_2 and flowing at 6.5 L/min for the membrane and 33 L/min for the column. The liquid flow rate is 3 L/min for the membrane and 5 L/min for the column.

Liquid concentration is the operating parameter with the most influence on K_{Og} with an increase in performance of 84% for the membrane and of 1381% for the column. Obviously, the column is way more dependent on the liquid concentration than the membrane.

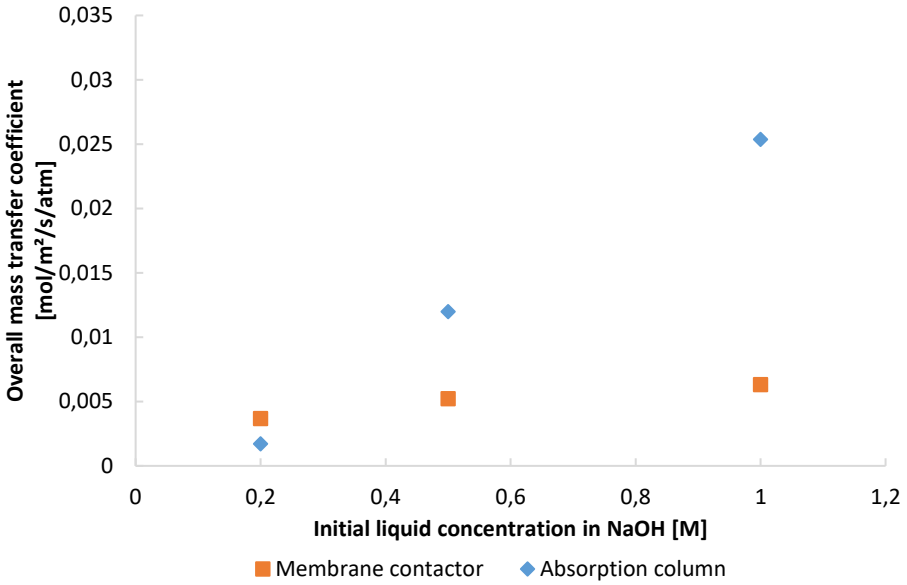

Figure 4.23: Comparison of the evolution of the overall mass transfer coefficient in function of the liquid initial concentration for the membrane contactor and the absorption column. Both devices use a flue gas composed of 15% CO_2 and flowing at 6.5 L/min for the membrane and 33 L/min for the column. The liquid flow rate is of 3 L/min for the membrane and of 5 L/min for the column

Gas concentration

Figure 4.24 presents the evolution of K_{Og} in function of the gas composition for the two devices. Both the column and the membrane use a liquid of initial concentration of 0.5M and flowing at 1L/min for the membrane and 5 L/min for the column. The gas flow rate is 6.5 L/min for the membrane and 33 L/min for the column.

The obtained data give a decrease in performance of 8% for the membrane contactor when using a gas composed of 15% CO_2 rather than 10% while the decrease is of 47% for the column. Once again, the column is more dependent than the membrane in terms of gas concentration.

In conclusion of the data presented in this section, it seems that the performance of the membrane varies more with the liquid and gas flow rates while the column depends on the liquid and gas concentrations more closely.

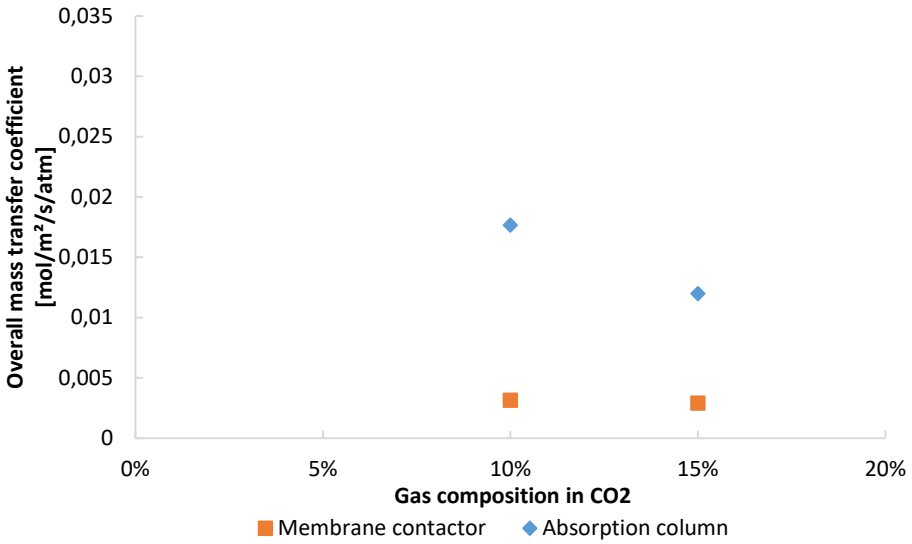

Figure 4.24: Comparison of the evolution of the overall mass transfer coefficient in function of the gas composition in CO_2 for the membrane contactor and the absorption column. Both devices use a liquid of initial composition of 0.5M and flowing at 1 L/min for the membrane and 5 L/min for the column. The gas flow rate is of 6.5 L/min for the membrane and of 33 L/min for the column

Furthermore, all the collected data highlight the power of intensification of the membrane contactor. Indeed, with an exchange surface twice as small as the column exchange area and for less intense gas and liquid flow rates, the overall mass transfer coefficient is always in the same range of values. The fact that the membrane is less dependent on the gas and liquid concentrations combined with the intensification makes it a powerful tool to compete with the absorption column. Indeed, the absorbent solutions do not need to be highly concentrated in NaOH to give proper results and the contactors are way more compact than the columns.

Conclusion

Being part of an overall work on the ability to capture and convert carbon dioxide into a valuable product – sodium carbonate – by using membrane contactors for every step involved in the process, this work aims to compare the absorption column and the membrane contactor technologies for the chemical absorption of CO_2 in liquid NaOH.

Firstly, the influence of operating parameters was studied on the efficiency of the absorption using an absorption column designed by Armfield Ltd. Increasing liquid and gas flow rates led to small increase in performance for this device while increasing the liquid concentration led to a huge increase in performance. The increase in gas concentration led to a marked decrease in performance.

Secondly, the same operating parameters were varied to study their impact on the overall mass transfer coefficient and the absorption efficiency for the membrane contactor designed by Liqui-Cel®. Again, the increase in liquid and gas flow rates led to an increase in efficiency about the same order of magnitude attained with the absorption column. The use of a more concentrated absorbent increased the overall mass transfer coefficient while a gas richer in CO_2 slightly decreased the efficiency of the contactor.

The conducted experiments lead to the conclusion that the most impacting operating parameter is the concentration of the liquid absorbent. Indeed, the continuous providing of fresh hydroxide to react with the injected CO_2 is the key parameter ensuring an efficient absorption. Therefore, the increase in liquid flow rate also have a higher impact than the increase of gas flow rate. An increased liquid flow rate allows to retard the fast saturation of the absorbent. The increase in gas concentration in CO_2 lowers the efficiency of the absorption because of the accelerated saturation in liquid film it involves.

After having analysed the influence of the operating parameters for both the devices, a comparison of performance was performed. The effective interfacial area of the membrane is twice as small as the one of the column and the liquid and gas flow rates achievable with the setup are lower than the one used with the column. Nonetheless, the overall mass transfer coefficient obtained while using the membrane contactor lies in the same range than the column coefficient. This highlights the power of the intensification which is a strong argument in favour of the membranes to be used as CO_2 capture devices.

The last part of this work aims to provide recommendations for future researches about the topic treated throughout the present report. Several aspects of the conducted experiments and of the used setups are analysed in order to propose improvements on their use.

5 Recommendations for future researches

This section aims to provide further lines of inquiry for future researches in order to address the experienced difficulties throughout the work that has been done. For each issue encountered, a setup or process modification will be presented.

5.1 Titration method

The titration method delivers good results in terms of the evolution of concentration species. Nonetheless, the calculation of the overall mass transfer coefficient is extremely difficult to compute with this method. Indeed, this calculation is based on the difference between the concentrations in inlet and outlet of the device studied and is flawed by the slightest manipulation error.

During the process of titration, the errors arise from the fact that the turn of methyl orange is difficult to detect and to reproduce exactly. To overcome this difficulty, a pH-meter could be used in addition to the coloured indicators. This would allow to determine more precisely the species concentrations in the solution. Another method would be to use a CO_2 electrode to measure the CO_2 concentration in the liquid samples as it was done in the work of Wang et al. [42].

Another way to improve the titration results is to use more precise measuring containers. All samples should be exactly the same volume to ensure the reproducibility of the titration.

Yet, it seems that the best way to evaluate the rate of absorption of CO_2 is by determining the CO_2 concentrations in the inlet and outlet gas as it was done for all the conducted experiments.

5.2 Experimental procedure

To ensure the reproducibility of the operation, a few steps must be followed. Once the desired operating conditions are reached, the system should operate for 10 minutes at the required conditions before the timer begins so that absorption has begun. The samples must be taken at the inlet and then the outlet at each time step to ensure the difference of the species concentration between outlet and inlet will not be flawed.

5.3 Setup modifications

5.3.1 Membrane contactor setup

Liquid flow

As explained in section 4.2.1, the liquid pressure is not sufficient to prevent the gas to flow through the membrane in the liquid bulk. This behaviour lowers the efficiency of the absorption process and must be avoided. For the conducted experiments, the pump used to circulate the liquid was the pump of the column setup placed in the sump tank. To get liquid at a higher pressure, another pump should be used. For example, a peristaltic pump with a valve to adjust the delivered pressure and ensure that it is larger than the gas pressure in the membrane contactor.

Gas flow

In section 4.2.1, it was mentioned that, in order not to flood the CO_2 sensors used to determine the composition of the inlet and outlet flue gas in CO_2, gas outlets had been made. This solution implies that not all the gas delivered by the lab compressor and the CO_2 cylinder flows in the membrane contactor.

To avoid this difficulty, a chromatograph could be used to continuously measure the composition of the gas inlet and outlet instead of the sensors of the column device.

The mixing of CO_2 and air was difficult to handle properly. Indeed, it was hard to determine exactly the pressure of both streams and ensure that the mixing was exact. A pressure regulator should be placed to regulate precisely the streams pressure and ensure a perfect mixing.

In order to get exact measurements of the inlet and outlet gas pressures and flow rates, addition of pressure gauges and digital bubble meters at both the inlet and outlet of the membrane could be made according to the work of Wang et al. [22].

5.4 Further experiments

- After the modification of the membrane contactor setup, higher gas and liquid flow rates should be achievable. This would allow to conduct experiment using the exact same operating conditions than with the absorption column.
- In addition of these experiments, it is of interest to invert the gas and liquid streams so that gas would flow on the shell side of the membrane and liquid on the lumen side. This would be interesting to evaluate the efficiency of the contactor in this configuration.
- The influence of the absorbent solution temperature could also be of interest according to what was stated by Kordylewski et al. [26].

References

1. **IPCC [Solomon, S., D. Qin, M. Manning, Z. Chen, M. Marquis, K.B. Averyt, M.Tignor and H.L. Miller (eds.)].** *Climate Change 2007: The Physical Science Basis. Contribution of Working Group I to the Fourth Assessment.* Cambridge : Cambridge University Press, 2007.

2. **Olajire, A.A.** CO2 capture and separation technologies for end-of-pipe applications - A review. *Energy.* 2010, 35, pp. 2610-2628.

3. **Luis, P.** Use of monoethalonamine (MEA) for CO2 capture in a global scenario: Consequences and alternatives. *Desalination.* 2015.

4. **Ruiz Salmón, I., Janssens, R. and Luis, P.** Mass and heat transfer study in osmotic membrane distillation-crystallization for CO2 valorization as sodium carbonate. *Separation and Purification Technology.* 2017, 176, pp. 173-183.

5. **World Meteorological Organization.** The state of greenhouse gases in the atmosphere based on global observations through 2014. *Greenhouse gas bulletin.* 2015, 11.

6. **NASA.** *Global climate change - Vital signs of the planet.* [Online] 8 may 2017. [Cited: 14 may 2017.] https://climate.nasa.gov.

7. **IPCC [Core Writing Team, R.K. Pachauri and L.A. Meyer (eds.)].** *Climate Change 2014: Synthesis Report. Contribution of Working Groups I, II and III to the Fifth Assessment Report of the Intergovernmental Panel on Climate Change.* Geneva : IPCC, 2014. p. 151.

8. **World Meteorological Organization.** The state of greenhouse gases in the atmosphere based on global observations through 2015. *Greenhouse gas bulletin.* 2016, 12.

9. **Center for Sustainable Systems, University of Michigan.** Greenhouse gases factsheet. *Center for Sustainable Systems, University of Michigan.* [Online] 2016. [Cited: 15 May 2017.] http://css.snre.umich.edu/factsheets/greenhouse-gases-factsheet.

10. **National Oceanic & Atmospheric Administration - Earth System Research Laboratory.** Trends in atmospheric carbon dioxide. *ESRL - Global Monitoring Division.* [Online] 5 May 2017. [Cited: 15 May 2017.] https://www.esrl.noaa.gov/gmd/ccgg/trends/.

11. **EPICA.** Carbon Dioxide and Temperature Measurements. *LafEnergy.* [Online] [Cited: 14 May 2017.] http://lafenergy.org/essays/gwfig1.php.

12. **United Nations Framework Convention on Climate Change.** The Paris Agreement. *UNFCCC.* [Online] 10 April 2017. [Cited: 15 May 2017.] http://unfccc.int/paris_agreement/items/9485.php.

13. **Kuckshinrichs, W. and Hake, J-F.** *Carbon Capture, Storage and Use - Technical, Economic, Environmental and Societal Perspectives.* s.l. : Springer International Publishing, 2015.

14. **Benson, S.M., et al.** Carbon Capture and Storage. *Global Energy Assessment - Toward a Sustainable Future.* Cambridge, New York, Laxenburg : Cambridge University Press, 2012, 13, pp. 993-1068.

15. **Wang, M., et al.** Post-combustion CO2 capture with chemical absorption: A state-of-the-art review. *Chemical engineering research and design.* 2011, Vol. 89, pp. 1609-1624.

16. **Pires, J.C.M., et al.** Recent developments on carbon capture and storage: An overview. *Chemical engineering research and design.* 2011, 89, pp. 1446-1460.

17. **Figueroa, J.D., et al.** Advances in CO2 capture technology - The U.S. Department of Energy's Carbon Sequestration Program. *International journal of greenhouse gas control.* 2008, 2, pp. 9-20.

18. **Steeneveldt, R., Berger, B. and Torp, T.A.** CO2 CAPTURE AND STORAGE Closing the Knowing-Doing Gap. *Chemical Engineering Research and Design.* 2006, 84, pp. 739-763.

19. **IPCC [Metz, B., O. Davidson, H. C. de Coninck, M. Loos, and L. A. Meyer (eds.)].** *IPCC Special Report on Carbon Dioxide Capture and Storage. Prepared by Working Group III of the Intergovernmental Panel on Climate Change.* Cambridge : Cambridge University Press, 2005. p. 442.

20. **OECD/IEA.** *CO2 Capture and Storage - A key carbon abatement option.* Paris : Head of Communication and Information Office, 2008.

21. **Gibbins, J. and Chalmers, H.** Carbon capture and storage. *Energy policy.* 2008, 36, pp. 4317-4322.

22. **Wang, M., et al.** Process intensification for post-combustion CO2 capture with chemical absorption: A critical review. *Applied Energy.* 2015, 158, pp. 275-291.

23. **Luis, P. and Van der Bruggen, B.** The role of membranes in post-combustion CO2 capture. *Greehouse Gas Science and Technology.* 2013, 3, pp. 1-20.

24. **Forster, M.** Investigations to convert CO2, NaCl and H2O into Na2CO3 and HCl by thermal solar energy with high solar efficiency. *Journal of CO2 Utilization.* 2014, 7, pp. 11-18.

25. **Yoo, M., Han, S-J. and Wee, J-H.** Carbon dioxide capture capacity of sodium hydroxide aqueous solution. *Journal of Environmental Management.* 2013, 114, pp. 512-519.

26. **Kordylewski, W., Sawicka, D. and Falkowski, T.** Laboratory tests on the efficiency of carbon dioxide capture from gases in NaOH solutions. *Journal of Ecological Engineering.* 2013, 14, pp. 54-62.

27. **Luis, P., Van Aubel, D. and Van der Bruggen, B.** Technical viability and exergy analysis of membrane crystallization: Closing the loop of CO2 sequestration. *International Journal of Greenhouse Gas Control.* 2013, 12, pp. 450-459.

28. **Fleischer, C., Becker, S. and Eigenberger, G.** Detailed modeling of the chemisorption of CO2 into NaOH in a bubble column. *Chemical Engineering Science.* 1996, 10, pp. 1715-1724.

29. **Seader, J.D. and Henley, E.J., Roper D.K.** *Separation process principles.* 3rd. s.l. : John Wiley & Sons, 2011.

30. **INHER S.A.** Random packing. *INHER S.A.* [Online] [Cited: 26 July 2017.] http://www.inhersa.co.za/products/process-engineering-equipment/column-internals/random-packing.

31. **Chabanon, E., et al.** Pushing the limits of intensified CO2 post-combustion capture by gas-liquid absorption through a membrane contactor. *Chemical Engineering and Processing.* 2015, 9, pp. 7-22.

32. **Khan, F.M., Krishnamoorthi, V. and Mahmud, T.** Modelling reactive absorption of CO2 in packed columns for post-combustion carbon capture applications. *Chemical Engineering Research and Design.* 2011, 89, pp. 1600-1608.

33. **Armfield Ltdt.** Gas Absorption Column - Instruction Manual - UOP7-MKII. August 2015. PC - 0054519.

34. **Onda, K., et al.** Saltins-out Parameters of Gas Solubility in Aqueous Salt Solutions. *Journal of Chemical Engineering of Japan.* 1969.

35. **Zeng, Q., et al.** Mass Transfer Coefficients for CO2 Absorption into Aqueous Ammonia Solution Using a Packed Column. *Industrial & Engineering Chemistry Research.* 2011, Vol. 50, pp. 10168-10175.

36. **Li, J.-L. and Chen, B.-H.** Review of CO2 absorption using chemical solvents in hollow fiber membrane contactors. *Separation and Purification Technology.* 2005, 41, pp. 109-122.

37. **Luis, P., Van Gerven, T. and Van der Bruggen, B.** Recent developments in membrane-based technologies for CO2 capture. *Progress in Energy and Combustion Science.* 2012, 38, pp. 419-448.

38. **Drioli, E., Criscuoli, A. and Curcio, E.** *Membrane Contactors: Fundamentals, Applications and Potentialities.* Amsterdam : Elsevier B.V., 2006.

39. **Rangwala, H.A.** Absorption of carbon dioxide into aqueous solutions using hollow fiber membrane contactors. *Journal of Membrane Science.* 1996, 112, pp. 229-240.

40. **Gabelman, A. and Hwang, S.-T.** Hollow fiber membrane contactors. *Journal of Membrane Science.* 1999, 159, pp. 61-106.

41. **Kim, Y.S. and Yang, S.M.** Absorption of carbon dioxide through hollow fiber membranes using various aqueous absorbents. *Separation and Purification Technology.* 2000, 21, pp. 101-109.

42. **Wang, R., et al.** Influence of membrane wetting on CO2 capture in microporous hollow fiber membrane contactors. *Separation and Purification Technology.* 2005, 46, pp. 33-40.

43. **Chabanon, E., et al.** Study of an innovative gas-liquid contactor for CO2 absorption. *Energy Procedia.* 2011, 4, pp. 1769-1776.

44. **Mansourizadeh, A., Ismail, A.F. and Matsuura, T.** Effect of operating conditions on the physical and chemical CO2 absorption through the PVDF hollow fiber membrane contactor. *Journal of Membrane Science.* 2010, 353, pp. 192-200.

45. **Kreulen, H., et al.** Microporous hollow fibre membrane modules as gas-liquid contactors - Part.1 Physical mass transfer processes. *Journal of Membrane Science.* 1993, 78, pp. 197-216.

46. **Luis, P., Van der Bruggen, B. and Van Gerven, T.** Non-dispersive absorption for CO2 capture: from the laboratory to industry. *Journal of Chemical Technology and Biotechnology.* 2011, 86, pp. 769-775.

47. **Ruiz Salmón, I.** *Thesis project (summary) - CO2 capture with NaCl: An approach based on membrane technology.* 2014.

48. **Liqui-Cel - Membrane Contactors.** *Design & Operating Procedures.*

49. **Mavroudi, M., Kaldis, S.P. and Sakellaropoulos, G.P.** A study of mass transfer resistance in membrane gas-liquid contacting processes. *Journal of Membrane Science.* 2006, 272, pp. 103-115.

List of figures

List of tables

Appendix A - Individual mass transfer coefficients

Membrane mass transfer coefficient

Based on the hypothesis that the only mechanism allowing the species to flow through the membrane is Knudsen diffusion, the membrane mass transfer coefficient is determined using Fick's law [36]:

$$k_m = D_{eff} \cdot \frac{\epsilon}{\delta\tau} \tag{A.1}$$

where ϵ, δ and τ are the membrane porosity, thickness and porosity respectively and $D_{eff} = \frac{2}{3} r_p \cdot \sqrt{\frac{8RT}{\pi M}}$ is the effective diffusivity of the diffusing species in the membrane (r_p is the pore radius, R the gas constant, T the temperature and M the species molecular weight). Eq.(A.1) is based on the assumption that the pores are uniform and cylindrical.

Tube side mass transfer coefficient (gas phase)

The tube and shell side mass transfer coefficients can be predicted by relations of this form [40]:

$$Sh = \frac{k_{l\ or\ g} \cdot d_{i\ or\ h}}{D_{i,g\ or\ l}} \propto Re^{\alpha} Sc^{\beta} f(geometry) \tag{A.2}$$

where Sh is the Sherwood number (ratio of convective mass transfer rate to diffusive mass transfer rate); Re is the Reynolds number and Sc the Schmidt number.

The tube side mass transfer coefficient is given by the Lévêque's equation [36]:

$$Sh_l = \frac{k_g \cdot d_i}{D_{i,g}} = 1.62 \left(\frac{d_i^2 \cdot v_g}{L \cdot D_{i,g}}\right)^{0.33} \text{ (L is the fibre length)} \tag{A.3}$$

This solution is applicable when assuming that the gas flows in laminar conditions in the fibres.

Shell side mass transfer coefficient (liquid phase)

Again, correlations based on eq.(A.2) can be found to evaluate the mass transfer coefficient of the liquid phase flowing in the shell side of the membrane contactor such as the following presented in [38] for gas absorption using membrane contactors:

$$Sh_l = \frac{k_l \cdot d_h}{D_{i,l}} = 1.25 \cdot \left(\frac{d_h^2 \cdot v_l}{L \cdot \nu}\right)^{0.93} \cdot \left(\frac{\nu}{D_{i,l}}\right)^{0.33} \tag{A.4}$$

where d_h is the hydraulic diameter of the fibre and ν the kinematic viscosity.

It is important to notice that the flow in the shell side mass is strongly dependent on the packing density of the membrane contactor which in turn influences the mass transfer coefficient [36].

Appendix B - Chemical absorption and enhancement factor

In previous sections were presented the mass transfer coefficient for the physical absorption of a gas species in a liquid solvent. Usually, in order to improve the efficiency of the process (see Figure B.1), the liquid is chosen so that a reaction can occur with the gas species. In that situation, the overall mass transfer coefficient will take this form:

$$\frac{1}{K_L} = \frac{1}{E \cdot k_l} + \frac{1}{H \cdot k_m} \cdot \frac{d_o}{d_{lm}} + \frac{1}{H \cdot k_g} \cdot \frac{d_o}{d_i} \tag{B.1}$$

$$\frac{1}{K_G} = \frac{H}{E \cdot k_l} + \frac{1}{k_m} \cdot \frac{d_o}{d_{lm}} + \frac{1}{k_g} \cdot \frac{d_o}{d_i} \tag{B.2}$$

where E is the enhancement factor due to the chemical reaction. By definition, this factor can be expressed as:

$$E = \frac{J_{chem}}{J_{phy}} \tag{B.3}$$

with J_{chem} and J_{phy} the absorption rate in the liquid in the presence of a chemical reaction and when only physical absorption occurs

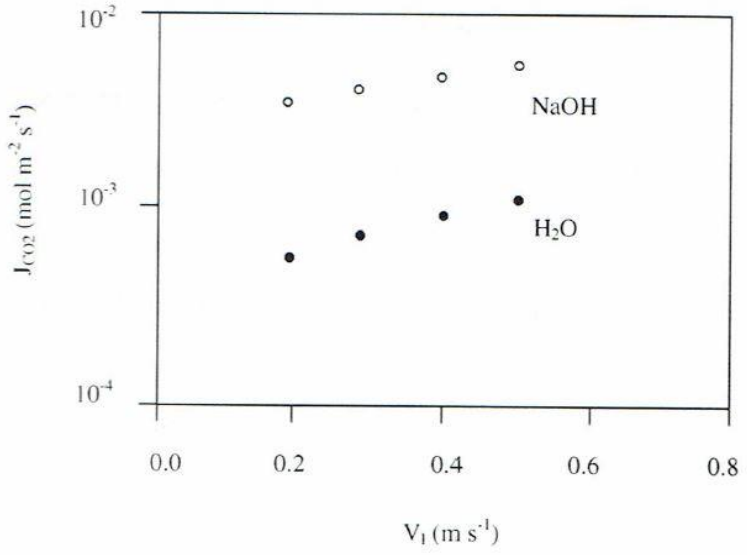

Figure B.1: Evolution of the CO_2 absorption rate with a varying fluid velocity for NaOH and H_2O (from [38])

Appendix C – Pictures of the setups

Absorption column

(a)

(b)

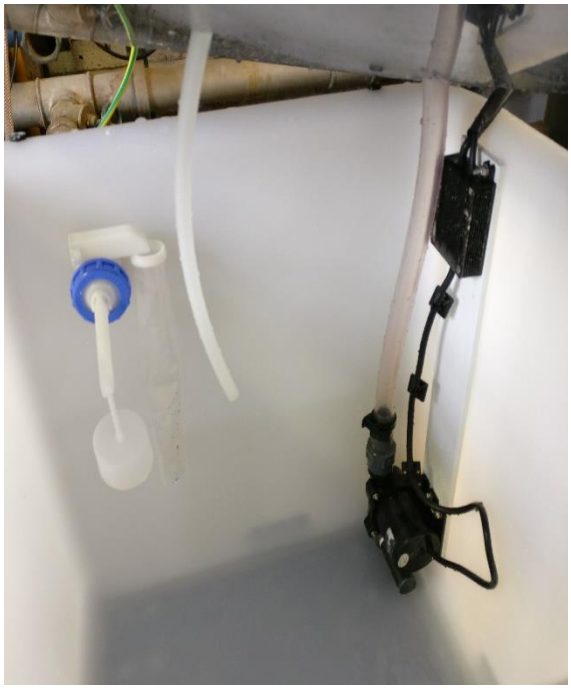

(c)

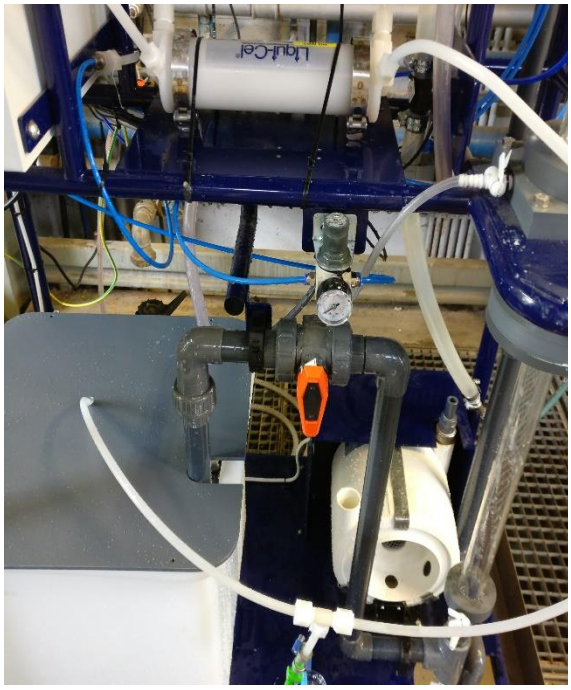

(d)

Figure C.1: Pictures of the absorption column setup. (a) Overall view - (b) Air blower - (c) Liquid pump - (d) Liquid line from the bottom of the column to the sump tank and CO_2 regulating valve

Membrane contactor

(a)

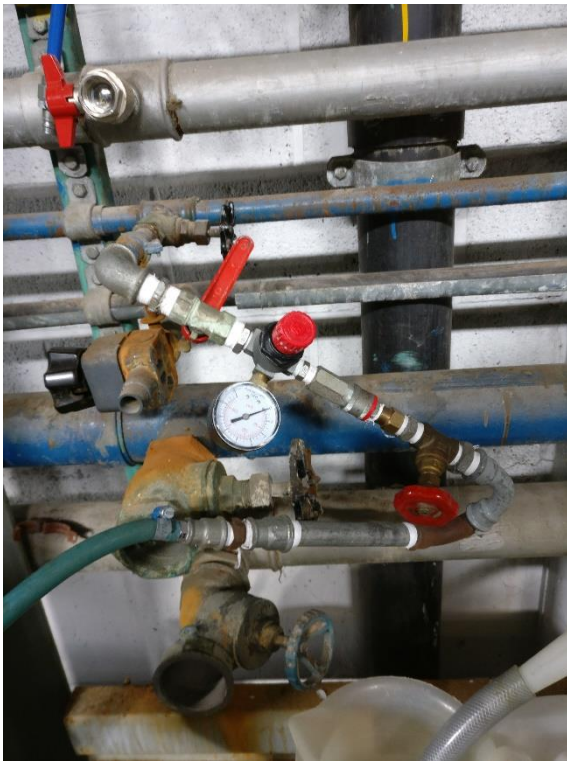

(b)

(c)

(d)

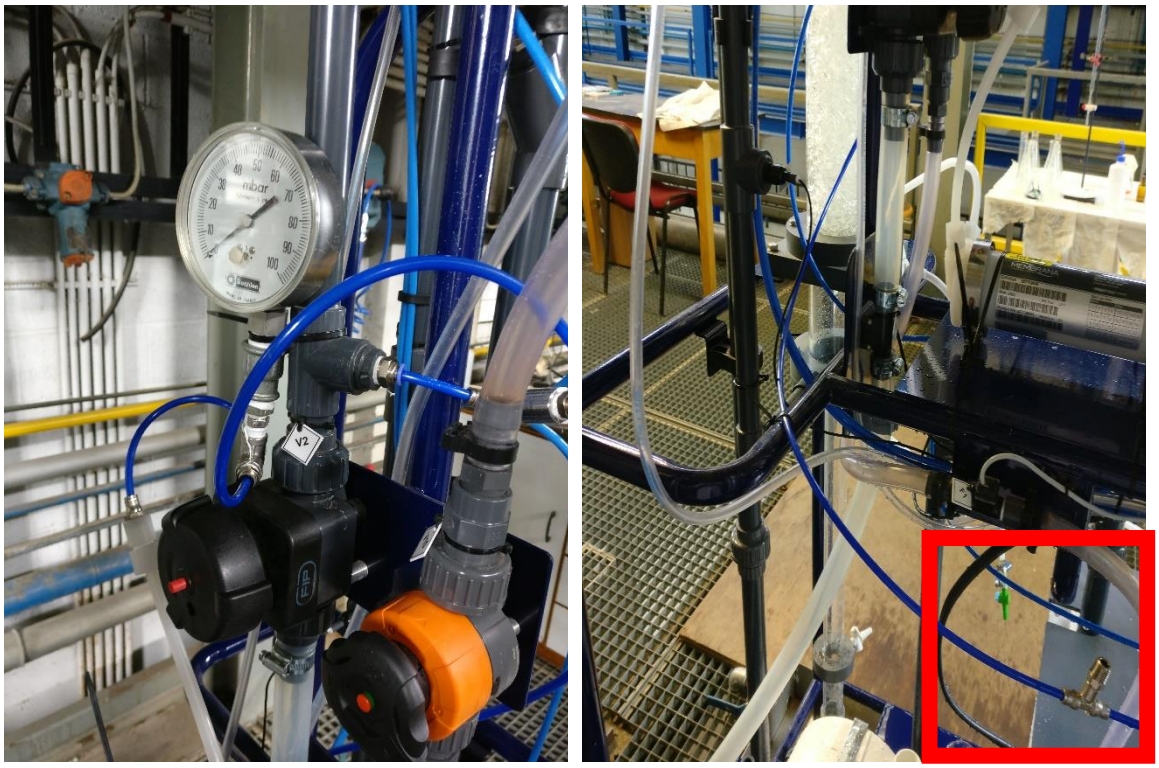

(e) (f)

Figure C.2: Pictures of the membrane contactor setup. (a) Overall view – (b) Lab air compressor – (c) Air conveyer – (d) Mixing of air and CO_2 before injection in membrane and deviation to CO_2 sensor – (e) Pressure gauge at the inlet of the column and liquid and air regulating valves – (f) gas outlet ensuring that the CO_2 sensor is not flooded

Appendix D – Graphs of evolution of species concentration and overall mass transfer coefficient

Absorption column

- Liquid: 0.2M – 3 L/min, Gas: 10% CO_2 – 33 L/min

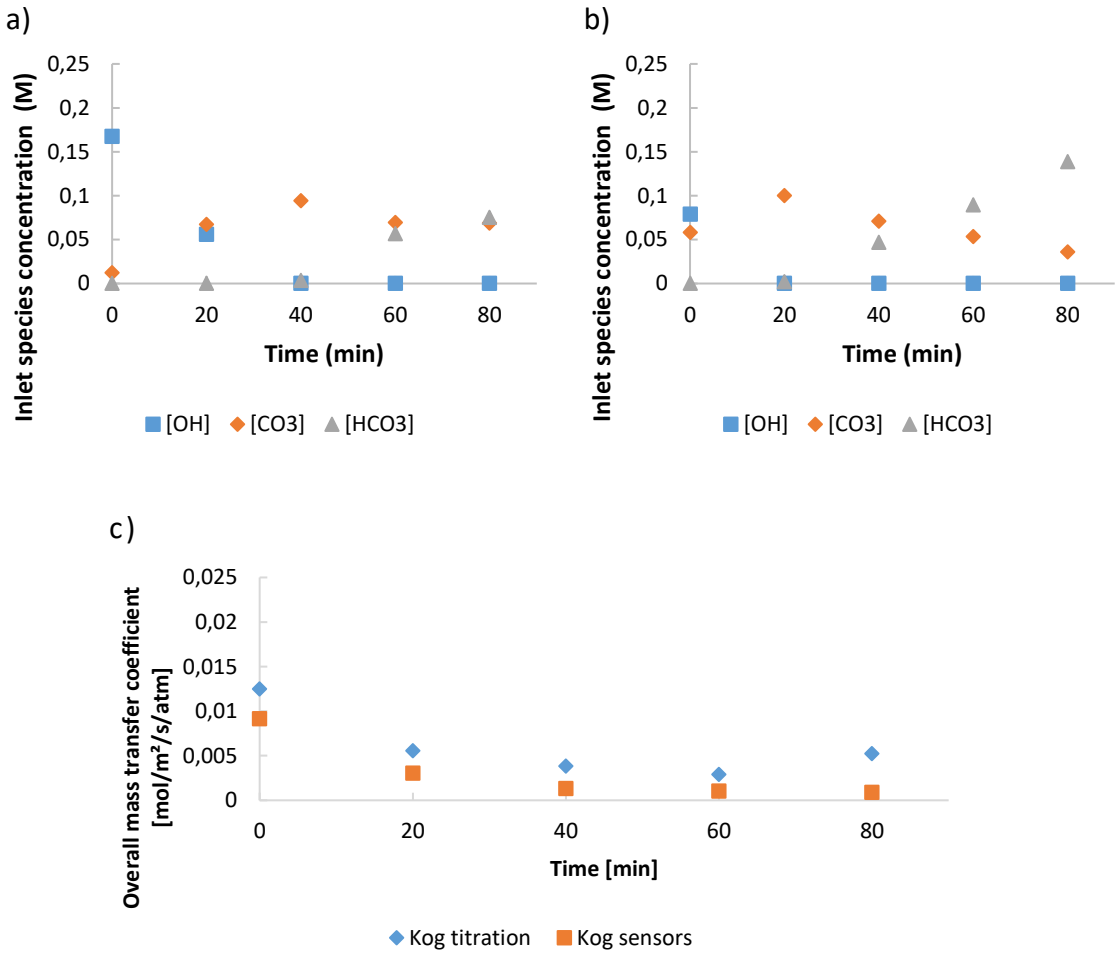

Figure D.1: (a) and (b) Evolution of the species concentrations in inlet and outlet - (c) Evolution of the overall mass transfer coefficient computed with the double indicator and the sensors methods

- Liquid: 0.2M – 7 L/min, Gas: 10% CO_2 – 33 L/min

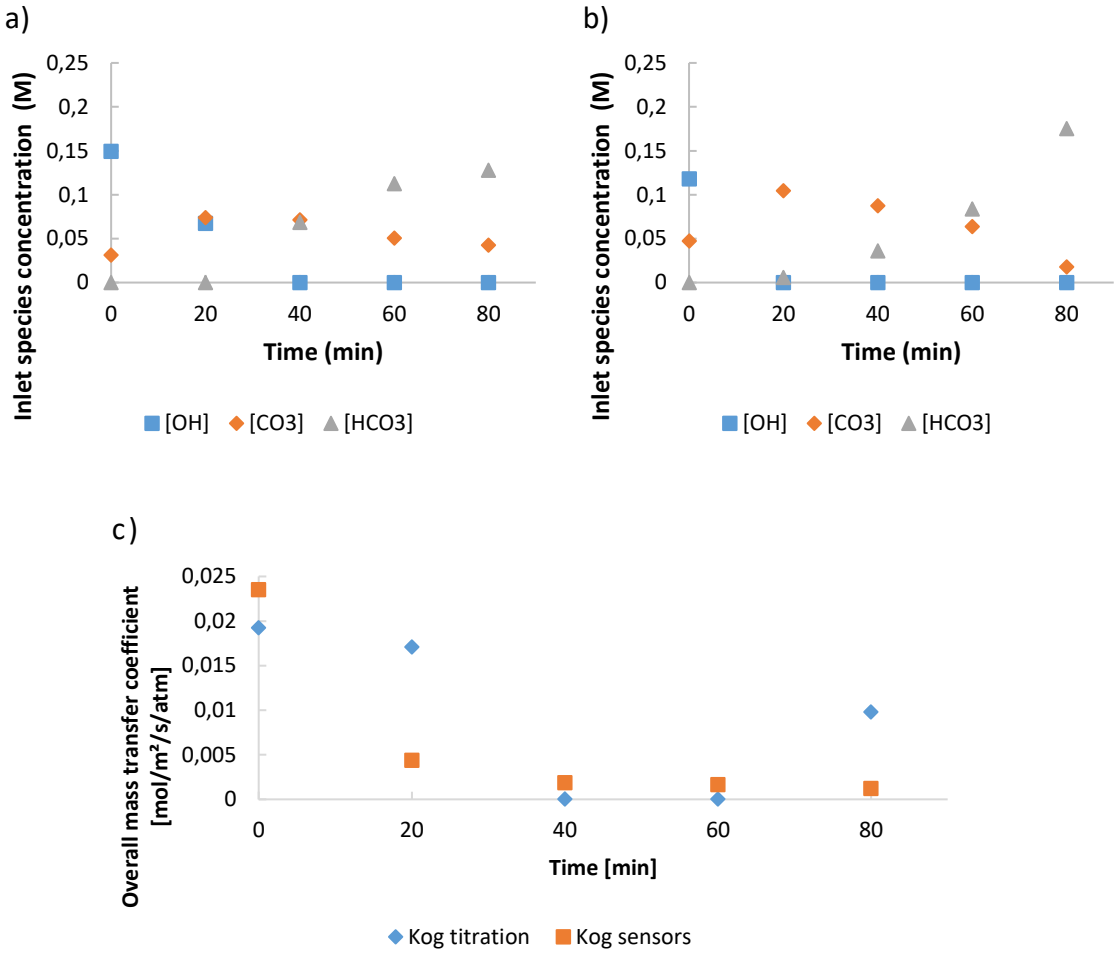

Figure D.2: (a) and (b) Evolution of the species concentrations in inlet and outlet - (c) Evolution of the overall mass transfer coefficient computed with the double indicator and the sensors methods

- Liquid: 0.5M – 5 L/min, Gas: 15% CO_2 – 33 L/min

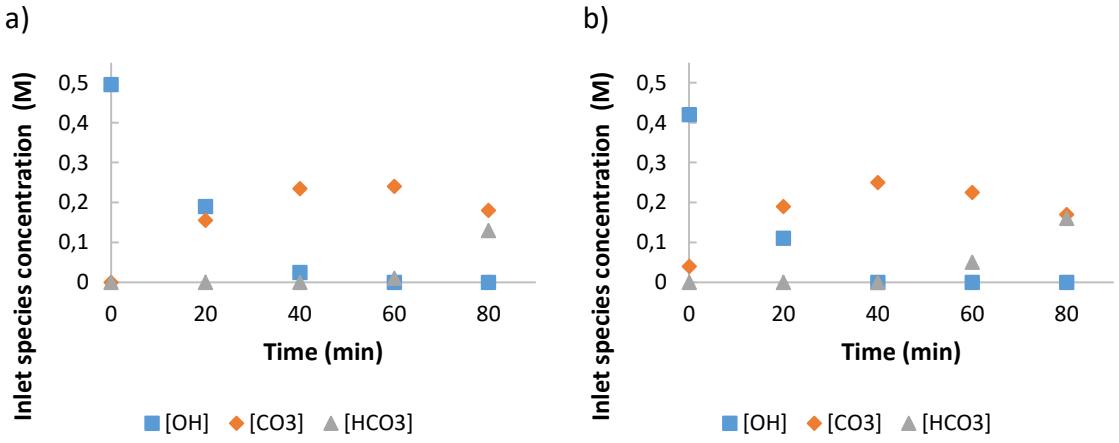

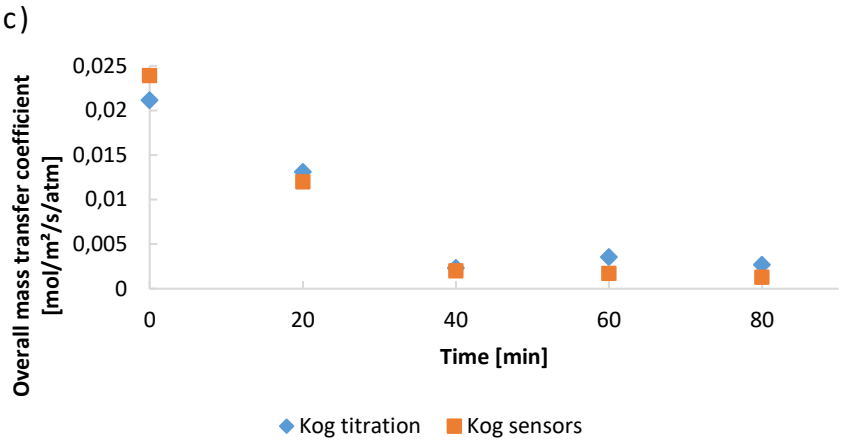

Figure D.3: (a) and (b) Evolution of the species concentrations in inlet and outlet - (c) Evolution of the overall mass transfer coefficient computed with the double indicator and the sensors methods

- Liquid: 1M – 5 L/min, Gas: 15% CO_2 – 33 L/min

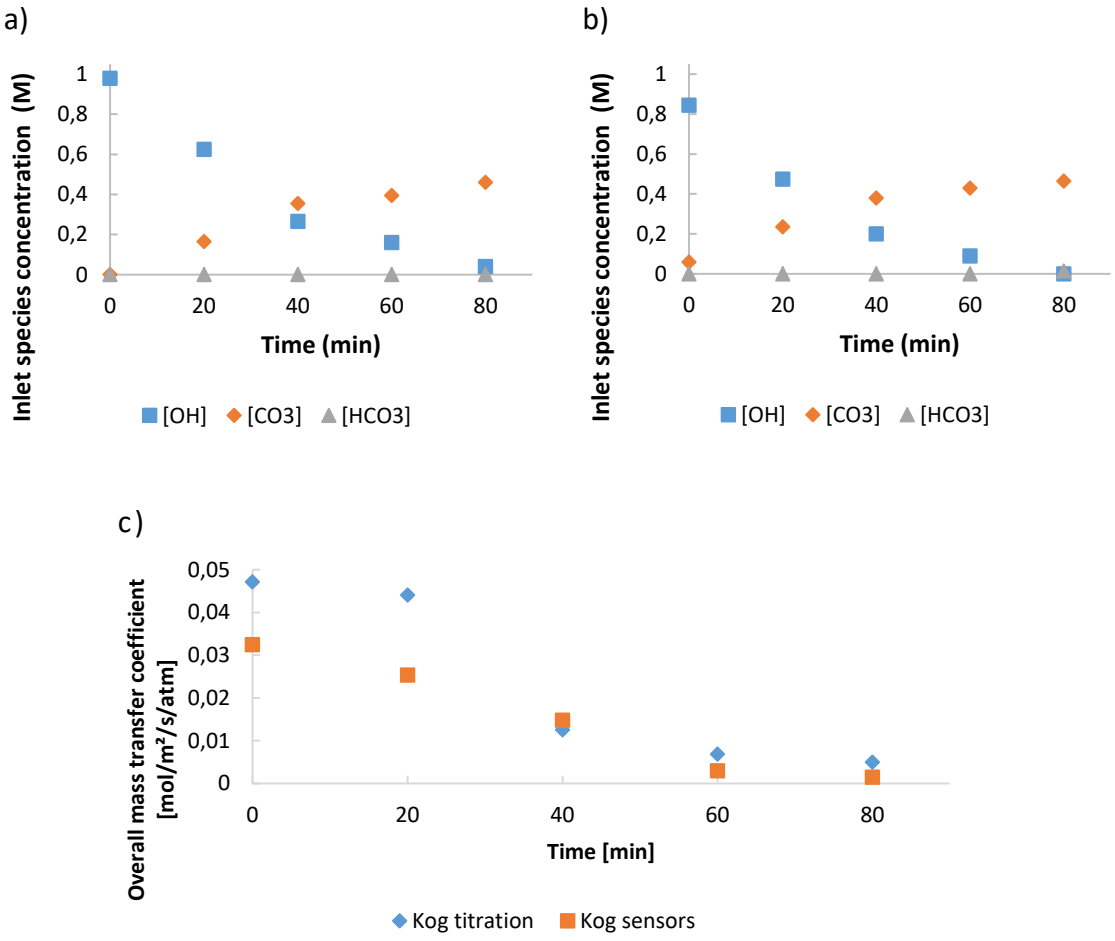

Figure D.4: (a) and (b) Evolution of the species concentrations in inlet and outlet - (c) Evolution of the overall mass transfer coefficient computed with the double indicator and the sensors methods

- Liquid: 0.2M – 5 L/min, Gas: 10% CO_2 – 66 L/min

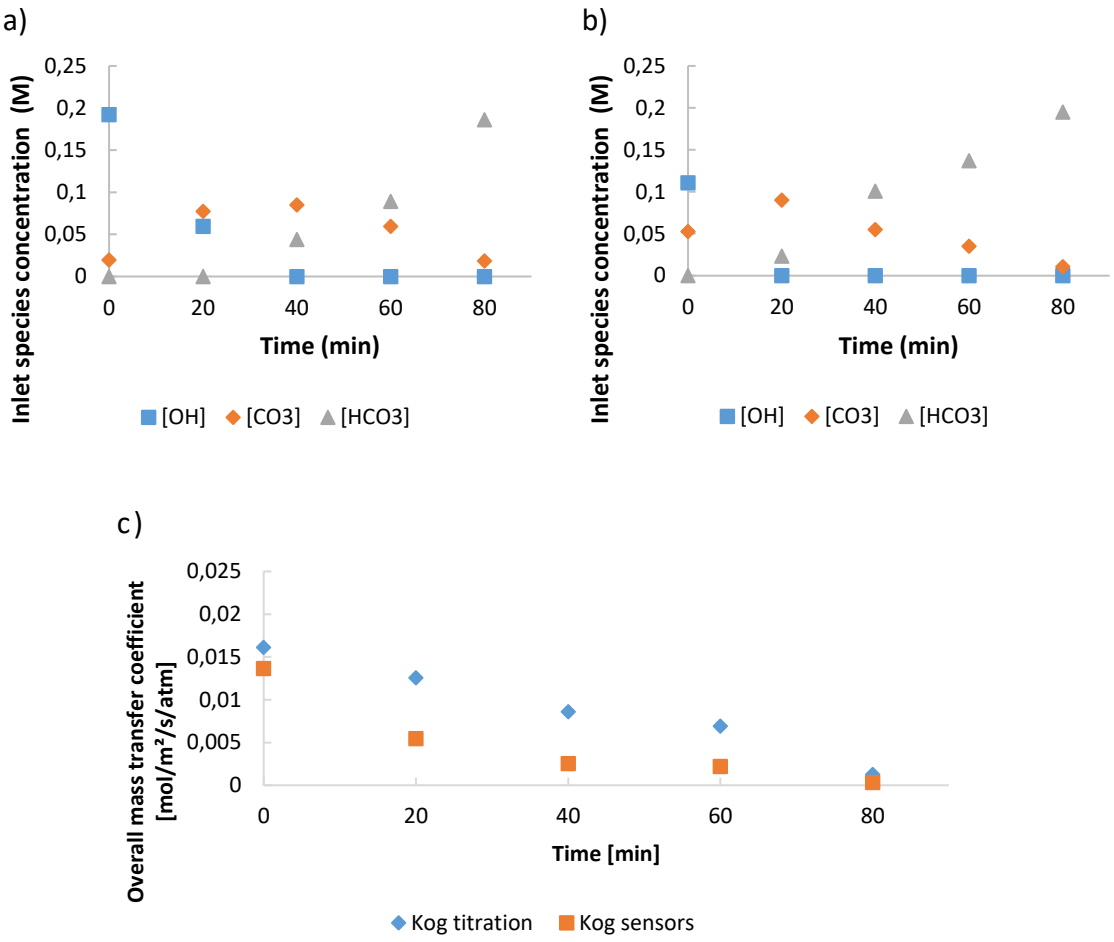

Figure D.5: (a) and (b) Evolution of the species concentrations in inlet and outlet - (c) Evolution of the overall mass transfer coefficient computed with the double indicator and the sensors methods

Membrane contactor

- Liquid: 0.2M – 1 L/min, Gas: 15% CO_2 – 6.5 L/min

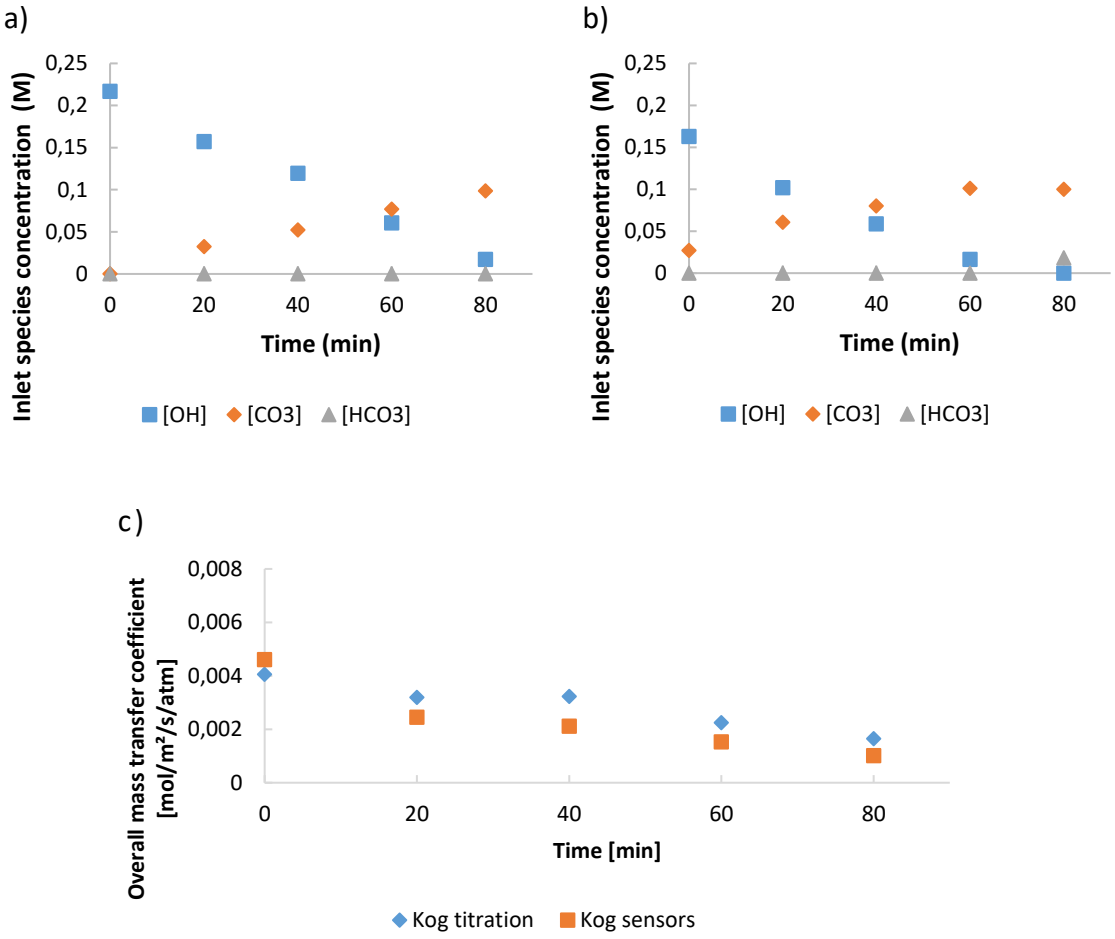

Figure D.6: (a) and (b) Evolution of the species concentrations in inlet and outlet - (c) Evolution of the overall mass transfer coefficient computed with the double indicator and the sensors methods

- Liquid: 0.2M – 3 L/min, Gas: 10% CO_2 – 33 L/min

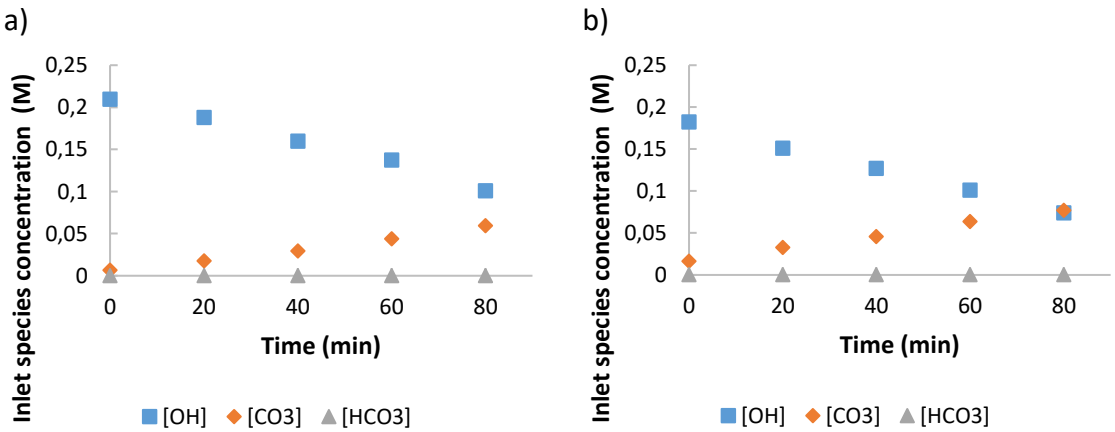

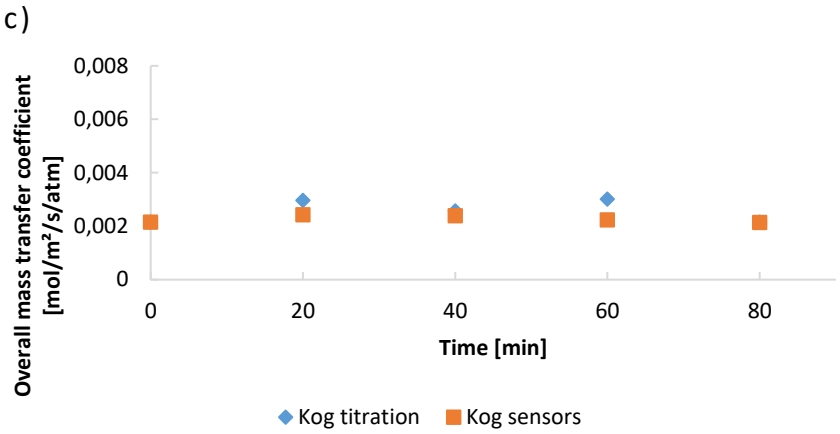

Figure D.7: (a) and (b) Evolution of the species concentrations in inlet and outlet - (c) Evolution of the overall mass transfer coefficient computed with the double indicator and the sensors methods

- Liquid: 0.2M – 1 L/min, Gas: 10% CO_2 – 10 L/min (closed gas exit)

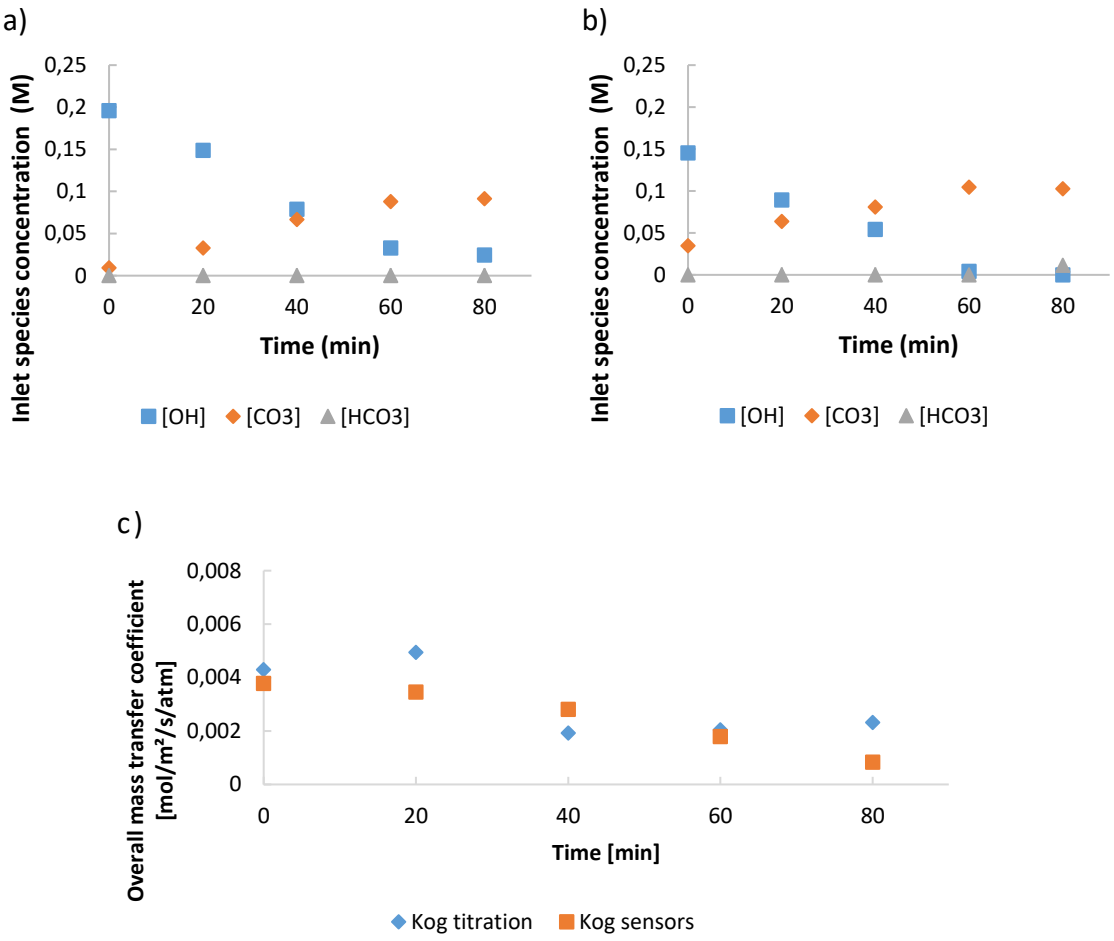

Figure D.8: (a) and (b) Evolution of the species concentrations in inlet and outlet - (c) Evolution of the overall mass transfer coefficient computed with the double indicator and the sensors methods

- Liquid: 0.2M – 1 L/min, Gas: 10% CO_2 – 6.7 L/min (closed gas exit)

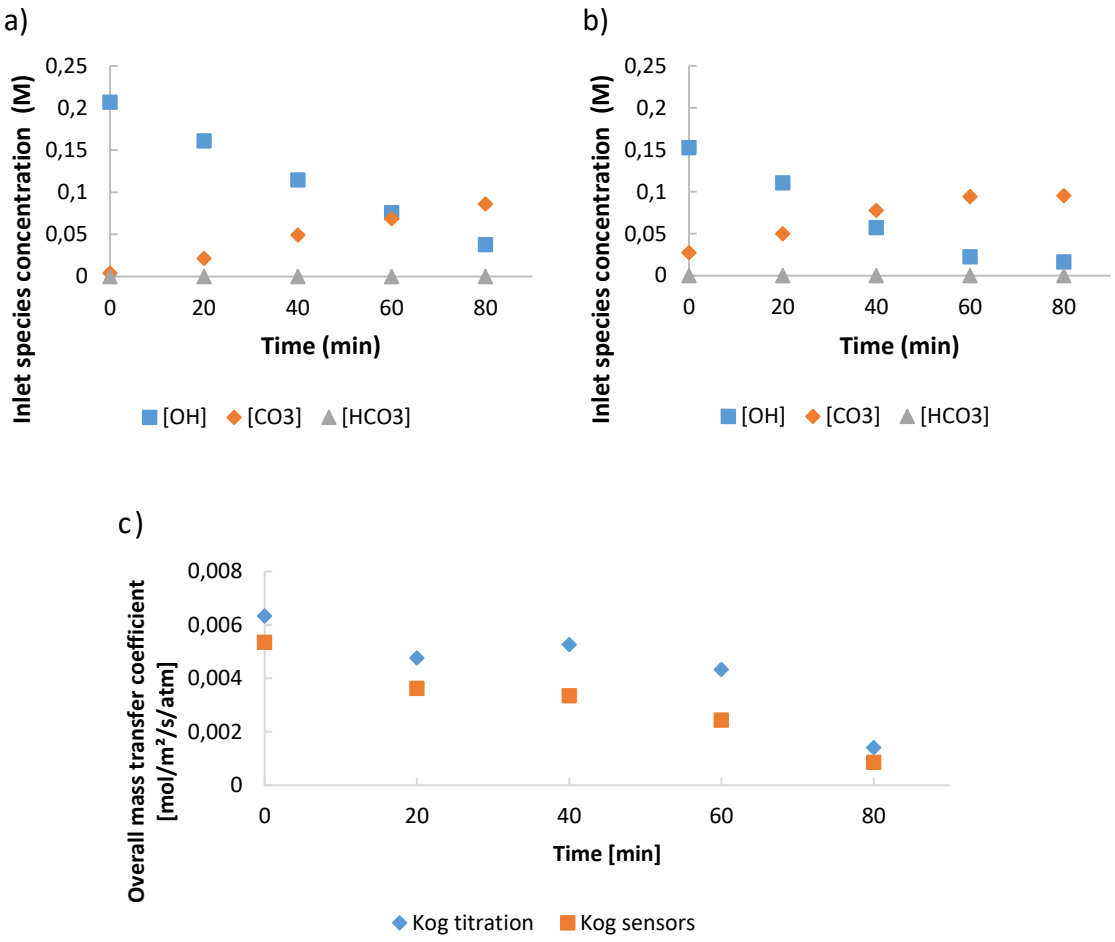

Figure D.9: (a) and (b) Evolution of the species concentrations in inlet and outlet - (c) Evolution of the overall mass transfer coefficient computed with the double indicator and the sensors methods

Rue Archimède, 1 bte L6.11.01, 1348 Louvain-la-Neuve, Belgium **www.uclouvain.be/epl**